SHEDDING LIGHT ON *E. COLI* PHOTOTAXIS

BY

TATYANA PERLOVA

DISSERTATION

Submitted in partial fulfillment of the requirements
for the degree of Doctor of Philosophy in Physics
in the Graduate College of the
University of Illinois at Urbana-Champaign, 2018

Urbana, Illinois

Doctoral Committee:

Professor Christopher Rao, Chair
Professor Martin Gruebele, co-Director of Research
Associate Professor Yann R. Chemla, co-Director of Research
Assistant Professor Diwakar Shukla

Abstract

My thesis work has been focused on phototaxis response in *E. coli*. I will review the current state of knowledge on chemotaxis and phototaxis and discuss the motivation behind this project in Chapter 1. In Chapters 2 and 3, I will describe a high-throughput framework for studying phototaxis in bacteria, which consists of the experimental setup and automated routine for data analysis, that I have developed over the course of this project. In Chapter 4, I will present experimental results that allowed us to pinpoint the role of individual components of the chemotactic network in phototaxis response and to characterize power dependence of the response. In Chapter 5, I will discuss the role of receptor-receptor interaction in determining the integrated phototactic response. In Chapter 6, I will quantify the effect of light on *E. coli* swimming velocity and its potential implication. In Chapter 7, I will discuss how various external parameters affect *E. coli* phototaxis response. Finally, in Chapter 8, I will present some preliminary results and discuss potential future directions of this project.

Acknowledgments

First and foremost, I would like to thank my advisors, Professor Yann Chemla and Professor Martin Gruebele, for being fantastic mentors, for showing me the way forward, for supporting and respecting me and my ideas. They taught me most of what I know about research: how to come up with new ideas, how to test them, how to combine experimental, analytical and computational approaches, and how to communicate scientific findings effectively. Martin's enthusiasm and Yann's cautious optimism have been my beacons in the night at times when I though that nothing is ever going to work. I could never have completed this work without their guidance and support.

I would like to thank senior students in Chemla and Gruebele lab, who I was working with when I just joined the lab, especially Patrick Mears and Hannah Gelman. Their competence, patience, and mentoring skills created an encouraging and stimulating learning environment.

I would like to especially thank my *E. coli* comrade, Roshni Bano, a younger student in the lab who joined a few years after me. It has been a pleasure to work with her: together we did multiple rounds of trap re-allignment, planned experiments for the CPLC summer school, mentored students and discussed papers. She has been incredibly supportive and patient with me, especially for the last couple of months, which I am sure was not easy. Roshni's curiosity, enthusiasm and initiative in the academic environment and beyond have been an example for me.

I would like to thank Alice Troitskaya for carefully proof-reading all of the texts without articles that I have written and patiently explaining why, when and where they have to be put in. I also thank Yann, Martin, Kevin Whitley, Roshni, Alice, Kaitlin Sumler, Clara Duarte and Nicole Curtis for proof-reading my thesis.

I would like to thank Ruopei Feng, our data analysis/computer hardware guru, for generously sharing his skills and knowledge.

I would like to thank all the former and current members of Chemla and Gruebele lab, for creating a great working and learning environment. In addition to those mentioned above, I would like to thank Max Prigozhin, Max Platkov, Irisbel Guzman, Anna-Jean Wirth, Lance Min, Barbara Stekas, Kiran Girdhar,

Vishal Kottadiel, Monika Makurath, Isaac Li, Sukrit Suksombat, Drishti Guin, Meredith Rickard, Lydia Kisley, Caitlin Davis, Kapil Dave and Shahar Sukenik.

I would like to thank several undergraduate students who have worked in the lab on some of the projects discussed in this work. Meredith Rickard, who is now a graduate student in Martin's lab, was an REU student in the lab and helped to set up a platform for heterogeneous illumination. Brett Barsanti and Kaitlin Sumler helped to develop protocols for growing *R. sphaeroides*.

I would like to thank a number of UIUC Professors. The classes I have taken with Professors William Metcalf, Rachel Whitaker and Klaus Schulten, have been incredibly helpful and instructive, both when planning further directions of my thesis project and when deciding on the area to pursue after my Ph.D. Professors Bob Gennis and Christopher Rao, have been extremely generous with their time and always willing to provide much-needed help and advice, and answer all of my naive biology questions. I would like to thank student in Chris Rao's group, Payman Tohidifar, for showing me how to do capillary assay. I would like to thank Professor Seppe Kuehn for help with PDMS chambers and career advice. I would like to thank Professors Tom Kuhlman and Seppe Kuehn for allowing me to use their equipment and sharing reagents. Additionally I would like to thank students in Kuehn and Kuhlman labs, Neil Kim, Harry Mikalide, Nick Sherer and Gloria Lee. I also thank Professor John Stack for his interest and support over the years. I also would like to thank Professor Diwakar Shukla for agreeing to be on my thesis committee on the last minute notice.

I would like to thank many other people in the Physics Department at the University of Illinois at Urbana-Champaign who helped me throughout graduate school. I would like to especially thank Professor Lance Cooper, Associate Head for Graduate Programs, for all his help and support and for making graduate student's well-being one of the priorites of Physics Department. I would like to thank Sharlene Denos and Katie Molohon, CPLC outreach postdocs, Angela Barragan, CPLC outreach fellow, and Professor Jaya Yodh, CPLC coordinator, for giving me the opportunity to participate in outreach and teaching activities, which has been a very rewarding experience. I would also like to thank Sandra Patterson, CPLC secretary, for all her help and, of course, her amazing sense of humor. I would like to thank Physics secretaries Melodee Schweighart and Wendy Wimmer. I would also like to thank CPLC lab manager, Betty Ujhelyi.

I would also like to thank a number researchers in the *E. coli* chemotaxis field. Professor John Parkinson have been extremely generous and provided majority of strains used in this work. I would like to thank Professors Yann Dufour, Shahid Khan, George Ordal, Barry Taylor, Thomas Shimizy and Thierry Emonet for helpful comments and discussion.

I would like to thank all of my friends in US, Russia and beyond, for their support and encouragement.

Eugene Moskovets, a senior-generation 'phystech', was the one to suggest that I should try to apply to graduate schools in America. I would like to thank my friend and mentor, Professor Michael Gorshkov, for his guidance and for his support of my decision to pursue a graduate degree in the US. I would like to thank, Nina Khristenko, Sergey Stepanyan, Nikita Gorshkov, my college friends who stayed in touch all throughout grad school, despite the distance and time zone difference. I would like to thank my friends in CU who taught me so many things beyond science, Rezvan Shahoei, Courtney Byard, Omid Alamdari, Vikyath Rao and Maryam Shakiba. I would like to thank many others who made my graduate school experience a fulfilling and rewarding one: Judi Chu, Anna Kukekova, Taras Pogorelov, Katka Golubeva, Grigory Polsyn, Hamed Shahoei, Martin Miller, John Rubins, Parisa Hosseinzadeh, Angela Barragan, Farshid Jafarpour, Zack Dell, Carolyn Kan, Barbara Stekas, Brandon Langley, Eric Petersen, Brittney Gorman, Robin Berthier, Brianne Gutman, Emily Cliff, Gloria Lee, Alice Troitskaya, Roshni Bano, Nadya Berkovich and Maria Dorofeeva.

I would like to thank my family, and most of all, my mother and my brother, Olga Perlova and Mihail Perlov, for their love and support, for believing in me and taking my successes and failures as their own. Finally, I would like to thank my partner and my best friend, Anton Goloborodko, for always having my back and for believing in me even when I did not believe in myself. I would not be able to get through this without him.

Table of Contents

Chapter 1

Introduction

Along with temperature, pH, and chemicals, light is an important environmental signal for many microorganisms. *Escherichia coli* is a surprising example of non-phototrophic bacteria, for which exposure to blue light results in changes in motile behavior, more specifically in increased 'tumbling'. This light-induced behavioral response is called phototaxis.

It is not known whether phototaxis in *E. coli* has any adaptive value for bacteria or whether it results in a movement towards or away from light. The exact mechanism of light sensing in *E. coli* is not understood either, but downstream from the receptors phototaxis is likely controlled by the same signalling network as chemotaxis, thermotaxis and other 'taxis' behavior (I will use chemotaxis as an umbrella term for all 'taxis' behaviors, which is accepted terminology in the field) [1].

Before talking about phototaxis *per se*, I will provide a broader picture of chemotaxis in section 1.1: I will introduce *E. coli* strategy for navigating environment gradients (1.1.1), discuss ecological role of chemotaxis and some of the open questions in the field (1.1.2). Then I will review what is currently known about phototaxis and discuss specific goals and motivation behind my thesis project in section 1.2.

1.1 What is chemotaxis

Very generally chemotaxis can be defined as a movement of an organism in response to environmental stimuli. The evolutionary advantage is obvious - in a heterogeneous environment, it is crucial to be able to move towards food and away from poison. So it is not surprising that chemotaxis is widespread throughout the tree of life from bacteria and archaea, to eukaryotes and higher organisms. However, there is a fundamental difference between chemotaxis in prokaryotic microbes and chemotaxis in eukaryotes. Eukaryotes can sense the chemical gradient along their body length, i. e. perform a spatial comparison of concentrations, and choose the direction of movement accordingly. Potential chemotactic strategies that can be employed by bacteria are fundamentally constrained by their small size ($\sim 2\,\mu m$ vs $\sim 50\,\mu m$ for eukaryotic cells). First of all, the time it would take a bacteria to perform statistically significant measurements of the difference in

chemical concentration across its body length is much larger than the time it would take a small molecule to diffuse across the same length [2]. Moreover, if bacteria actually absorbs the molecules it encounters, the gradient of concentration along bacteria body length will not be informative [2]. So instead of performing spatial comparisons as eukaryotes do, bacteria perform temporal ones: do things get better or worse? Secondly, bacteria are subject to rotational Brownian motion and bacteria swimming at a speed of $20\,\mu m/s$ will steer off course by more than 90° in 10 s and therefore will 'forget' which direction it was moving in before [3]. The two effects set upper and lower limits on 'counting time' and 'memory time' - the time it takes bacteria to 'forget' its previous measurement. How do bacteria manage to navigate their environment and search for optimal conditions within these constraints?

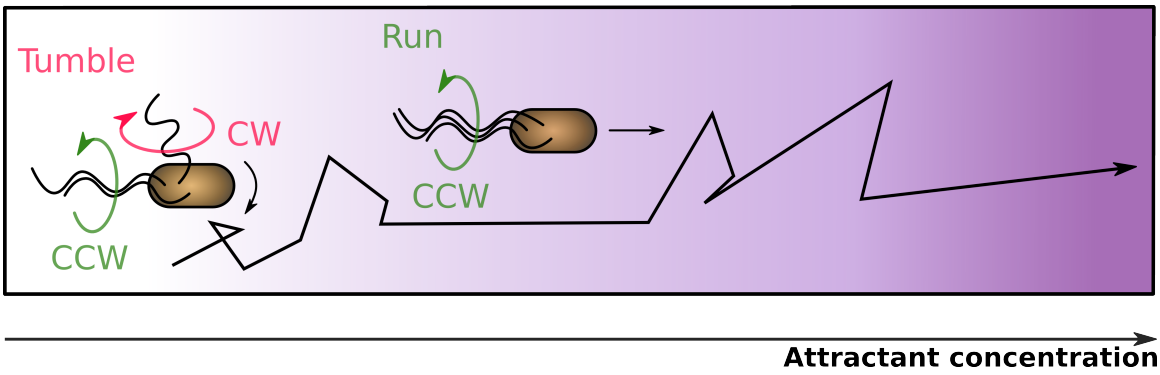

Figure 1.1: *E. coli* taxis is a biased random walk

1.1.1 How bacteria navigate their environment: *E. coli* paradigm

There is a lot of variability between chemotactic strategies across different bacterial species, which I will discuss later in this section [4]. However, there is also a common theme which can be illustrated by the example of *E. coli* - one of the best studied bacterial species.

E. coli motility is governed by a few simple principles that allow it to find the most favorable environment efficiently. *E. coli* is propelled by a bundle of helical, rotating flagella and swims by alternating between two types of motion: runs, during which cells swim in one direction along an approximately straight path, and tumbles, during which cells randomly reorient in one spot (1.1). *E. coli*, like many other bacteria, modulate the fraction of time spent tumbling (the tumble bias) in response to changes in the environment sensed by extracellular receptors, a behavior known as taxis. Using its surface receptors, a bacterium assesses whether its surroundings are getting better or worse as it propels itself forward. If the environment is improving, the bacterium continues to swim in the same direction, if it stays the same or is getting worse the bacterium tends to randomly change direction. The net effect of this response is that *E. coli* run lengths become longer

in favorable directions (i.e. toward high nutrient concentrations) and cells migrate effectively to a better environment (1.1).

Taxis behavior in *E. coli* is governed by a relatively simple biochemical network with a common core shared by many prokaryotic organisms [5], which I will describe in detail in Chapter 4. This network is characterized by its (1) extreme sensitivity: an *E. coli* cell responds to concentration changes as small as ∼3 nM, corresponding to just a few molecules per cell volume [6]; (2) wide dynamic range: a cell is sensitive to changes of up to 5 orders of magnitude in concentration; and (3) the ability to integrate diverse extracellular cues: not just concentrations of various chemicals (chemotaxis), but temperature (thermotaxis), pH (pH-taxis), and, as it turns out, light (phototaxis) [7–9].

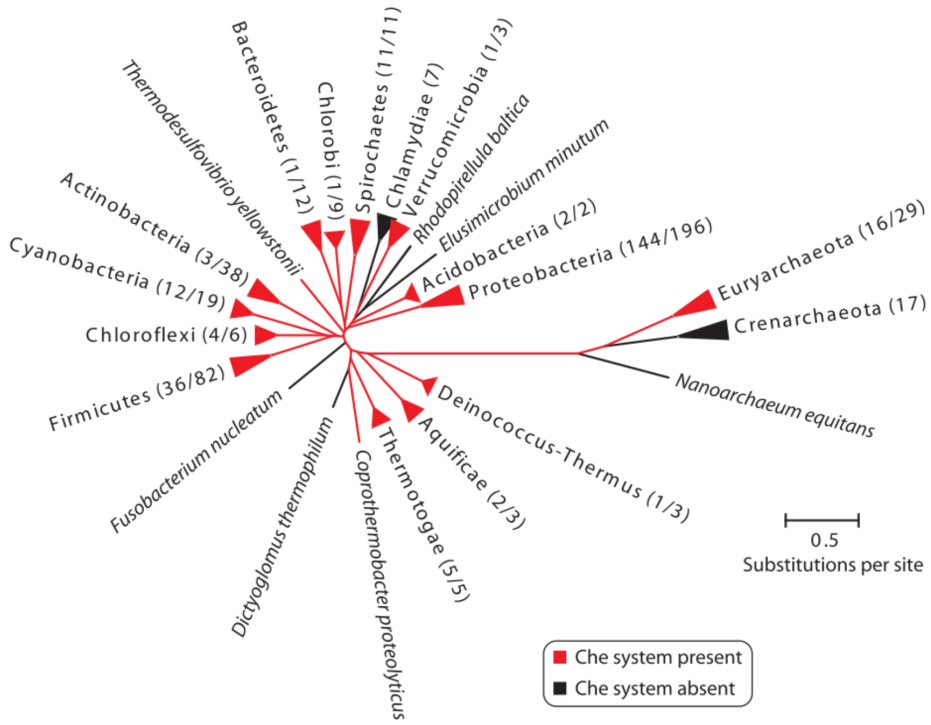

Figure 1.2: Phylogenetic distribution of the chemotaxis system. Phyla containing representatives with chemotaxis system components are shown in red. The number of these representatives versus the total number of analyzed genomes within the clade is shown in parentheses. Figure from [5].

1.1.2 Why study chemotaxis

Chemotaxis in *E. coli* has been studied extensively and serves as a paradigm for the way living cells modulate their behavior based on environmental signals [3, 10, 11]. But what is the relevance of chemotaxis beyond *E. coli* and laboratory environment? I do not claim to present here a comprehensive picture of the current state of knowledge nor to predict the further developments in the field, but I would like to discuss some

questions that are important to me and that motivated at least in part my thesis work.

Ecological role of chemotaxis

Bacterial lifestyle in the natural environment is very different from the single-cell planktonic state that we are used to in the lab. According to current understanding, most bacteria spend the majority of their time in the attached or immotile state as part of complex microbial communities [12]. However between dispersion from and attachment to biofilm bacteria can be motile and potentially guided by chemotaxis.

While immotile microorganisms explore and compete for physical space through growth, motile chemotactic bacteria can actively navigate towards the optimal microenvironment [13, 14]. Chemotaxis and motility may, therefore, play a role in determining where and when bacteria are going to settle and transition to the sessile state. It has been shown for example that different stages of chitin microparticles colonization by bacteria correspond to different abundances of genes associated with chemotaxis to chitin degradation products [15]. These results suggest that along with other processes, such as metabolism and quorum-sensing, chemotaxis might drive the succession of different species in particle-attached microbial communities [15]. Chemotaxis plays a role in defining the spatial structure of microbial communities as well. One very clear manifestation of that is a vertical stratification of the species in microbial mats and water columns due to energy taxis - chemotaxis in gradients of components that affect the flow of electrons through an electron-transport chain, such as oxygen, alternative electron acceptors, and carbon sources [8, 16].

Finally, several studies suggest that chemotaxis to informational cues, such as self-excreted amino acids or quorum-sensing signals, may contribute to the formation of bacterial communities as it allows bacteria to actively look for each other [17–21]. In other words rather than relying on chance encounters bacteria may use chemotaxis in order to reach a local quorum density necessary for expression of biofilm-associated genes [17, 21]. For example, it has been shown that chemotaxis towards autoinducer AI-2, a quorum-sensing signalling molecule for intra-species communication, mediates autoaggregation and promotes expression of biofilm-associated genes in *E. coli* [21]. In another study, researchers have demonstrated that both *B. subtilis* and *P. aeruginosa* are attracted to extracellular potassium emitted by *B. subtilis* biofilms and this attraction is mediated by chemotaxis [22].

In summary, the ability to follow environmental gradients can give bacteria important fitness advantage in heterogeneous environment [23–25]. So it is not surprising that chemotaxis is ubiquitous in the microbial world. As of 2010 more than half of sequenced prokaryotic genomes contained chemotaxis genes and most of the major prokaryotic phyla contain representatives with chemotaxis system components (fig. 1.2) [5]. Chemotaxis plays role in diverse ecological processes across the wide range of bacterial habitats and lifestyles.

For example, marine bacterium *Vibrio fisheri* is guided by chemotaxis towards the squid light organ, where it achieves high enough density to become luminescent [26]. Chemotaxis in *Pseudomonas fluorescens* is important for colonization of tomato plant rhizosphere [27]. And pathogenic bacterium *Helicobacter pylori* uses chemotaxis to navigate towards the mucus lining of the stomach [28].

As discussed above chemotaxis is an environmentally relevant behavioral response and studying different aspects of chemotaxis may provide important insights about natural bacterial communities. In that regard, I find the following questions especially intriguing. How do bacteria handle the diverse range of navigational problems they can face in the wild? And what is the connection if any between chemotaxis and other processes in bacteria?

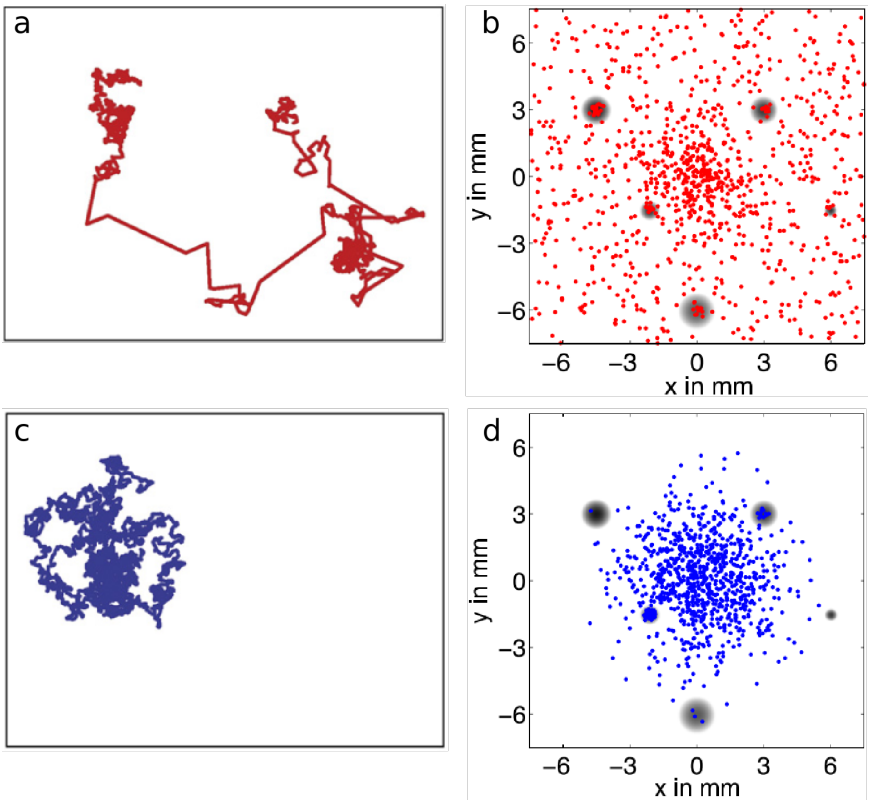

Figure 1.3: According to simulation distribution of run lengths affects population performance in a patchy nutrient landscape. (a) Example of the trajectory with power law distribution of run intervals and (b) population of such bacteria at the end of the simulation with superimposed gradients of attractants indicated by gray patches. (c) and (d) Example of the trajectory and bacterial positions for the population of bacteria with run intervals distributed exponentially. Figure adapted from [23].

What is optimal chemotaxis strategy?

Until recently the dominant view in the field of chemotaxis was that *E. coli* chemotactic network is designed for optimal performance [2, 29, 30]. However it is becoming increasingly obvious that optimal chemotaxis

strategy is dictated by the environment, type of stimuli and typical gradients bacteria encounter [4, 31, 32]. As discussed above bacteria can face very different types of navigational problems and ecological tasks, which is reflected in behavioral variability in the individual bacteria [23, 33], in the phenotypic variability within clonal bacterial populations [25, 34–36], and in the variability of chemotaxis and motility strategies across species [4, 5, 24, 37, 38].

At the single-cell level, the source of the behavioral variability is signalling noise in the chemotaxis network [33]. Due to temporal fluctuations in the abundance of the active form of the chemotaxis signalling molecule CheY-P, run intervals are distributed according to a power law, rather than exponentially as was previously believed [33]. At the behavioral level, it means that bacteria perform superdiffusive Levy-walk, alternating between local search and long-distance exploration (fig. 1.3a). According to simulations in an environment with sparse nutrient sources, populations of such superdiffusive bacteria explore space and find nutrient sources more efficiently than bacteria with an exponential distribution of run intervals (fig. 1.3) [23].

There is a trade-off, however, between different aspects of chemotactic performance as well as between chemotactic performance in different environments. For example in an environment with steep and stable gradients, superdiffusive bacteria are at a disadvantage due to their reduced precision of localization and slower adaptation [23]. Another theoretical study has shown that the speed of advancement along the gradient, the so-called drift velocity v_D, used as a measure of chemotactic efficiency, depends on the ratio of chemotaxis protein concentrations $[CheR]/[CheB]$ [32] (see Chapter 4 for detailed description of the chemotaxis network). Moreover the ratio $[CheR]/[CheB]$ that maximizes v_D depends on the steepness of the gradient [32]. Finally different ecological tasks require different chemotaxis strategies as well: modeling shows that the range of phenotypes maximizing nutrient uptake during foraging is different from the ones winning the arrival race in the colonization challenge [25].

It is reasonable to assume therefore that chemotactic diversity is a selectable trait that enables adaptation to environmental variability and for a population of bacteria in a diverse and ever-changing environment it would be advantageous to have a range of chemotaxis phenotypes [25]. But there is little experimental evidence to corroborate this. Waite *et al.* have shown that non-genetic diversity affects functional performance of the bacterial population in a stable gradient of attractant leading to spatial separation of different phenotypes based on their chemotactic drift velocity [35]. However it is far from clear how the diversity of chemotaxis strategies would affect the performance of the population in a more realistic environment where nutrients might be sparse, gradients are short-lived and a large number of different stimuli need to be taken into account at the same time.

E. coli bacteria dwell in the lower intestines of warm-blooded animals. Between switching from one host to another it lives in ponds, sediments, and soil [39]. Its chemotactic apparatus has therefore evolved to allow optimal navigation within the constraints of this lifestyle (although laboratory strains of *E. coli* might be very far off from its wild-type free-living ancestor [40]). Other bacteria have developed distinct chemotactic strategies adapted to their ecological niches so there is a large degree of variation in different aspects of chemotaxis and motility across studied species [4, 5, 24, 37, 38]. For example, there is more than an order of magnitude variation in swimming speed between *E. coli* and some marine bacteria [24] (fig. 1.4a). Motility patterns are highly variable as well: while *E. coli* runs and tumbles, *R. sphaeroides* runs and stops, and many marine bacteria run and reverse instead (fig. 1.4b) [4]. Bacterial species also differ in their chemotactic efficiency, or how fast they can move up the gradient compared to how fast they swim. Thus marine bacteria *P. haloplanktis* has more than 10 times faster chemotactic response compared to *E. coli* which enables them to exploit short-lived nutrient gradients, a critical skill in the fast-changing and nutrient-sparse ocean environment [24, 38]. Finally, there is also a lot of variation in the type of stimuli that bacteria respond to.

Behavioral differences result from diverse architectures and complex regulation of chemotaxis pathways in different species. The *E. coli* chemotactic network is, in fact, one of the simplest among the studied networks. Bacterial chemotactic networks in other species feature numerous forms of signalling proteins [5, 41], additional feedback loops for more precise adaptation [42], cytoplasmic and periplasmic receptor clusters [41, 43], and even multiple chemotactic systems in a single organism [5].

In summary, a number of theoretical and a few experimental studies suggest that diversity of chemotactic strategies on all levels, within populations of bacteria and across species, has developed to ensure efficient navigation in the natural habitat, whatever that might be for a particular species of bacteria. There have been theoretical attempts to 'reverse-engineer' natural microenvironment of bacteria based on the knowledge about their chemotactic apparatus [44]. Bridging the gap between gradients that bacteria might encounter in the wild and those that can be generated experimentally is necessary for experimental validation of this hypothesis and further investigation of the factors important for chemotactic performance, which requires creative approaches to setting up chemical gradients [38] or developing entirely new ways to stimulate a tactic response.

1.1.3 Chemotaxis and other processes in bacteria

Chemotaxis does not function in isolation, it is regulated by and potentially contributes to the regulation of other important cellular processes such as metabolism, growth, quorum-sensing and lifestyle switches. I

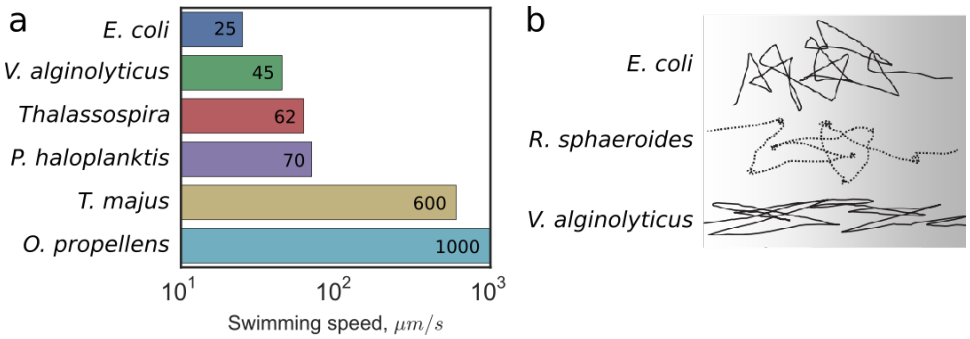

Figure 1.4: Variability in chemotactic strategies across different bacterial species. (a) Swimming velocity, based on data from [24]. (b) Motility patterns: *E. coli* runs and tumbles, *R. sphaeroides* runs and stops, *V. alginolyticus* runs and reverses. Adapted from [4].

have already discussed above some examples of chemotaxis to quorum-sensing signalling molecules and the role of chemotaxis in biofilm formation in the previous section. Chemotaxis, growth, and metabolism are also linked in several ways. Chemotaxis can be directly guided by metabolism. In metabolism-dependent chemotaxis mode, response to a certain nutrient requires its transport and metabolism, and is mediated by binding of metabolized intermediates to intracellular receptor clusters or by the change in the electron flow through the electron-transport chain in case of 'energy-taxis', a type of metabolism-dependent chemotaxis [8, 16, 45]. Regulation of chemotaxis and motility appear to depend on growth as well. It is known, for example, that whether or not bacteria will be motile and therefore able to perform chemotaxis depends on the growth substrate: bacteria are immotile when grown in rich media such as LB and motility is impaired during growth on glucose [46], their preferred carbon source [47], possibly due to downregulation of cAMP [48].

During growth on the same substrate throughout the growth curve bacteria can regulate flagellar motor output and therefore swimming velocity [49], as well as chemoreceptor ratio, resulting in a change of pH, temperature and amino acid preference [9, 50, 51]. However, it is not clear whether the change is caused by the increase in the cell density or alternatively by nutrient depletion.

Interdependence between chemotaxis, growth, and metabolism is not surprising as one of the functional roles of chemotaxis is to find nutrients that can be metabolized and provide building blocks for making new cells and therefore more efficient chemotaxis means higher fitness. However, to the best of my knowledge, there has been no experimental work connecting the chemotactic performance to fitness benefits. On the contrary, a majority of studies on chemotaxis try to decouple chemotaxis from metabolism by using non-metabolizable analogs of attractants [52].

1.1.4 Where next for chemotaxis research

Chemotaxis in *E.coli* and other bacteria has been studied extensively at several levels of complexity - from molecular details of signalling to behavioral patterns in single cells and populations of bacteria [35, 53, 54]. However, on each level, there is a lot left to discover. On the molecular level, we still do not know for example how different players in the chemotactic network interact with each other, although several recent papers bring us closer to a complete understanding of the signal transduction mechanism and organization of receptor complexes [55–57].

There are a number of open questions on systems and behavioral levels as well, some of which were discussed in the previous sections. I consider the following research directions promising for uncovering the ecological role of chemotaxis as they have already provided some important insights: (1) chemotaxis of bacterial populations in different types of environment - more realistic gradients, patchy nutrient landscapes (fig. 1.3b), simultaneous gradients of different types of stimuli, (2) chemotaxis in bacterial species beyond *E. coli*, (3) chemotaxis within the context of other processes in bacteria, such as metabolism, quorum-sensing, growth and life-style switches.

1.2 Phototaxis

I believe that studying **phototaxis**, which is a type of taxis behavior regulated by light, can contribute to answering some of the questions I formulated in the previous section. Unlike chemicals, light is easy to control both in time and in space and it is also easy to combine with other types of stimuli. Many species of bacteria are phototrophic or photosynthetic and therefore phototaxis is directly dependent on and affecting their metabolism and fitness. Finally, it has been demonstrated that non-phototrophic bacteria such as *E. coli* and *Salmonella* respond to light as well [58]. Phototaxis in *E. coli* has been the focus of my thesis work for two main reasons. First of all the phenomenon of light-induced motility changes in non-phototrophic organisms is intriguing on its own and has not received a lot of attention. And secondly *E. coli* is an easy to culture model organism with developed genetic approaches and a vast library of chemotactic mutants and therefore can be used for testing experimental and data analysis approaches for studying phototaxis at the development stage. Below I will discuss in more details what is known about phototaxis in phototrophic and non-phototrophic organisms as well as motivations and goals of my thesis work.

1.2.1 Phototaxis in phototrophic organisms

Phototaxis, the light-dependent movement of microorganisms, was first observed as early as the 19th century for a species of purple bacteria [59]. Along with halobacteria and cyanobacteria, purple bacteria are phototrophic, i.e. they can capture light and use its energy in their metabolism. Phototaxis has an obvious advantage for phototrophic bacteria as it allows them to migrate towards optimal illumination conditions [60, 61].

There are several species of phototrophic bacteria, in which phototaxis has been studied more extensively, among them purple nonsulfur bacteria *R. sphaeroides* and *Rhodospirillum centenum* [62, 63] and cyanobacteria *Synechocystis sp.* [64–67].

R. sphaeroides is a metabolically diverse photosynthetic bacteria living in soil and freshwater habitats. It can perform both aerobic and anaerobic respiration as well as photosynthesis when grown under appropriate conditions [68]. When grown phototrophically *R. sphaeroides* is phototactic: it demonstrates increased probability of stopping or increased stopping bias in response to a step decrease in light intensity, which is analogous to tumbling response in *E. coli* [63]. At the same time *R. sphaeroides* fails to accumulate in a light beam so no migration towards light has been shown [62]. There has been no evidence of photokinesis or change in swimming velocity in response to light exposure [63]. I will review what is known about taxis behavior of *R. sphaeroides* in more details in Chapter 8.

Synechocystis is photoautotrophic unicellular freshwater cyanobacterium and it exhibits phototaxis mediated by Type IV pili when gliding on solid agar surfaces [65]. *Synechocystis* senses the direction of light, rather than an intensity gradient although the mechanism is unclear: when presented with several light sources from different directions, bacteria exhibit phototaxis along the vector sum of these directions [67]. *Synechocystis* also differentiates between different wavelengths of light: red to green wavelengths cause changes in motility bias, while blue inhibits motility [66]. The signalling network underlying phototaxis behavior in *Synechocystis* is unknown.

1.2.2 Phototaxis in *E. coli* and other non-phototrophic organisms

E. coli is a surprising example of non-phototrophic bacteria, for which exposure to blue light results in changes in motile behavior [1, 58, 69, 70]. And *E. coli* is not unique in that sense. Light-modulated motility responses have also been observed for chemotrophic *Salmonella typhimurium* and *Acinetobacter calcoaceticus* [69].

A phototaxis response to blue light in *E. coli* and *S. typhimurium* was first demonstrated in 1975 by Taylor and Koshland [69]. *E.coli* responded by initial tumbling after a short exposure, smooth swimming

after medium exposure and paralysis resulting from prolonged exposure. In 1979, Taylor and co-workers showed that a functioning electron transport chain is required for response to terminal electron acceptors (e.g. oxygen or nitrate) and to blue light, both of which are mediated by the Aer receptor, which was not known at the time. They have observed the response in both aerobic and anaerobic conditions as long as bacteria were respiring [58]. Finally, Wright *et al.* have shown that paralysis of bacteria, reported by previous papers, was caused by photo-excited dyes present in non-transparent growth media, such as LB [1]. They have demonstrated that blue light illumination causes tumbling response in respiring *E. coli*, and indentified two receptors essential for the response. I will describe what is known about *E. coli* phototaxis in more details in the Chapter 4.1.

1.2.3 Why study phototaxis: goals and motivation of the project

There were several reasons behind choosing *E. coli* phototaxis as the subject of my thesis work. First of all, the phenomenon of light-induced motility changes in non-phototrophic organisms is intriguing on its own and has not received much attention. As discussed above, there have been only a handful of studies on its phototactic response, and the mechanism of photosensing in *E. coli* is unclear [1, 58, 69, 70]. Secondly, whether or not phototaxis in *E. coli* has an adaptive value for the bacteria or is only an artifact, light can be used as a tool. Downstream from the receptors, phototaxis is controlled by the same biochemical network as chemotaxis; therefore light can be used to perturb the network as an easy-to-use alternative to chemical stimulation. Light-induced changes in motility behavior suggest that light gradients can cause drift of the *E. coli* population and therefore light can potentially be used to control the distribution of bacteria. Finally, I was interested in studying the motility of bacterial populations in a realistic environment, for example in a landscape with sparse gradients of tactic stimuli. Experimental studies of chemotaxis in realistic gradients have been limited due to challenges associated with controlling the distribution of chemicals. Developments in the field of microfluidics made it possible to create precisely controlled temperature or chemical gradients [71, 72], however, no matter how ingenious the approach, chemical gradients are fundamentally limited by diffusion, which is why I was interested in using light as an easy-to-control, spatially and temporally resolved stimulus.

The reasons discussed above led to the formulation of several aims for my thesis work. My first goal was to develop a platform for studying phototaxis in bacteria, including the experimental setup and data-analysis tools. I will discuss the details of the experimental setup used for studying phototaxis at the population level in homogeneous illumination patterns in Chapter 2, and the automated workflow for data analysis in Chapter 3.

My second goal was quantitative characterization of *E. coli* phototaxis including quantifying the role of individual receptors and the power dependence of phototaxis response (Chapter 4), contribution of individual receptors to the response in multiple-receptor mutants (Chapter 5), effect of light on other processes in bacteria (Chapter 6), and role of environmental parameters (Chapter 7).

Finally in Chapter 8, I will show my preliminary data and discuss future projects that can build on the experimental and data analysis tools that I have developed: an experimental setup for creating heterogeneous illumination patterns, single-cell level phototaxis experiments, phototaxis in *R. sphaeroides* and light-induced migration in *E. coli* and *R. sphaeroides*.

Chapter 2

Experimental Methods

As I have discussed in the previous Chapter, in their natural habitat bacteria have to navigate gradients that might be very different from those encountered in lab conditions (1.1.2). However, experimental studies of chemotaxis on the population level in realistic gradients have been limited due to challenges associated with controlling the distribution of chemicals. Light, on the other hand, can be controlled with high spatial and temporal resolution, which makes light especially attractive to use as a complex external stimulus in bacterial studies. Therefore, one of the goals of my thesis project was to develop a platform for high-throughput time-resolved measurement of phototaxis behavior in bacteria including designing and building the instrument, troubleshooting protocols for culturing bacteria and preparing samples, and writing routines for automated analysis of the raw data. In this Chapter, I will first review chemotaxis behavioral assays, methods used to create chemical gradients for chemotaxis studies and experimental frameworks used to study phototaxis (section 2.1). In section 2.2 I will describe the instrumentation, then in section 2.3 I will discuss some of the consideration behind the choice of experimental conditions.

2.1 Background

2.1.1 Chemotaxis behavioral assays

In the pioneering experiments on tracking single bacteria in 3D, Howard Berg have shown that *E. coli* movement consists of two types of discrete motions: smooth translocations - runs, and erratic reorientations - tumbles (see also section 1.1.1) [73]. Later in experiments with bacteria tethered to the glass by their flagella, it was established that runs correspond to clockwise (CW) rotation of the flagellar bundle and therefore tumbles correspond to counterclockwise (CCW) rotation of the flagellar bundle [74, 75]. Both of these methods allow quantifying steady-state chemotaxis behavior or kinetics of chemotactic response to different chemicals either by identifying runs and tumbles in the bacterial trajectories or by detecting CW and CCW rotation of the bacterial body or flagella filament.

Advances in optics, electronics, and data analysis methods enabled development of sophisticated instru-

ments and assays that allow more accurate determination of motility states, observing bacteria for longer periods of time or tracking a larger number of bacteria at a time. The original tethered assay has essentially been 'inverted': now the bacterial body is immobilized on the slide and flagellar rotation is measured by tracking microbeads attached to flagella [33, 76]. Compared to the original tethered assay, in the inverted version flagella motors operate under low load, which better represents free-swimming behavior [77, 78].

The optical trap assay is another single-cell behavioral assay. Optical traps are used to immobilize a single *E. coli* bacterium by holding each end of the cello [79, 80]. Despite immobilization by the traps, cells display motile behavior, detected as oscillatory signals by the quadrant photodiodes. Regions of alternating oscillatory and non-oscillatory, or erratic, signals correspond to runs and tumbles of the cell, respectively [80, 81]. This method allows very accurate long-term characterization of bacterial motility behavior, which results from the integrated action of all flagellar motors.

Tracking assays have not changed conceptually since Berg's time, rather the major developments have been due to better microscopes and better tracking algorithms. Higher contrast and resolution of modern optical microscopes allows detecting bacteria within a larger field of view. And therefore it is possible to record long trajectories of individual bacteria without moving the optical stage [35, 36, 73, 82–84]. Novel algorithmic approaches have been developed to enable accurate tracking of bacteria in both in two [35, 36, 84] and in three dimensions [85, 86].

2.1.2 Chemotaxis in chemical gradients

The behavioral assays discussed above allow studying steady-state bacterial motility as well as chemotactic responses to chemical stimuli. The latter requires combining behavioral assays with tools that enable exposure of bacteria to chemical gradients in these assays. Over the past century the field of chemotaxis has come up with a variety of different experimental approaches that enable studying *E. coli* motility in the gradient of a chemical, some of which I will introduce below.

Tethered bacteria can be exposed to a chemical gradient using a micropipette filled with an attractant or a repellent [87]. A chemical is released from a micropipette resulting in diffusing chemical gradient, which can be treated as step-wise or as a pulse stimuli, depending on the amount of chemical [87]. Accurate quantification of the profile of chemical concentrations that bacteria experience, and how it changes in time, is complicated.

In the classic capillary assay developed by Adler *et al* the capillary with the compound of interest is inserted in a pond with bacterial culture (fig. 2.1a) [88]. Diffusion of a chemical from the capillary results in a gradient that bacteria respond to - move away or towards the opening of the capillary [88]. Chemotaxis

can be then quantified by the number of colonies grown from the bacteria that moved inside the capillary. The capillary assay is a quantitative and high-throughput method that allows characterization of chemotaxis response to a variety of different compounds, however, it offers no control over the resulting chemical gradient.

In another classic chemotaxis assay, the so-called swarm assay, bacteria swim through pores in semisolid agar and navigate gradients created by nutrient consumption [39]. The presence of chemotaxis is indicated by a chemotactic ring - a higher density front of expanding bacterial colony [39]. The swarm assay allows fast qualitative characterization of chemotaxis phenotype and has been used extensively to isolate chemotaxis mutants [39]. However, it is not purely a behavioral assay, as it requires consumption of the nutrient in addition to functional chemotaxis [39].

There are several examples of chemotaxis studies that make use of caged compounds [89–91] (fig. 2.1b). Caged compounds are light-sensitive probes that functionally encapsulate biomolecules in an inactive form [92]. An active molecule is liberated when exposed to light, usually in the UV range. Use of caged compounds allows more temporal and spatial control over resulting gradients. However, there are several disadvantages to this method: the number of readily available caged compounds is limited, accurate quantification of absolute concentrations of released chemical requires involved calibration procedures [93], UV light used for photolysis is damaging to bacteria, and, finally, after the light pulse, temporal development of the gradient is solely due to diffusion and therefore cannot be controlled experimentally.

Developments in the field of microfluidics made it possible to generate flow-free, steady gradients of arbitrary shape (fig. 2.1c) [71, 72]. Microfluidics have been widely used in the studies of chemotaxis and allowed to gain important insights that would have been hard if not impossible to obtain otherwise. For example, Kalinin *et al* used a microfluidic device to generate two opposing chemoattractant gradients and showed that *E. coli* relative response strength to Asp *versus* Ser depends on the ratio of corresponding chemoreceptor, which changes with bacterial culture density. However, our ability to create more complex, heterogeneous distributions similar to those that bacteria might encounter in nature is still limited. Creation of microfluidic devices requires expensive microfabrication facilities and changing the parameters of the gradient is usually not possible without redesigning the microfluidic device.

The optical trap assay makes use of the combination of optical trap with the microfluidic chamber [80] (fig. 2.1d). In this case, a gradient is formed by merging of fluid flows from different channels containing a different concentration of chemoeffectors. When a bacterium is moved between channels it experiences a temporal gradient. The shape of the gradient is determined by the convolution of the speed with which bacteria is moved and the actual gradient. This method allows one to expose bacteria to precisely controlled gradients of defined shapes, however, it is limited by a very low throughput.

In a state-of-the-art experiment, Stocker *et al.* took a step closer towards observing bacterial chemotaxis in realistic gradients. They model a marine particle by a sinking PDMS cylinder leaking dissolved organic matter and characterize accumulation of bacteria in the resulting nutrient plume [38] (fig. 2.1e).

Essentially all of the methods described above by definition are limited by diffusion and therefore allow little control over spatial and temporal characteristics of the gradients, which is why I wanted to use light as stimuli instead.

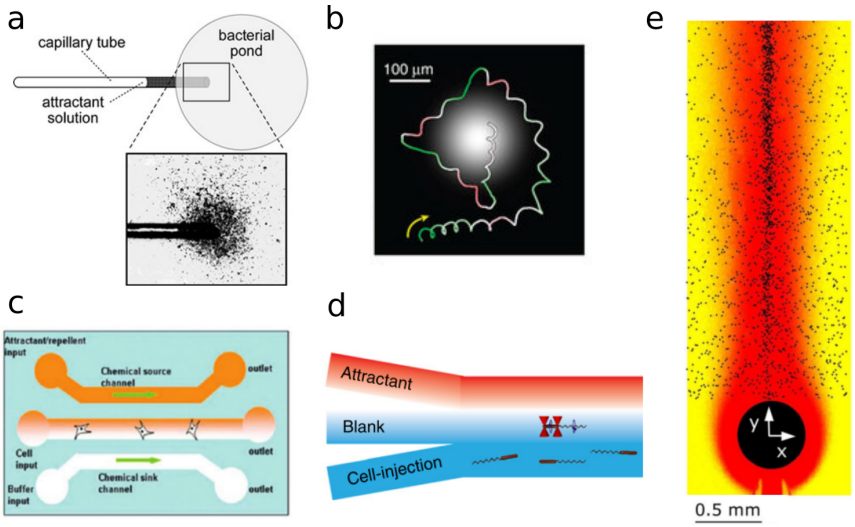

Figure 2.1: Methods used to create chemical gradients in the studies of chemotaxis. (a) In a capillary assay, gradients develop due to diffusion of a chemical from the capillary to the pond with bacteria (figure from `http://chemotaxis.biology.utah.edu/Parkinson_Lab/projects/ecolichemotaxis/ecolichemotaxis.html`) [88]. (b) A trajectory of the sea urchin sperm in a gradient of photolysed chemoattractant [91]. (c) Diffusion of chemicals from upper and lower channels through agarose allows creating stable linear gradients in the middle channel in the absence of the fluid flow [72]. (d) An optically trapped bacterium experiences the step-wise increase in the concentration of attractant as it is moved from the middle to upper channel of the microfluidic chamber [80]. (e) Marine bacteria *P. haloplanktis* accumulate in the nutrient plume created by the sinking particle [38].

2.1.3 Phototaxis

Phototaxis has received considerably less attention than chemotaxis and the range of experimental approaches is therefore more narrow. Different phototaxis assays are reviewed in [94] and can be classified depending on the type of motility employed by the organism under study as it dictates the choice of surface. For example, cyanobacteria move by gliding or twitching on surfaces and phototaxis in cyanobacteria has been studied by quantifying its motility on agar towards or away from the source of light [65, 67].

Phototaxis in Purple Nonsulfur bacteria *Rhodospirillum centenum* and *Rhodobacter sphaeroides* was studied in liquid culture by observing accumulation of bacteria in the light beam or by measuring light-

induced changes in motility patterns of a tethered bacterium [62, 63].

Finally Wright *et al* studied light response of swimming *E. coli* exposed to step-wise increase or decrease in light intensity. The response was quantified by analyzing bacterial trajectories and calculating average angular velocity or RCD (rate of change in direction) across multiple trajectories as a population measure of the *E. coli* phototactic response [1]. This approach allows temporally resolved and high-throughput measurements of the phototactic response and it served as a starting point for the experimental platform I have developed.

2.2 Instrumentation

General setup of the intrument

The schematic of the instrument is shown in figure 2.2a. The full list of the components used for this setup including optomechanics and electronics can be found in the appendix A. The setup is based on the inverted optical microscope. I use a 20x objective, which is suitable for the phase contrast regime, has high enough magnification to resolve individual bacteria and large field of view - 1150 μm in diameter (fig 2.2b). For observation, bacteria are illuminated from the top by a halogen lamp (fig 2.2a HAL lamp). Light from the lamp is heat filtered and passes through the phase contrast mask. As discussed in section 1.2.2 *E. coli* responds to light in the range 400-500 nm with the highest response amplitude at about 440 nm [1]. To exclude the possibility of cross-excitation of bacteria by observation light, the illumination beam from the lamp passes through the 500 nm long-pass filter (fig 2.2a 500 nm LP). The power density of the illumination light measured by the power meter placed roughly at the level of microscope stage varied from 0.7 to 5 mW/cm^2, which is significantly lower than power density I used for stimulation.

Excitation light from the blue LED (fig 2.2a LED) is introduced from the back port. The camera is attached to the side port by the dual side port adaptor. The dual side adaptor has the relay optics that extends the infinity space from the existing side port on the microscope stand out to the dual remote ports to allow the formation of the image 60 mm from the end of the port. The dichroic or mirror in the slider of the dual adaptor splits the image plane and allows one to introduce an additional light source. The motivation behind using the dual adaptor was to enable patterned light applications which will be discussed in more details in one of the later Chapters (8.2.2). For all of the experiments discussed in this work, we used the silver mirror (fig 2.2a M2) in the slider position to project the field of view on the camera chip.

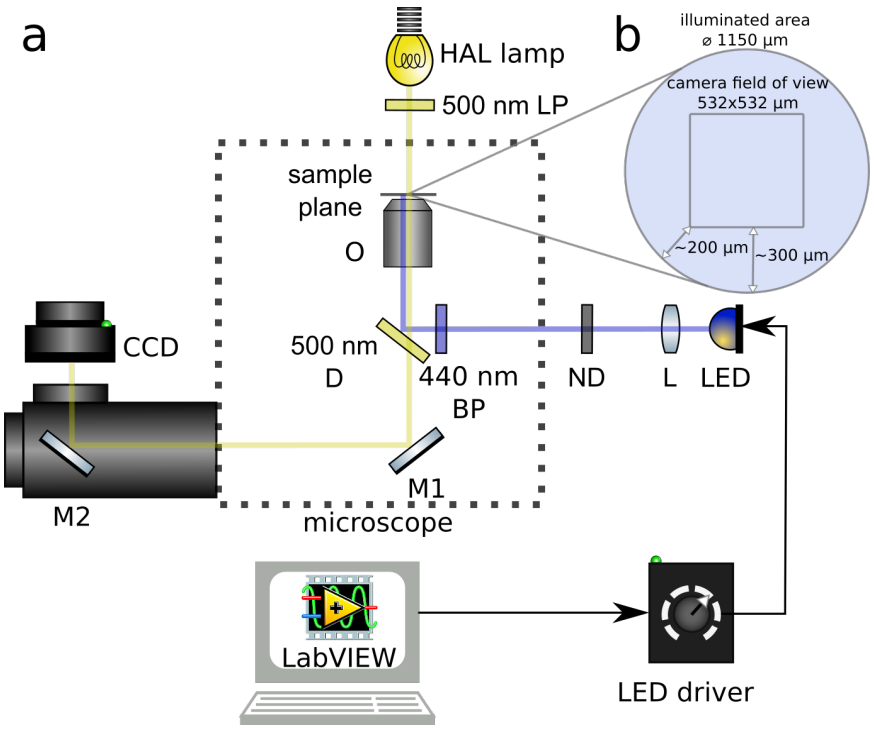

Figure 2.2: Experimental setup. (a) Schematic of the setup with the light paths indicated by yellow (wide-range visible light from HAL lamp) and blue (blue LED) lines. Components are labeled as follows: LP - long-pass filter, O - 20x objective, D - dichroic, BP - bandpass filter, ND - neutral density filter, L - collimating lens, LED - light emitting diode, M1, M2 - fully reflective mirrors, CCD - Charge-Coupled Device Camera. (b) Area captured by camera compared to the total illumination area equal to the objective's field of view. Minimal and maximal distances that unexposed bacteria need to swim to reach the observation area are shown.

Excitation light source

Excitation light from a blue LED is introduced through the back port of the microscope (2.2a LED). The blue LED with a collimation assembly was mounted using a backport adaptor. Excitation light passes through a $440 \pm 5nm$ bandpass filter (2.3a BP) and is directed towards the field of view by 500 nm dichroic mirror (2.3a D). As discussed in section 1.2.2 this bandwidth corresponds to the maximum amplitude of the phototaxis response in *E. coli* according to previous work [1].

To achieve even illumination of the field of view we followed the standard procedure to set up Koehler illumination. The first luminous field stop and aperture irises were centered by placing them in the luminous field stop slot and adjusting them so they were visible in the field of view. The aperture stop was fully open and the field diaphragm was closed so that its edges appeared in the field of view. The distances between the LED and collimation lens, and between the LED assembly and microscope backport, were varied to bring the field diaphragm in focus. Then, the field diaphragm was opened so that its edges just disappeared from the field of view and therefore the illumination area was equal to the objective field of view (2.2b).

Output light intensity of the LED is determined by the current from the LED driver (2.2a LED driver) which is controlled by the modulating voltage supplied by the DAQ card and defined using a LabView interface. Neutral density filters of ND 1.0 and ND 0.5 were installed in the filter slider (2.2a ND) to have finer control over the resulting light intensity. Light intensity at the sample plane as a function of driving voltage for both ND filters at different modulating voltages was measured using a power meter placed on the microscope stage. To calculate light intensity, total power was divided by the total illuminated area, equal to the objective field of view (2.3b). The error bars correspond to 10% deviation from the measured power (see fig. 2.5 and corresponding discussion).

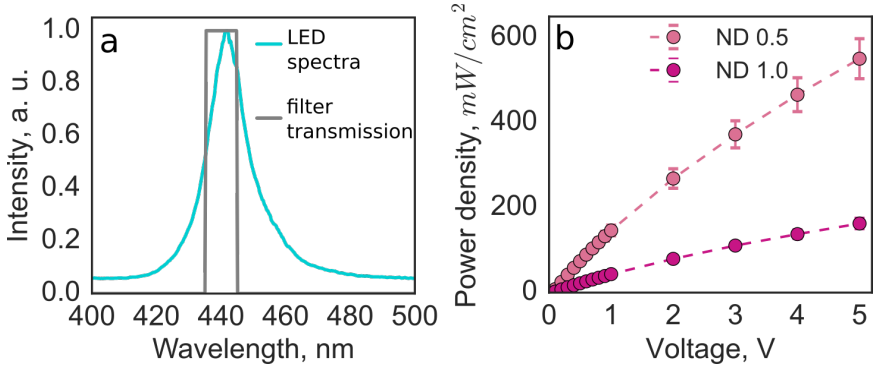

Figure 2.3: Excitation light characterization. (a) Excitation light spectrum with overlayed bandpass filter transmission. (b) Power density of the blue light in the sample plane versus modulating voltage. Measurement was performed with neutral density filters ND 1.0 and ND 0.5.

Camera

We used a CCD camera mounted at the microscope side port to record movies of swimming bacteria. The criteria for choosing a camera were sensor size, resolution (number of pixels), and frame rate. The first camera I used from ImagingSource had the chip size of 4.5x2.8 mm so it only allowed us to capture a small fraction of the field of view (23 mm in diameter in the image plane), and therefore the number and duration of bacterial trajectories were limited. The resolution was too low (744x480 pixels), to allow enlarging a captured image by a relay lens. So I switched to a camera from PointGrey, which had the largest available sensor size at that moment (11.3x11.3 mm) so we were able to image a larger fraction of the field of view and capture more bacterial tracks. The camera also has high enough resolution to resolve individual bacteria (2048x2048 pixels) with individual pixel size $5.5\mu m$. The pixel size in the sample plane can be estimated as pixel size in the image plane divided by the objective resolution, which gives us about 0.27 μm per pixel. That means that a typical 1x0.5 μm bacteria will occupy $\sim$ 10 pixels, which should be more than enough. Camera calibration using USAF target 1951 gave us an estimate of the pixel size of about 0.26 μm, which

is close to what we expected from the calculation (2.4). This estimate is used for all further image analysis. The size of the observation area in the sample plane was 532x532 μm (see 2.2b for comparison between camera field of view and total illuminated area). Importantly, the illuminated area is still larger than the observation area captured by the camera, so the fraction of bacteria that would be swimming in from outside of the illuminated area is small (see section 3.3 for more detailed discussion).

As long as the camera is not saturated we can estimate the evenness of the blue light illumination in the sample plane from the focused image measured by the camera (2.5b). Indeed, we have shown that pixel intensity averaged over all of the pixels in a frame changes linearly with light intensity measured in the sample plane (2.5a). From the background-subtracted image, we estimate that standard deviation of the normalized pixel brightness distribution is about 10% of the mean. We use that as our error for determining light power density in the sample plane (2.3b).

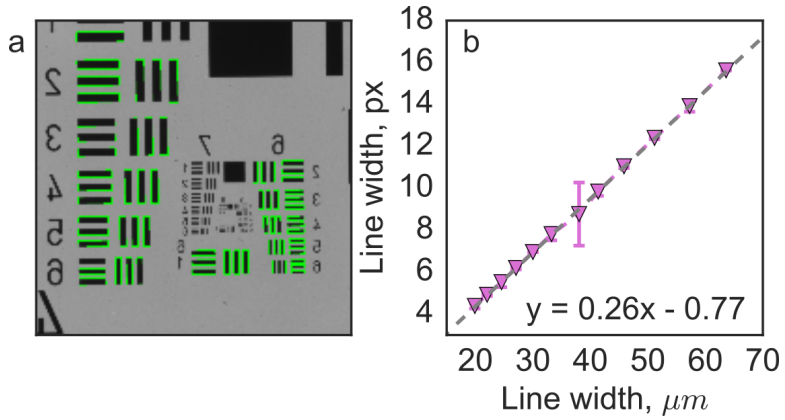

Figure 2.4: Camera calibration. (a) Image of the USAF target 1951 taken with the camera at 20x magnification, detected lines from groups 5 and 6 are shown with green outline. (b) Line width in pixels versus line width in microns, line slope gives size of the camera pixel in the sample plane

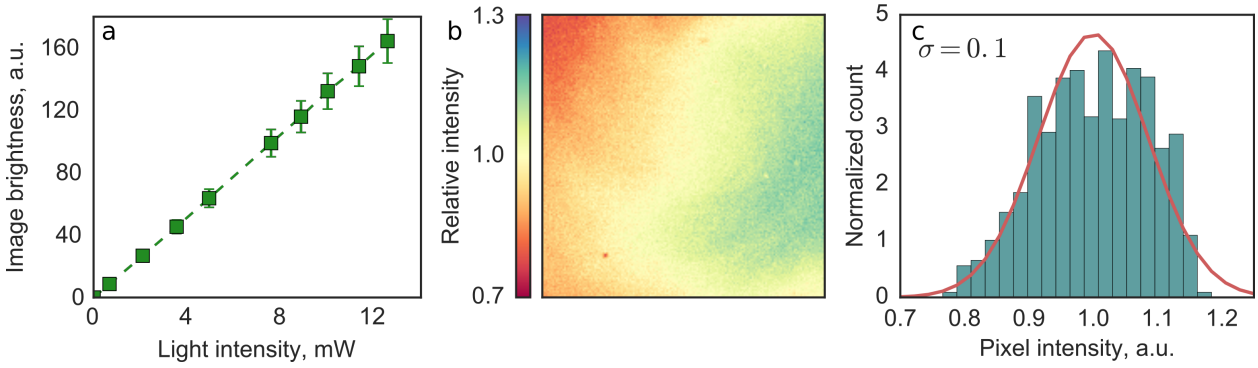

Figure 2.5: Estimating unevenness of the illumination profile. (a) Image brightness is linearly proportional to the intensity of the excitation light. (b) Illumination profile. (c) Distribution of the normalized pixel brightness. Standard deviation is shown.

2.3 Experimental conditions

The protocols for growing and preparing bacteria as well as assembling the experimental chamber can be found in Appendix C. In this section, I will discuss some of the consideration behind the experimental procedures.

Growing and preparing bacteria

According to earlier experiments, exposure to blue light caused paralysis in swimming *E. coli* and *S. typhimurium* bacteria [69]. However Wright *et al.* have shown that paralysis was due to flavin dyes contained in non-transparent growth media such as Luria-Bertani Broth (LB) was not observed in transparent motility buffer [1]. I performed initial experiments with bacteria grown in Tryptone Broth (TB). TB is less nutritious media than LB so it supports the growth of motile bacteria. Similar to LB, TB appears yellow, which indicates the presence of dyes, although the color is less intense compared to LB. Bacteria were washed and resuspended in transparent motility buffer prior to the experiments to minimize the potential effect of dyes. I did not observe paralysis. However, I did observe a decrease in swimming velocity. Eventually, I decided to switch to M9 minimal growth media, as it would have been impossible to confirm that there is no growth media left in the final suspension and that some of the observed trends were not in fact caused by interaction with excited leftover dyes.

Another reason for using the media with defined composition was the potential coupling between the mode of metabolism and light response. Taylor *et al.* have shown that phototaxis requires a functioning electron transport chain and therefore can only be observed in anaerobically or aerobically respiring bacteria [58]. Therefore, I wanted to have bacteria with a defined mode of metabolism, which can only be controlled by providing a specific growth substrate. TB, on the other hand, is media of undefined composition and can support both aerobic and anaerobic respiration as well as fermentation. I used succinate as a growth substrate in the M9 media as it is non-fermentable and can support only respiration [95]. For some of the experiments, I used glycerol similarly to Wright *et al* [1]. Motility buffer contained succinate as a carbon source and I have found that using lactate or glycerol instead does not affect the results.

Experimental chamber

Wright *et al.* have used a bridged coverslip chamber where a quartz coverslip was positioned over two standard glass coverslips lying on top of the glass slide [1]. Coverslips were used as spacers in this case and defined the thickness of the chamber - 170 μm. This is much larger than the depth of focus of an objective, so bacteria can swim in and out of focus, and analysis requires three-dimensional tracking. I wanted to limit

the path length of the chamber so it is comparable with objective's depth of focus, which would effectively confine bacteria in two dimensions, allowing for easier tracking of individual bacteria as well as for measuring a change in the density of bacteria over time in response to light.

The 20x objective that I used has a depth of focus equal to 5.8 μm which defines the approximate path length of the experimental chamber. I tried several options: glass capillaries, PDMS chamber, slide-coverslip chambers with double-sided tape as a spacer and slide-coverslip chamber sealed with epoxy. VitroCom offers capillaries of different dimensions including ones with a path length of 10 μm. All bacteria inside these appeared in focus. The problem is that width-to-path length ratio cannot be larger than 10 to prevent the collapse of the middle of the capillary during fabrication. So capillaries with 10 μm path length were only 100 μm wide, so I was only able to use the small fraction of the field of view.

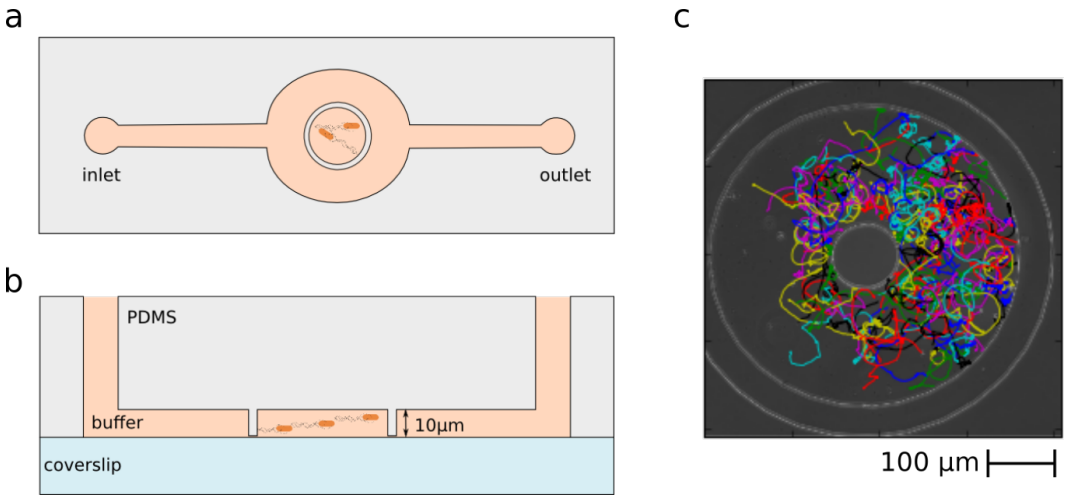

Figure 2.6: Microfluidic chamber design from Jordan et al. (a) Top view, (b) side view, (c) microphotograph of the central part of the chamber with overlayed bacterial trajectories. Scale bar corresponds to 100 μm

I also tried using PDMS (polydimethylsiloxane) chambers, with a design adapted from [96]. The schematic representation of the chamber with top and side views is shown on fig. 2.6. The PDMS chambers are made by pouring the mixture of defined ratio of the curing agent to the silicone elastomer base on the silicon wafer mold. The path length of the chamber is defined by the height of the features on the mold and can be accurately controlled during the fabrication of the wafer. The PDMS chambers can be covalently bound to the glass after plasma cleaning [71, 97]. The central ring of the chamber shown in fig. 2.6 is masked during the plasma bonding step and therefore does not bind to the coverslip. Therefore, when we push the media through the chamber this ring is lifted under the pressure and allows bacteria to flow inside. When the flow stops, the ring touches the coverslip so the bacteria are now trapped inside the ring, which creates an additional advantage of bacteria being confined to the field of view. Detected bacterial trajectories overlayed

on top of the microphotograph of the ring are shown in fig. 2.6. PDMS is also oxygen-permeable, although its permeability is affected both by plasma treating and exposure to Bovine Serum Albumin (BSA), which I use to prevent bacteria sticking to the surface [98]. Nutrients can be supplied by slowly flowing media through the channel, which should not affect the bacteria inside the central ring. Therefore, bacteria can be observed for longer periods of time as they do not exhaust nutrients or oxygen. Overall, PDMS chambers suited my purposes very well and probably should be adapted for future experiments with patterned illumination. However, the amount of effort required for fabrication of silicone molds and individual chambers made it impractical to use PDMS chambers for the short-term experiments on bacterial response to step-up increase or decrease in light intensity, which is what I have mainly focused on in this work.

I tried using several variations of the glass chamber formed by a slide and a coverslip with spacers in between, including double-sided tape and thin aluminum foil. The problem with both of these methods was 'trapped' air bubbles at the interface between the spacer and liquid, which I wanted to avoid as much as possible to observe the effect of light decoupled from other environmental parameters, such as oxygen concentration.

Eventually, for the majority of my experiments, I used a slide-coverslip chamber without spacers, where the path length was defined by the thickness of the liquid layer. To prevent bacteria sticking, slides and coverslips were precleaned in acetone and KOH and passivated with BSA [99]. The chamber was sealed with epoxy to prevent drying and drift and therefore did not allow the flow of oxygen. However dissolved oxygen in the buffer can support bacterial respiration for some time. Succinate, which I use as a carbon source in the motility buffer, does not support fermentation, so when the oxygen is exhausted - usually within half an hour - bacteria slow down and stop swimming, which means that I can use swimming velocity and/or tumble bias to monitor the 'energy state' of bacteria. As you can see in figure 2.7a and b, both swimming velocity and tumble bias stay approximately constant within the first 30-35 min after chamber assembly, which is what I used as a cutoff for the duration of one experiment.

I also used the oxygen indicator Resazurin to quantify bacterial oxygen consumption in a sealed reservoir. As bacteria consume oxygen, Resazurin is reduced, which can be monitored by absorbance at 610 nm or by the change in color [100–102]. I measured the absorbance of a suspension of *E. coli* bacteria grown in TB or minimal media and resuspended in motility buffer with $100\mu g/ml$ Resazurin in a sealed spectrophotometer cuvette (fig. 2.7c). As you can see, it takes about 3 hours for the absorbance to stop changing when bacteria are grown in minimal media, which means that at least within this time bacteria are respiring dissolved oxygen. This observation further supports the feasibility of using sealed chambers as long as bacteria stay normally motile within the duration of the experiment.

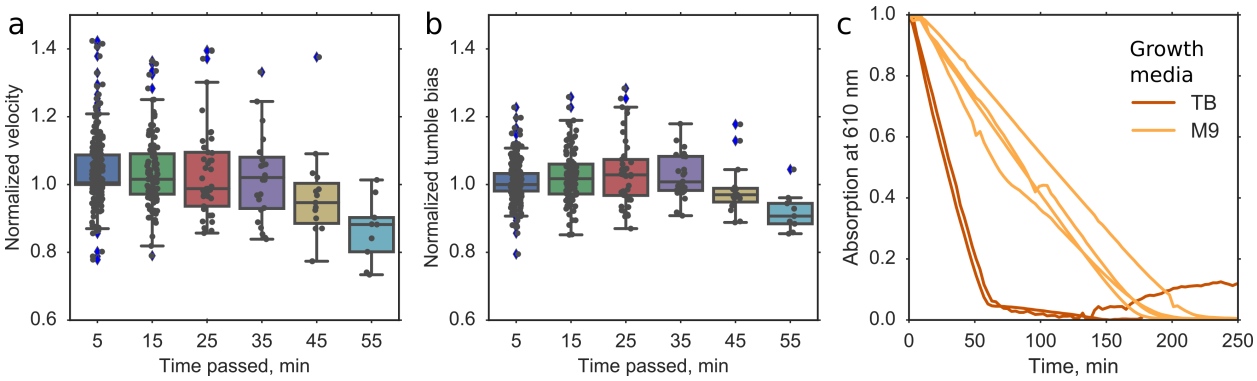

Figure 2.7: Characterizing bacteria 'energy state' in a sealed reservoir. (a) Normalized swimming velocity as a function of time passed after chamber assembly. Each point corresponds to velocity averaged over one movie. Velocity is normalized to the average velocity of the first movie recorded in the chamber. (b) Normalized tumble bias as a function of time passed after chamber assembly. (c) Resazurin absorption at 610 nm changes as a function of time as *E. coli* bacteria grown in M9 minimal media (light orange) or TB (dark orange) consume oxygen in a sealed reservoir.

Video recording parameters

I used the change in average intensity of the movie frame as an indicator of the light turning on or off. It is possible because a small fraction of incident blue light gets reflected from the glass surface in the sample plane towards the camera chip. So, I set the exposure time such that light turn on results in a noticeable but small change of the overall intensity to minimize the change in signal to background ratio (fig. 2.8). At the maximum light intensity that I used, 550 mW/cm^2, exposure time was set to 2.5 ms and was increased for lower light intensities.

The frame rate should be high enough so that individual tumbles can be resolved and that frame-to-frame displacement of bacteria is much smaller than a pair-wise distance between bacteria at the current density. According to literature, average tumble time from bundle breaking to bundle consolidation is $0.4 \pm 0.2\,s$ [103]. From our trap data, I got $0.9 \pm 0.8\,s$ with the majority of tumbles above $0.2\,s$ as shown by cumulative distribution in the fig. 2.9. Based on that, I used the framerate of 12 frames per second for all of my experiments.

At this frame rate and a typical density of bacteria, the majority of bacteria ($OD_{600nm} = 0.15$) are further apart than average frame-to-frame displacement $< r >$ (fig. 2.10a and b). And on average 10% of bacteria are closer to each other than $2 < r >$, which is reasonable, although will cause some problems with correct linking of coordinates into trajectories (fig. 2.10c). Please refer to section 3.3 for discussion of the density effect on the trajectory mislinking.

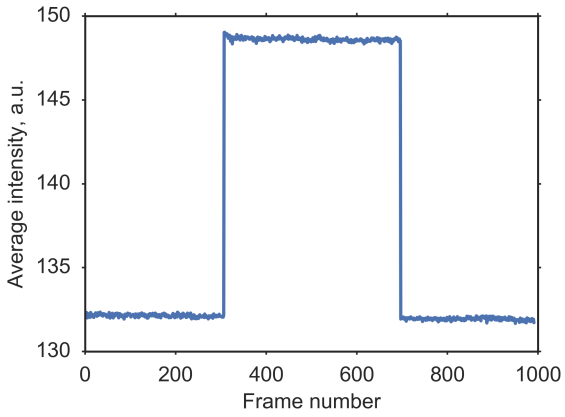

Figure 2.8: Frame intensity averaged over all pixels as a function of frame number within one movie. Light intensity in the sample plane was 500 mW/cm^2. Light exposure is clearly indicated by step-wise increase in the intensity.

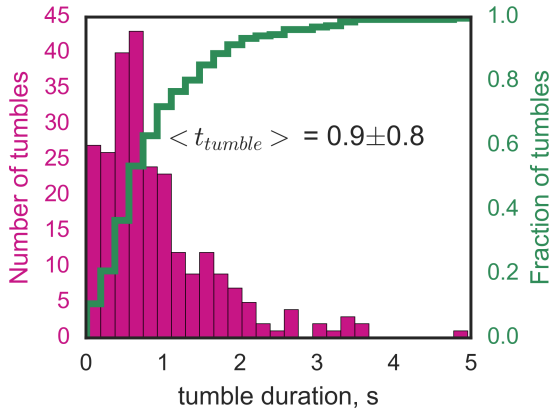

Figure 2.9: Distribution of tumble times from the trap data with cumulative normalized distribution shown in green

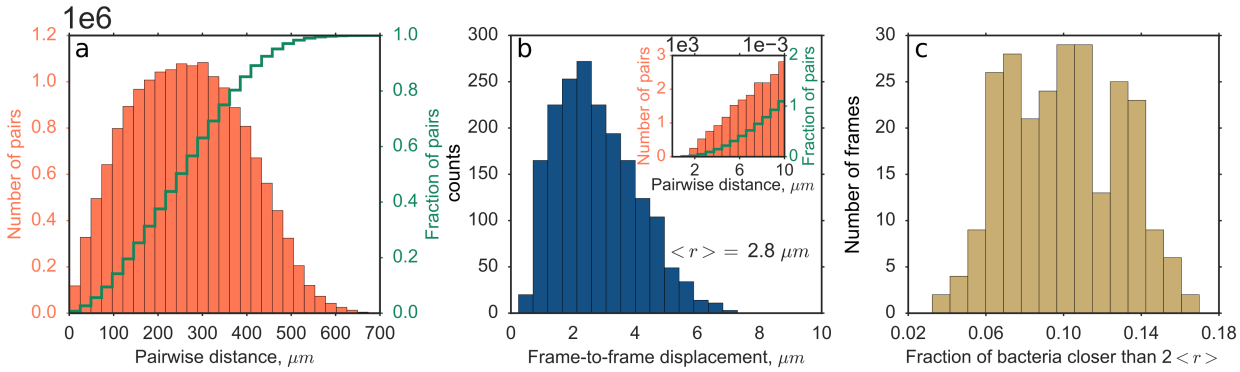

Figure 2.10: Pairwise distance *versus* frame-to-frame displacement of bacteria. (a) Distribution of pairwise distances in each frame of the movies with a typical density of bacteria with cumulative normalized distribution shown in green. (b) Distribution of frame to frame displacement r, $< r >= 2.8\mu m$. Inset - the tail of the pairwise distance distribution corresponding to lower values. (c) Distribution of the fraction of bacteria that were closer than $2 < r >$ in each frame of one movie.

Chapter 3

Data analysis

In this Chapter, I will first discuss algorithmic methods developed over the years to quantify bacterial chemotaxis at both the single-cell and population level in different behavioral assays (3.1). I will then introduce the automated framework that I have developed (3.2). Finally in section 3.3 I will discuss potential sources of error.

3.1 Background

3.1.1 Quantitative measures of chemotaxis

Specific approaches to data analysis are dictated by the type of data obtained in an experiment. Chemotaxis assays discussed in Chapter 2.1 can be classified by the type of data they provide - single-motor *versus* single-cell level bevavior. The natural quantitative outcome of the tethered assay is the CW bias: the fraction of time that the motor spends rotating CW - $\tau_{CW}/(\tau_{CW} + \tau_{CCW})$ [52, 74]. Bacterial behavior in trap experiments can be characterized by the tumble bias, the fraction of time bacteria spend tumbling - $\tau_{tumble}/(\tau_{tumble} + \tau_{run})$.

The path from 2D or 3D bacterial trajectories to tumble bias is less straightforward, however. Uri Alon *et al.* have developed criteria for assigning runs and tumbles based on instantaneous swimming and angular velocities [82]. These criteria are based on the empirical observation that tumbles corresponds to periods of slow swimming and fast reorientation and, therefore, high angular velocity or RCD (rate of change in direction). A tumble is detected when the swimming speed is below the threshold value and the angular velocity is above the threshold value. The threshold value for swimming velocity was defined as $v_{run}/2$, where the running speed v_{run} is an average of the top 10% of the velocities for each bacterial trajectory. Threshold values for angular velocity were set to $3\,rad/s$. It was shown that threshold values can be changed considerably without significantly affecting the tumble assignment [82]. However, motile behavior can be more complex than the binary logic of runs and tumbles: this analysis would not be robust to variations in running speed within one trajectory, which was demonstrated in experiments with optically trapped bacteria

[80].

Shahid Khan *et al* have shown that RCD can be used as a temporally resolved, high-throughput population measure of run-tumble bias for the analysis of chemotactic responses [89, 90]. It is unbiased in the sense that it does not depend on the choice of threshold values. The absolute values of RCD are non-meaningful however and therefore do not allow direct comparison between experiments: even bacteria with zero tumble bias might have high RCD values due to hydrodynamic interaction with the glass surface that results in circular trajectories (3.1) [104, 105].

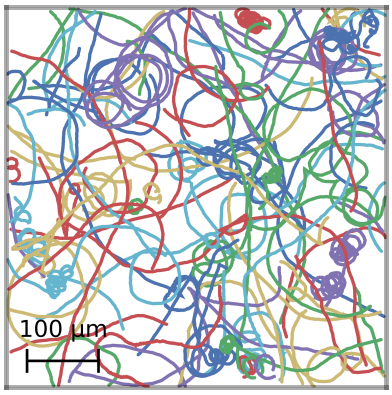

Figure 3.1: Circular trajectories of a running *E. coli* mutant CR20 with non-functional CheY, scale bar represents 100 μm.

Finally, Yann Dufour *et al.* have developed tumble detection analysis that is robust to variation in bacterial velocity [36]. Bacteria are assumed to be in one of the three states - run, tumble or intermediate state recovering from a tumble. Each state corresponds to a certain distribution of motility parameters - velocity, acceleration and angular acceleration. Distributions of motility parameters for each state are determined by fitting a tri-variate Gaussian mixture model to the pooled distributions of velocity, acceleration, and angular acceleration. Rather than relying on rigid threshold values, in this approach, each motility state is represented by a tri-variate Gaussian distribution of motility parameters.

After testing Alon's criteria and using RCD to characterize the response of bacteria to light, I finally adopted a procedure similar to the one described by Dufour *et al.* In section 3.3 I compare different methods of analysis and show that my results are robust to the analytical method used.

3.2 Data analysis workflow

I have developed an automated workflow implemented in Python to extract and analyze trajectories of individual bacteria from the raw data, consisting of movies of swimming bacteria. The scheme of the

analysis is shown in fig. 3.2. We start by detecting bacterial coordinates in each frame; the coordinates are then linked into trajectories. I calculate the instantaneous parameters of the trajectories, velocities, accelerations, angular velocities and angular accelerations; remove spurious trajectories; and assign run and tumble states. Tumble bias is calculated in a moving time window for all the trajectories in a movie, and then averaged across several movies, again in a moving window. In the following section, I will describe the process in more details. Also see Appendix A.3 for functions and their parameters.

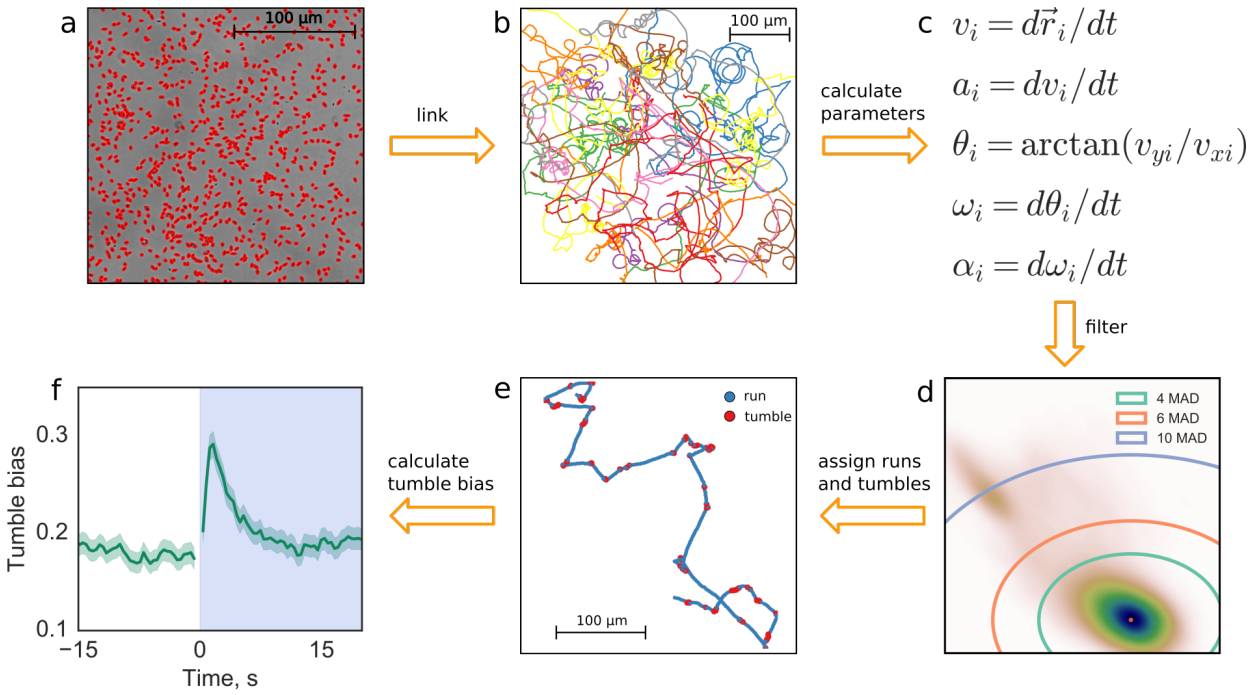

Figure 3.2: Data analysis workflow

3.2.1 Detecting bacteria, linking trajectories and calculating motility parameters

We detect bacteria in each frame of a movie using the `openCV` computer vision library [106]. Frames, when the light has been turned on or off, are detected by a change in the mean intensity of the frame (see fig. 2.8). Backgrounds that correspond to two illumination conditions are obtained by weighted accumulation of ~ 300 frames before and after the light is turned on. Each movie frame is background-subtracted and converted to binary format, at which point bacteria can be detected as connected white pixels on the black background.

Coordinates are linked into trajectories using the Python package `trackPy` [107]. The basic idea is that for each particle or bacteria in ith frame the algorithm looks for its counterpart in $i+1$th frame. For N

particles, this means evaluating $N!$ sets of pairs of bacteria and choosing the best configuration, the one in which the largest number of bacteria have a suitable pair. This problem becomes computationally expensive for a large number of particles. To limit the number of candidates, `trackPy` restricts its search to a region of a defined radius supplied by the user: the search range, centered on the particle position. I set the search range, which ideally should be larger than the maximum distance that bacteria can travel between frames, to $45/(framerate * pixel\ size)$ pixels, which corresponds to the tail of velocity distribution (fig. 3.5a). I also allow for the possibility that bacteria might be missed for 1 frame, perhaps due to noise in the video, and then seen again. See section A.3 for more details.

Finally, instantaneous velocities, accelerations, angular velocities, and accelerations are calculated using a 1-frame window [36].

3.2.2 Filtering trajectories

Despite passivation of the glass prior to the experiment, a significant fraction of bacteria (10-30%) end up stuck or tethered to the glass. They continue to rotate, and as a result background subtraction does not eliminate them. There are also bacteria that are drifting rather than swimming. Trajectories that belong to stuck or drifting bacteria decrease signal-to-noise ratio, as their run-tumble statistics are not meaningful. I have developed the following procedure to filter such spurious trajectories. For every trajectory, I calculate the average angular velocity and the 95th percentile of the velocity. The resulting two-dimensional distribution of trajectories in these coordinates contains two clusters: one corresponds to normally swimming bacteria, while the other contains trajectories of very slow or stuck bacteria (fig. 3.3a, b). For each bacterial strain I have used, I find the coordinates of the maximum of the 'swimming' cluster - the most probable values of angular velocity and the 95th percentile of velocity, - and keep only the trajectories that lie within a radius R from the maximum of the distribution. With the exception of a few strains, I define R as $R = 4 < MAD >$, where $< MAD >$ is median absolute deviation (MAD) from the maximum of the distribution averaged across all strains with a functional chemotaxis network (fig. 3.3). Most likely values of the 95th percentile of velocity and angular velocity with corresponding values of MAD as error bars for different strains grown in M9 minimal media with succinate are shown on the fig. 3.4. Note that filtering does not affect trajectories of the bacteria that are exposed to light disproportionately: the fraction of trajectories within $4 < MAD >$ for bacteria before, during and after light exposure is roughly the same.

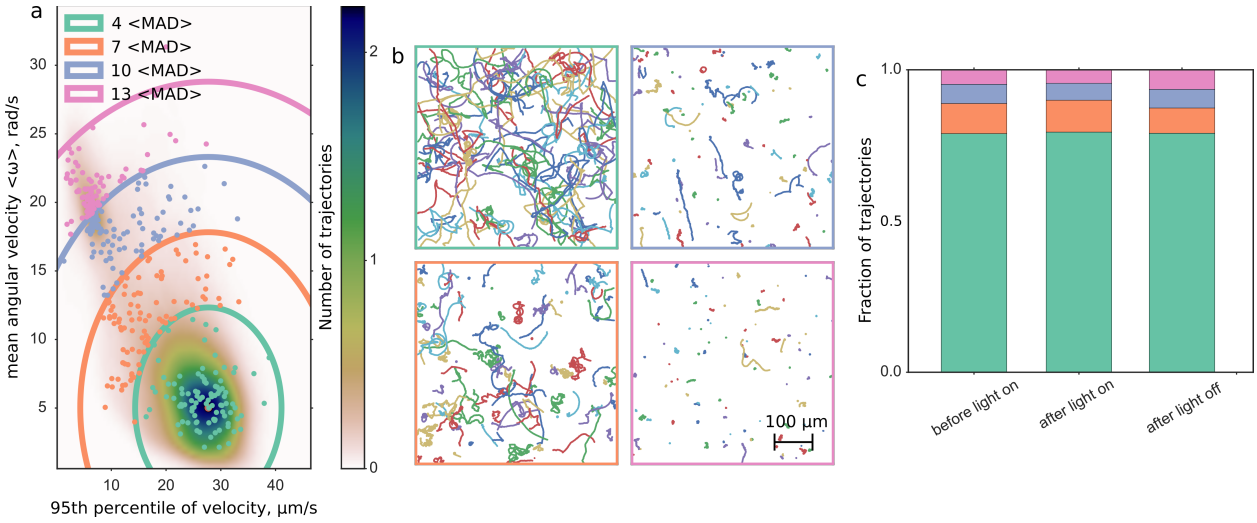

Figure 3.3: Filtering spurious trajectories, data for wild-type RP437 strain. (a) Two-dimensional distribution of trajectories in the coordinates of the 95th percentile of velocity and mean angular velocity. Trajectories outside the green circle with radius $4 < MAD >$ are removed from further analysis. Dots indicate randomly selected trajectories shown in panel (b). (b) Each square contains 100 randomly selected trajectories from within each circular layer on the panel (a), the color of the border indicate which circle trajectories come from on the panel (a). (c) Fraction of trajectories below $4 < MAD >$ and above $4 < MAD >$ as indicated by the color before during and after light exposure.

3.2.3 Assigning runs and tumbles

As I have already mentioned above (3.1), to assign run and tumble states we use a procedure similar to the one described by Dufour *et al* [36]. We use Hidden Markov Model (HMM) with Gaussian emissions, implemented in the Python package `hmmlearn`, to infer the sequence of the hidden states from the sequence of the observable parameters - velocity, acceleration and angular acceleration [108]. Parameters of the model - the transition probability matrix and the emission probabilities of the observables - are estimated from a reference dataset: more than 20 000 pre-stimulus trajectories of the wild-type *E. coli* bacteria. Training is done iteratively. At each iteration velocities and accelerations are normalized by average swimming velocity (the 95th percentile of the velocity is used on the first iteration), model parameters are estimated from the resulting sequence of observables, and optimal sequence of the states is inferred. The process is repeated until the change in normalized velocity between two consecutive iterations is below 2%, which usually takes 3-5 iterations. To account for the variation in swimming velocity within one trajectory we used a three-state model - fast run, slow run and tumble. Running velocity at each iteration was calculated from states corresponding to a 'fast run'. The resulting distributions of parameters for each motility state is shown on fig. 3.5. Note that I only use 'slow run' state at the assignment stage: for all the further analysis I consider 'slow runs' as 'run' states (3.6a-c).

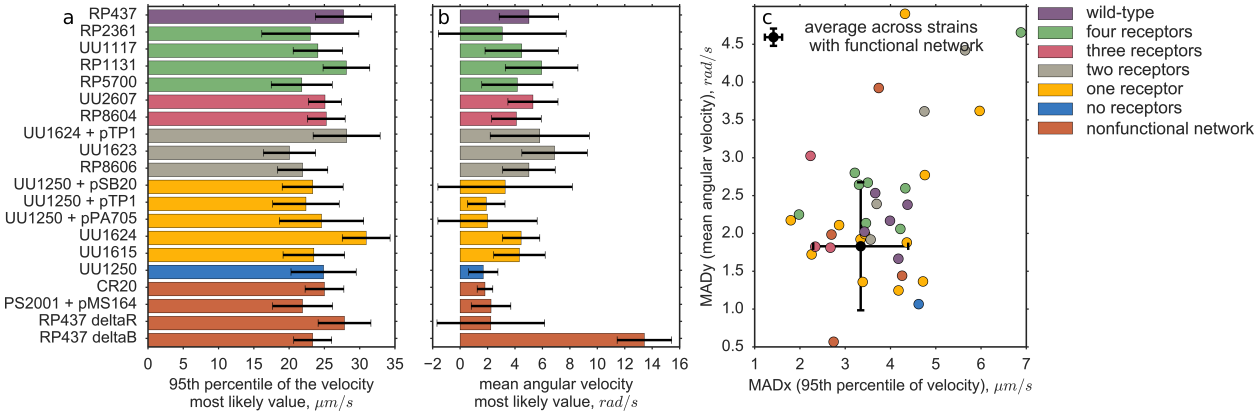

Figure 3.4: Distrubution of the trajectory parameters across different *E. coli* strains, strains are grouped by the number of receptors or by functionality of the network. (a) Most likely value of 95th percentile of velocity for different strains, errorbars represent median absolute deviations from the most likely value (MADx). (b) Most likely value of mean angular velocity (MADy). (c) MADy vs MADx for different strains, average values used for filtering are shown in black.

I wanted to compare the HMM method to Alon's criteria for tumble assignment (see section 3.1), according to which a bacterium is considered to be tumbling if its velocity is below threshold values and its angular velocity is above the threshold [82]. The velocity threshold for each trajectory was defined as the 95th percentile of velocities divided by two. The angular velocity threshold was set to 5 radians per s. The resulting distributions are shown on fig. 3.6d and e. As you can see, the main difference is that Alon's method finds significantly fewer tumbles than the HMM method. If we compare tumble assignment for a specific trajectory, it turns out that both methods largely agree on the location of the tumble, with the HMM method locating more 'tumbling' frames (fig. 3.7). So both methods give consistent results, and, as I will show in section 3.3, the choice of method does not affect the trends we observe: light-induced changes in motility.

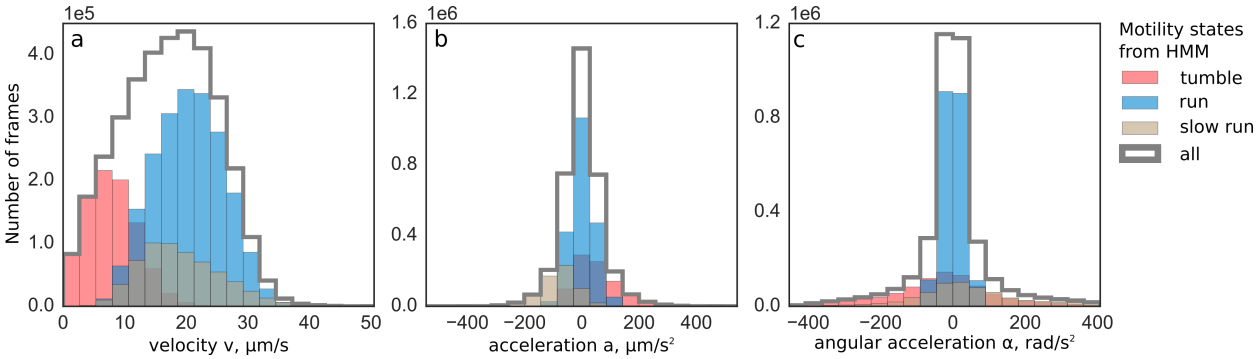

Figure 3.5: Distrubutions of the trajectories' parameters depending on the bacteril motility state: red - during tumble, blue - during run, grey - during slow run

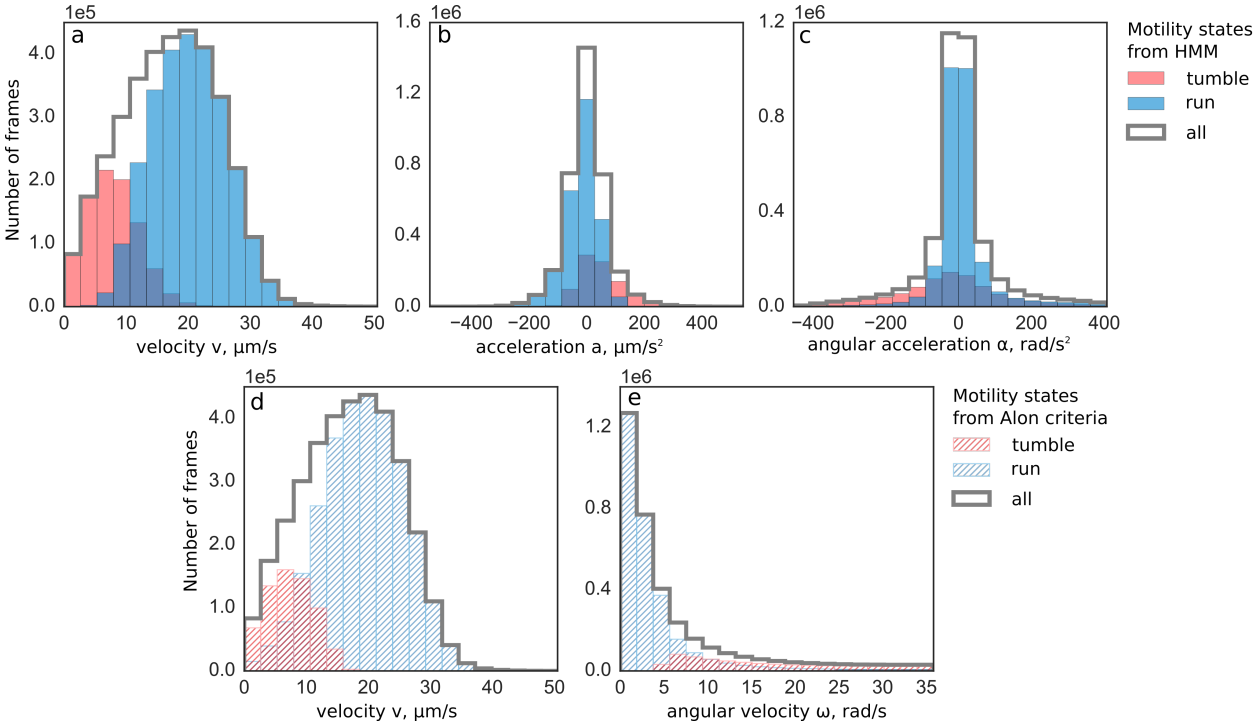

Figure 3.6: Distrubutions of the trajectories' parameters depending on the bacterial motility state: red - during tumble, blue - during run

3.3 Analysis of errors

In this section I will discuss several factors that contribute to the measurement errors in the analysis of bacterial trajectories.

3.3.1 Bacteria swimming in and out of the field of view

The area accessible to bacteria in the slide-coverslip chamber that I use for experiments (section 2.3) is much larger than the field of view. Consequently, 'unexposed' bacteria swimming from outside of the area illuminated by blue light might swim into the field of view, and affect the observed kinetics of the adaptation to light turn off and light turn on. However, as discussed in section 2.2, the illuminated area is still larger than the observation area captured by the camera and bacteria have to swim 200 - 300 μm to reach the field of view (2.2b). To estimate on what timescale these bacteria might contribute to the observed kinetics, I calculated the Mean Square Displacement (MSD) for trajectories of the wild-type *E. coli* (strain RP437) as a function of time (fig. 3.8). As expected, *E. coli* motility is super-diffusive, rather than diffusive as indicated by power-law exponent greater than 1 [23]. From the power law fit, I can estimate that it will take bacteria 30 - 50 s to reach the field of view from outside the illuminated area, although the time will vary for

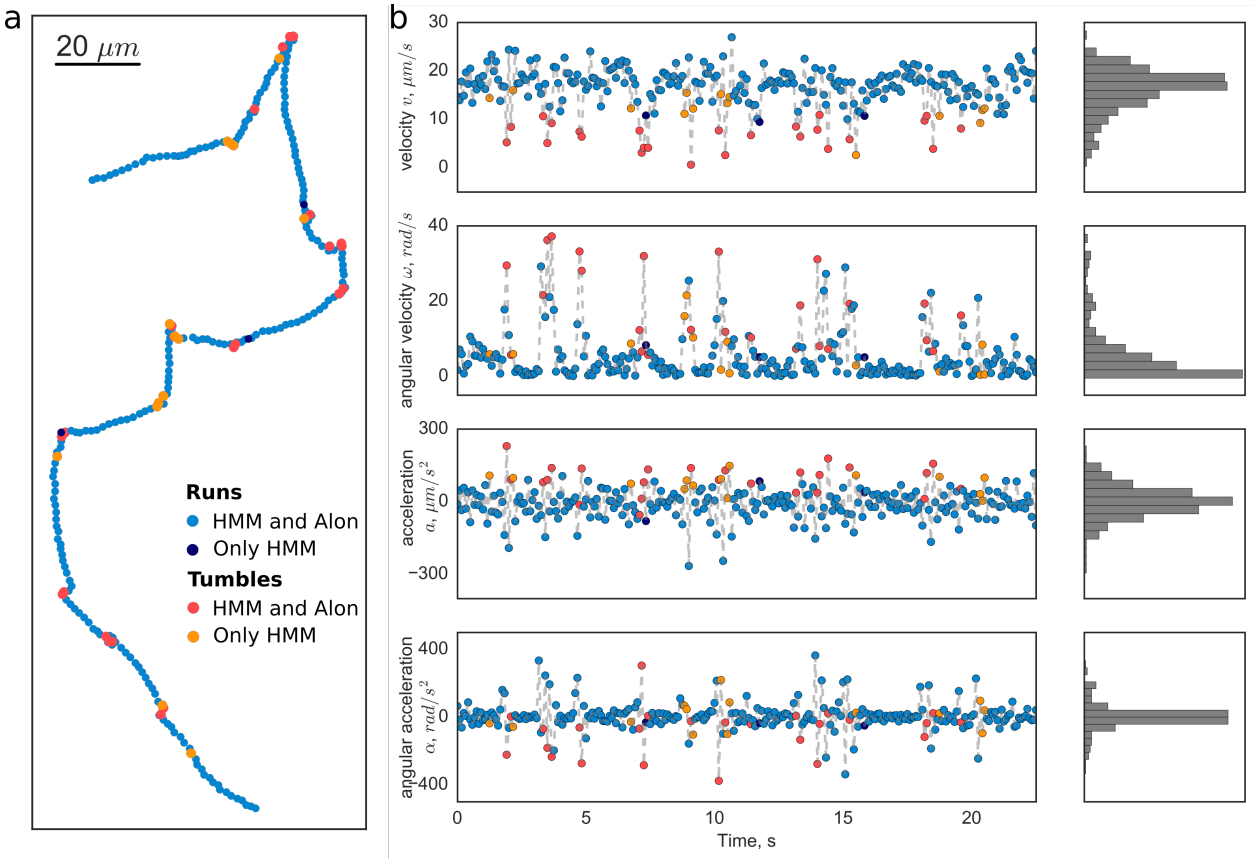

Figure 3.7: Tumble assignment using the HMM and Alon methods. Light blue and red dots indicate runs and tumbles respectively assigned both by HMM and Alon methods. Dark blue: runs assigned only by the HMM method, yellow: tumbles assigned only by HMM method. (a) Trajectory with assigned runs and tumbles. (b) Time traces of trajectory parameters used for tumble assigment with corresponding distributions.

different strains depending on the swimming velocity and tumbling frequency (3.4). Based on this estimate I limit the duration of time for which I record bacteria after the light is turned off to 30 s, as adaptation kinetics observed on the time scale longer than that likely result from previously unexposed bacteria and therefore do not reflect the internal dynamics of the chemotaxis network.

3.3.2 Errors in trajectory linking

When trajectories of different bacteria intersect there is no way for the linking algorithm to tell one from another, so the intersection of trajectories might result in linking errors: trajectories breaking or mis-linking (fig. 3.9). This can affect the results in several ways. First of all, mis-linking can actually introduce artifact tumbles as shown on figure 3.9b, when it replaces straight trajectories with turning ones. The opposite is possible as well, if mis-linking happens for bacteria that run into each other and tumble at the intersection. However, this is less probable as bacteria spend $\sim 80\%$ of the time running. If two bacteria have different

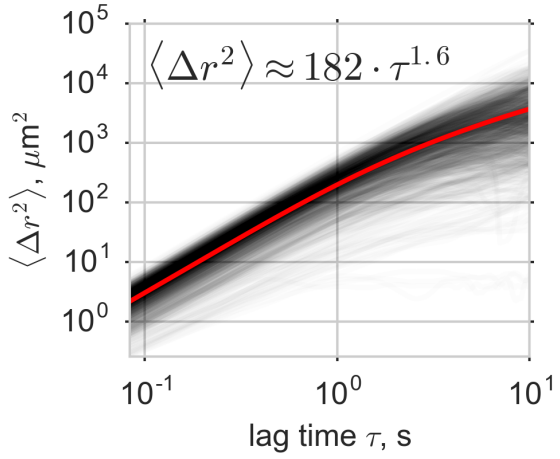

Figure 3.8: Mean square displacement $< r^2 >$ of wild-type *E. coli* bacteria (strain RP4347) as a function of lag time τ. MSD was calculated for more than 20000 trajectories that were at least 20 s long. Black lines shown MSD calculated for 1000 randomly selected trajectories. The equation is a power law fit to the ensemble MSD (red line).

swimming characteristics, e.g. one is slow and the other is fast, mis-linking may affect assignment of runs and tumbles. Finally, the breaking of trajectories will reduce the number of points available for calculating running velocity, making normalization and run-tumble assignment less reliable (3.2) [36]. This can be avoided by keeping only the trajectories longer than a certain threshold; however, that decreases the total amount of data available for the tumble bias calculation and therefore decreases signal-to-noise ratio.

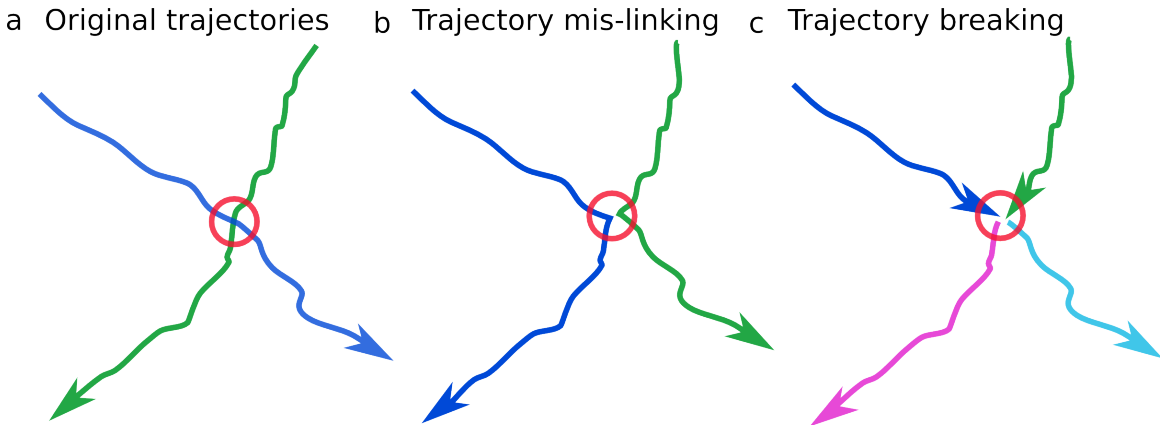

Figure 3.9: Intersection of trajectories (a) may lead to mis-linking (b) or breaking (c).

To assess the effect of mis-linking on detected motility statistics and tumble assignment, I performed simulations of bacteria swimming inside a 2D square with periodic boundaries, with step-wise addition and removal of attractant using RapidCell [32]. The number of bacteria was kept constant, while the accessible area was varied between simulations to gauge the density of bacteria at which the effect of mis-linking or

breaking becomes large enough as to obscure the observed trends. Simulations were run with 450 bacteria, swimming at $20\mu m/s$ with rotational diffusion of $0.062 rad/s^2$, and the concentration of the attractant Asp during the step was $0.5 - 0.8\mu m$. The simulation time step was set to 0.083 or 1/12th of a second to match the experimental framerate.

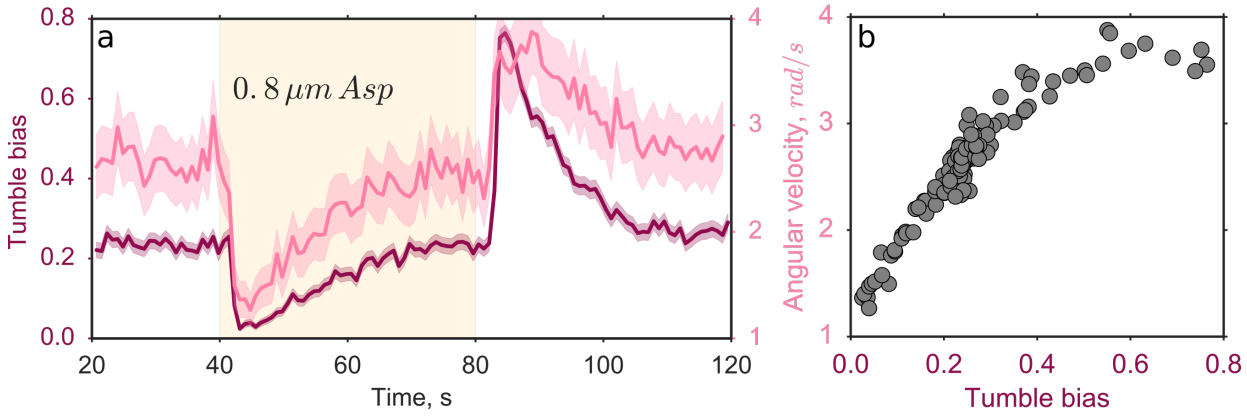

Figure 3.10: RCD or angular velocity changes linearly with tumble bias. (a) Temporal traces of tumble bias (dark red) and RCD (pink), highlighted area indicates addition and removal of $0.8\mu m$ Asp. Tumble bias was calculated from run-tumble states provided by simulations, RCD was calculated from orginal trajectories. (b) Correlation between angular velocity and tumble bias.

As discussed above, errors in trajectory linking may affect run-tumble assignment as well as alter the original trajectories. To decouple one effect from another, I used RCD as an independent measure of population run-tumble bias (section 3.1). The output of the simulations provided 450 bacterial trajectories with coordinates and run-tumble state of each bacterium in every frame (hereafter called 'original' trajectories), to which I added calculated RCD. I then used only the coordinates as an input for the data analysis workflow described in section 3.2 to get trajectories (hereafter called 're-linked trajectories'), motility parameters and run-tumble states.

Khan *et al.* have shown that RCD is linearly propotional to CCW bias in the range of 1 to 0.35, above which it plateaus [89]. That means that RCD should be proporional to tumble bias roughly in the range 0 - 0.65, although the relation between CW rotation of flagella and tumbling is not straightforward [54]. Indeed, RCD for simulated trajectories is propotional to tumble bias up to values of ~ 0.5 and changes in response to attractant addition or removal, although the signal-to-noise ratio is lower than that for tumble bias trace (3.10). To stay within the linear regime all the further simulations were perfored at lower concentration of attractant - $0.5\,\mu m$ instead of $0.8\,\mu m$.

To assess how the intersection of trajectories affects the accuracy of my analysis for each set of original and re-linked trajectories resulting from a simulation at a defined bacterial density, I calculate several

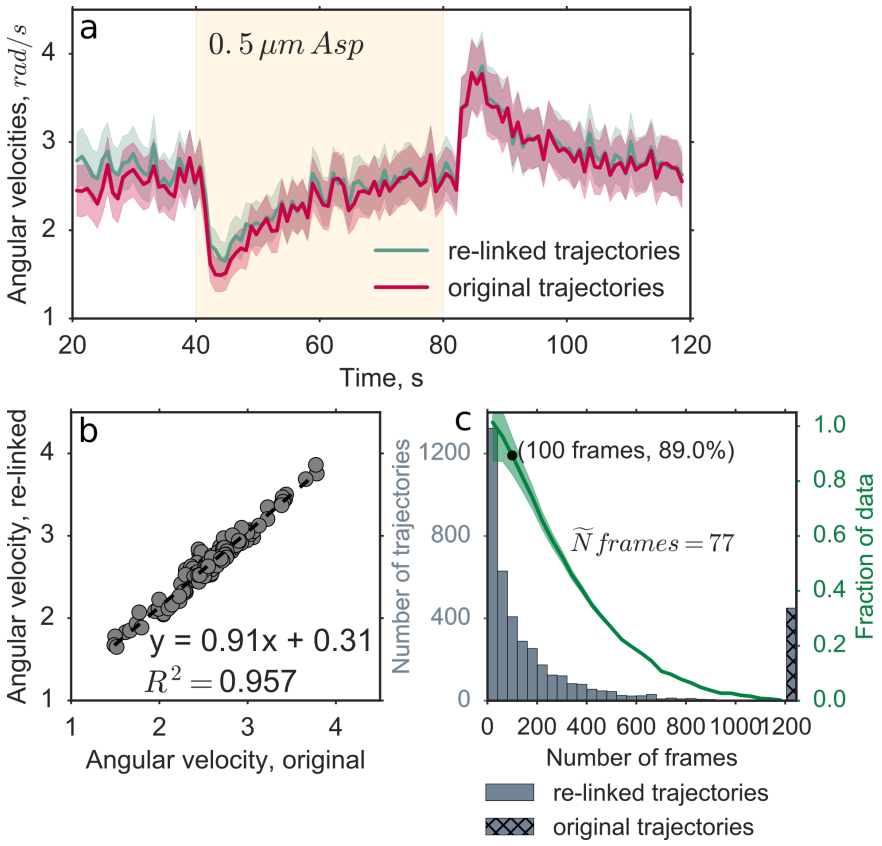

Figure 3.11: Comparison of original and re-linked trajectories. This simulation was performed at a density of bacteria typical for my experiments - 450 bacteria per 0.25 mm^2. (a) Temporal traces of angular velocity for original (red) and re-linked trajectories (green). (b) Correlation between angular velocity for re-linked and original trajectories with linear fit shown. Each point is a population average. (c) Histogram of trajectory lengths in frames for re-linked (gray) and original (gray crossed) trajectories. Median trajectory length is shown for re-linked trajectories. The green line shows the fraction of data as a function of length cutoff. For example, if cutoff is set to 100 frames, after removing all trajectories shorter than that I would still keep $\sim 90\%$ of the total number of frames.

parameters. Artifact tumbles due to mis-linking should increase the observed RCD so I compare RCD for the original and the re-linked trajectories. More specifically, I calculate the correlation coefficient R^2 and the linear coefficient of proportionality between the two (fig. 3.11a and b). The breaking of trajectories can be quantified by a median length of re-linked trajectories (fig. 3.11c). I am also interested in what fraction of the data (total number of frames) I will lose if I exclude short trajectories from consideration to improve the reliability of run-tumble assignment, so I calculate the fraction of data left after removing trajectories shorter than 100 frames (fig. 3.11c) (according to Dufour *et al.*, tumble assignment for trajectories shorter than 10 s is inaccurate [36]). The results of these calculations are shown in figure 3.12. As you can see, although the median length of trajectories decreases rapidly with the density of bacteria, the other parameters stay roughly constant within the range of density in my experiments (shaded gray area on fig. 3.12).

Finally to determine whether the observed RCD can be used to characterize the response to stimuli, I calculate the normalized amplitude of the response to addition (running response) and removal of attractant (tumbling response), defined as the maximum absolute increase in the RCD compared to the prestimulus value divided by the prestimulus value, both for original and for re-linked trajectories (fig. 3.13). As you can see up to the density of 3000 bacteria per mm^2 (which is higher than the typical density in my experiments), the RCD of the re-linked trajectories can reliably capture the scale of the response (fig. 3.13).

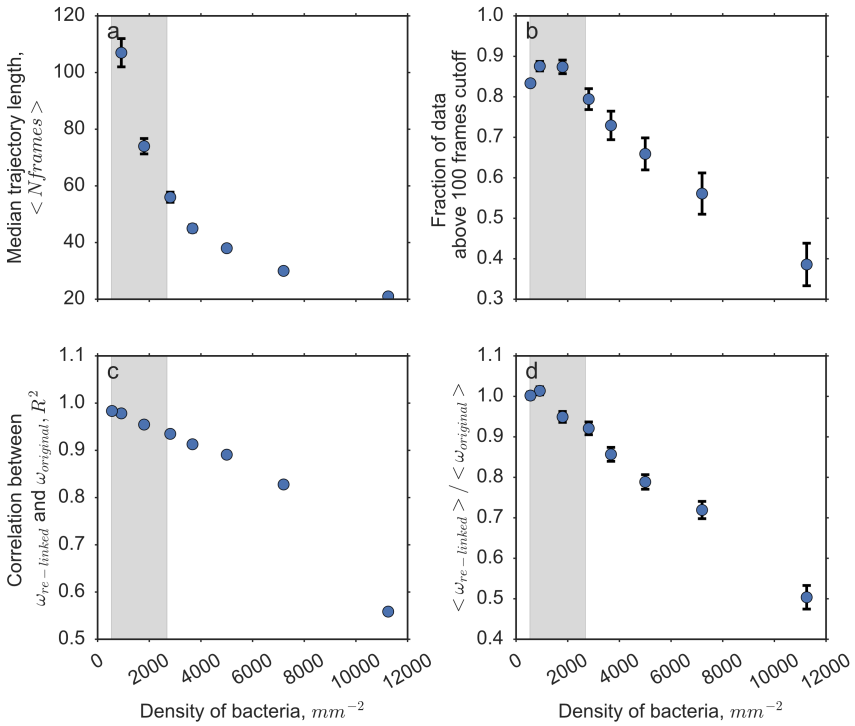

Figure 3.12: Effect of bacterial density on data analysis. The grey shaded area indicates the range of densities in my experiments. (a) Median length of trajectories in frames *vs* density. (b) Fraction of data above 100 frames cutoff *vs* density. (c) Correlation coefficient R^2 between angular velocities ω for re-linked and original trajectories as a function of density. (c) Linear coefficient of proporionality between angular velocities ω for re-linked and original trajectories as a function of density.

In summary, within the range of densities used in my experiments, artifact tumbles introduced by mis-linking trajectories (fig 3.9b) do not affect the observed values of RCD (fig. 3.12c and d). Similarly, the fraction of data above the 100 frames cutoff does not decrease significantly due to the breaking of trajectories (fig. 3.12b). This analysis does not address the effect of trajectory mis-linking on run-tumble assignment; however, it has demonstrated that observed RCD can be used as an independent measure of tumble bias.

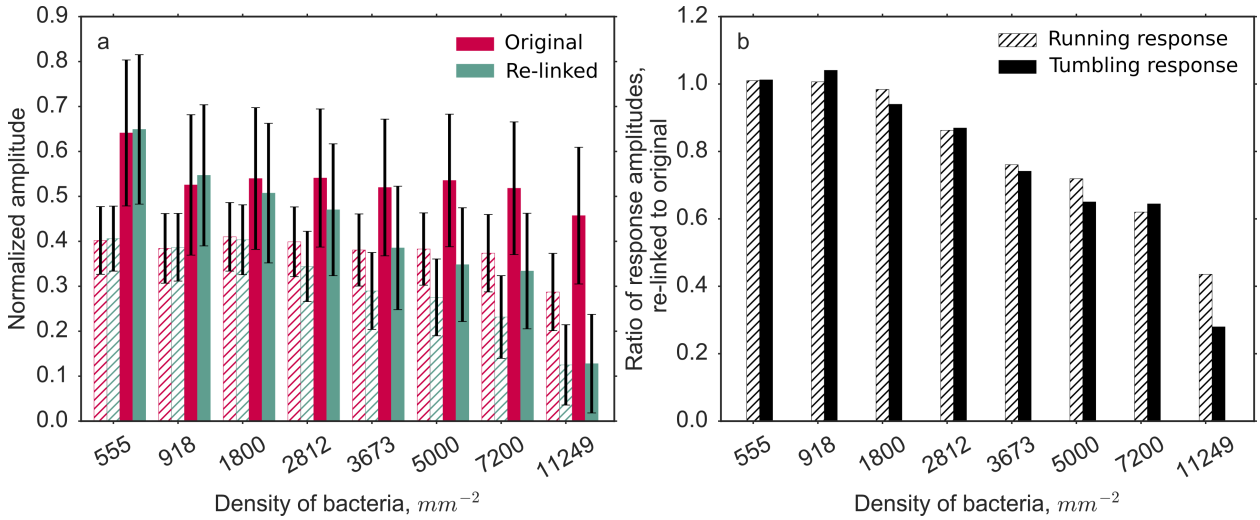

Figure 3.13: Effect of bacterial response amplitude from RCD traces. (a) Barplot of the normalized amplitudes of the running (hatched) and tumbling response (solid) for the original (red) and re-linked (green) trajectories at different bacterial densities. (b) Ratio of the response amplitudes, re-linked to original at different bacterial densities.

3.3.3 Erroneous assignment of runs and tumbles

Errors in tumble assignment can arise due to mis-linking of trajectories, poor statistics, or due to an inaccurate description of tumbling state in the assignment method. As discussed above, RCD can be used as an independent measure to verify the tumble-assignment procedure. RCD and tumble bias traces calculated using Alon's criteria and the HMM method described in the previous section (section 3.2) are shown on the figure 3.14. As you can see, although the absolute values depend on the specific method, the trends - response and adaptation to light exposure, - are very similar across different methods of tumble assignment. Similar trends are observed in the RCD traces as well. This allows me to conclude that the results I observe are robust to the method of analysis.

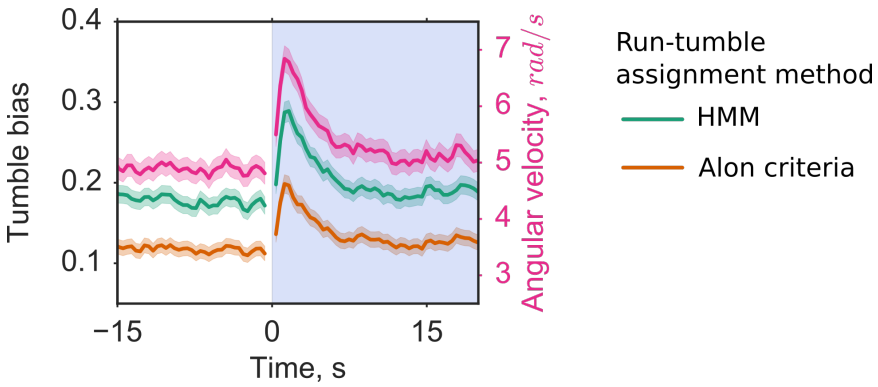

Figure 3.14: Different methods of quantifying chemotactic response. Angular velocity or RCD is shown in red, tumble bias calculated using Alon's criteria - in orange and tumble bias from the HMM method - in green. Blue shaded area indicated light exposure. This response trace comes from trajectories of the Tar-only UU1624 *E. coli* strain.

Chapter 4

Response to blue light is controlled by the chemotaxis network

To determine the contribution of chemotaxis network to light-induced taxis response, I have performed experiments with a number of chemotaxis mutants, missing different components of the network, or expressing only a single type of chemoreceptors. In this Chapter, I will first review the molecular basis of chemotaxis behavior, including the architecture of *E. coli* signalling network and distinctive features of each of the five *E. coli* chemoreceptors (4.1). I will then show the results I have obtained on light responses in *E. coli* chemotaxis mutants missing different components fo chemotaxis network (4.3). Finally, I will discuss my results on single-receptor *E. coli* mutants suggesting that all 5 *E. coli* receptors are able to independently mediate light-induced changes in tumble bias (4.4).

4.1 Background

On one end of the chemotaxis network are receptors sensing the extracellular and intracellular changes of relevant parameters (fig. 4.1), on the other end are flagellar motors that produce behavioral output, run or tumble, by rotating CCW or CW respectively. In addition to receptor-dependent chemotaxis there exist receptor-independent branch, where chemotaxis response to sugars is mediated by the interaction between core chemotaxis protein and components of sugar uptake system [109], however, I am not going to discuss it here. As I have discussed in Chapter 1 there is a lot of variability between the architectural organization of chemotaxis network between different species of bacteria, but the common core is shared and can be illustrated by *E. coli*.

4.1.1 Chemotaxis signalling network

The architecture of the chemotaxis network is shown in the figure 4.1. The behavioral output of the chemotaxis network, flagellar motors, is connected to its sensory input - transmembrane chemoreceptors, through signalling molecule *CheY*. In its phosphorylated form, *CheY-P* binds to the motors causing the switch of the direction of rotation from CCW to CW. *CheY* is phosphorylated by the kinase *CheA*, and dephosphorylated

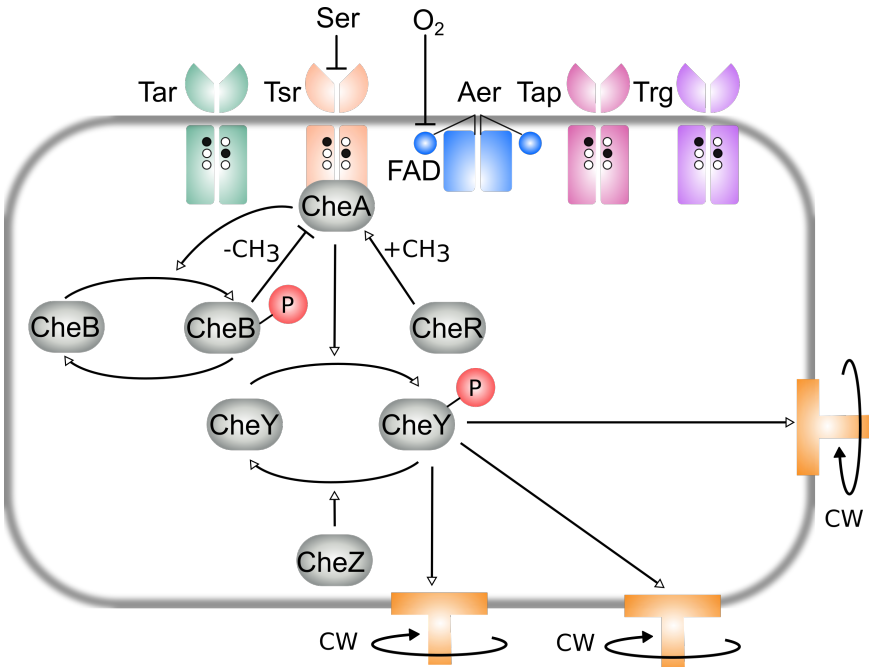

Figure 4.1: Schematic of the chemotaxis network. Receptor activity modulates the activity of the kinase *CheA*, which phosphorylates the signalling molecule *CheY*. In its phosphorylated form *CheY* binds to the flagella motors and causing them to rotate CW. White and black circles on the receptors indicate methylation sites, that methyltransferase *CheR* and methylesterase *CheB* act on. *CheR* is constitutively active and transfers methyl groups to the glutamate residues on the receptor backbone. *CheB* de-methylates receptors, but only in its phosphorylated form, *CheB-P*. *CheB* is phosphorylated by active *CheA*. Methylation increases and demethylation decreases, receptor and, therefore kinase *CheA* activity.

by the phosphatase *CheZ*. *CheA* interacts with the receptor complex through a coupling protein *CheW* (not shown on the fig. 4.1) and its activity is modulated by the environmental conditions. For example binding of repellents to the receptors cytoplasmic domains causes conformational changes in the receptors, resulting in consequent increase of the *CheA* activity, higher concentration of the *CheY-P* and therefore higher probability of CW motor rotation and higher tumble bias. *Vice versa* binding of attractants causes deactivation of *CheA* resulting in lower tumble bias. Therefore if the environment is improving, the bacterium continues to swim in the same direction, if it stays the same or is getting worse the bacterium tends to randomly change direction. The net effect of this response is that *E. coli* run lengths become longer in favorable directions (i.e. toward high nutrient or lower repellent concentrations) and cells migrate effectively to a better environment.

While several recent papers bring us closer to the understanding of the molecular mechanism behind the signal transduction in the chemotaxis network (4.1.2), it is completely unclear how does binding of attractants and repellents have the opposite effect at the molecular level.

Chemotaxis network has a built-in feedback loop that enables bacteria to adapt to the new conditions and therefore continue to be sensitive to the environmental changes. In addition to ligand-binding, the activity

of the receptors is regulated by their methylation state, which is determined by the relative activities of the methyltransferase *CheR* and methylesterase *CheB* (fig. 4.1). *CheR* is constitutively active and transfers methyl groups to the glutamate residues on the receptor backbone. *CheB* de-methylates receptors, but only in its phosphorylated form, *CheB-P*. *CheB* is phosphorylated by active *CheA*. Therefore activation of the receptor due to repellent binding will eventually cause its demethylation and subsequence decrease in receptor activity and lowering its affinity for repellent [110]. Adaptation allows *E. coli* to extend the dynamic range of chemotaxis network to over five orders of magnitude [111].

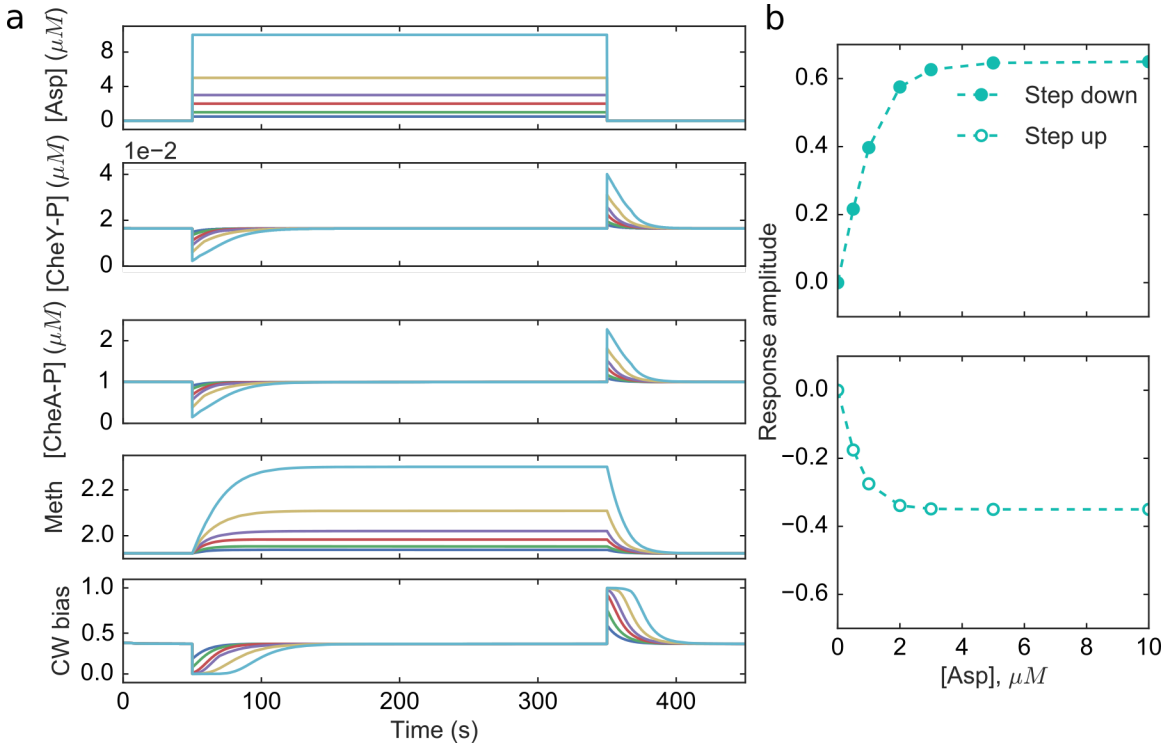

Figure 4.2: RapidCell simulations of the response to step and step down in Asp - attractant for Tar receptor [32]. (a) - temporal traces of the signal - [Asp], and corresponding chemotaxis network output - [CheA-P], [CheY-P], receptor methylation [Meth] and CW bias. (b) - Amplitude of the step up and step down responses as a function of [Asp].

Temporal traces of [CheA-P], [CheY-P], receptor methylation level, CCW and tumble bias obtained from simulating bacteria responding to stepwise addition and removal of Aspartate are shown on the figure 4.2a. The simulation was done using RapidCell [32]. [CheA-P], [CheY-P] and CW bias, below saturating concentration of Asp, traces closely follow each other. Addition and removal of Asp cause sharp decrease and increase of [CheA-P], [CheY-P] and CW bias, respectively followed by gradual adaptation due to methylation. Response and adaptation timescales are separated: timescale of adaptation is much slower than that of receptor activation due to ligand binding. Note that methylation level does not return to its prestimulus

level after adaptation which means that accurate adaptation to the stimuli is limited by maximum receptor methylation level. Note that saturation happens at the level of CheY-P - motor interaction.

Dependence of the motor bias on the *CheY-P* concentration is described by a highly cooperative sigmoid curve with Hill coefficient of ~ 10 which was measured by Cluzel and co-workers [76, 112]. The cooperative binding of the *CheY-P* to the motors was ruled out by FRET assays [77]. Instead steep dependence of the CW bias on the *CheY-P* concentration is explained by the interaction between bi-stable subunits of the flagellar rotor, so-called, conformational spread model. Each of the ~ 34 subunits can be in either CW or CCW states, and binding of the *CheY-P* increases the probability of the CW state [77]. The model states that there is a free-energy penalty for adjacent subunits being in different states, therefore the most stable conformation of the rotor correspond to all subunits being in the same state, all CW or all CCW [77].

4.1.2 *E. coli* receptors

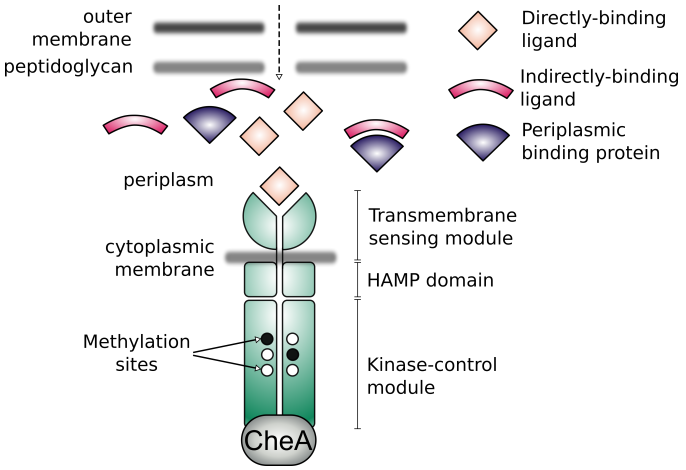

Figure 4.3: Domain organization of the chemoreceptor.

E. coli has five types of receptors that sense and respond to a range of environmental signals. Each receptor is responsible for sensing a set of repellent and attractant signals, although there is some crosstalk between different receptors [9]. The functional sensing unit of chemotaxis is a heterotrimer of receptor homodimers. I will discuss the interaction between receptors and underlying higher-order organization in more details in Chapter 5 and here I would like to review the molecular architecture of individual receptors.

Receptor dimer consists of three modules, that are functionally and structurally distinct that are shown in the figure 4.3. The transmembrane sensing module is a combination of the periplasmic ligand-binding domain and transmembrane domain [113, 114]. Note that, as schematically depicted on fig. 4.1, Aer receptor, unlike the other four does not have periplasmic sensing domain, instead it has cytoplasmic FAD-binding PAS

domain which I will discuss in more details below. The rest of Aer architecture is similar to that of the other four receptors. When ligand binds to the periplasmic domain, directly or via periplasmic binding protein, it causes conformational changes in the domain that are transferred to the 'signal-conversion' module - membrane-adjacent cytoplasmic HAMP domain, then further to 'kinase-control' module and finally to the end of the cytoplasmic helix bundle that binds and regulates kinase CheA [113, 114].

Adaptation part of 'kinase-control' module contains glutamate residues that get methylated or demethylated during adaptation. Tar and Tsr receptors also contain pentapeptide sequence (NWETF or NWESF) in that region that serves as a docking site for CheR and CheB enzymes [115, 116].

In a recent paper Gushchin and co-authors have cristallized ligand-bound and unbound states of the nitrate/nitrite transmembrane sensor NarQ [57]. Their results demonstrate that the ligand binding causes piston-like shifts of the transmembrane receptor helices which result in the leverlike motions of the HAMP domain [57]. Similar mechanisms might be at play for chemotaxis receptors as well [53, 56].

3D structures of the 'kinase-control' module and of the HAMP domain are highly conserved between different receptors and across bacterial species. Not unexpectedly the most variable part is transmembrane sensing domain, however, the basic fold is shared across species as well [114].

Table 4.1: *E. coli* receptors

Receptor	Repellent stimuli	Attractant stimuli	Periplasmic domain	Methylation sites	CheR/CheB binding	Receptor abundance
Tar	pH, Ni	Asp, MeAsp maltose, T	Yes	Yes	Yes	12000
Tsr	T, Leu Indole	Ser, Cys, pH PMF	Yes	Yes	Yes	12000
Aer	redox, oxygen carbon sources		No	No	No	500
Tap	phenol	dipeptides pyrimidines	Yes	Yes	No	500
Trg	phenol	galactose, ribose	Yes	Yes	No	900

Table 4.1 summarizes the basic information about different types of *E. coli* receptors [51, 95, 115–120], which I will now review in more details.

Tar and Tsr

Tar and Tsr are two of the most abundant *E. coli* receptors (table 4.1). Tar stands for taxis to aspartate and from repellents, Tsr - for taxis to serine and from repellents [95]. Both Tar and Tsr respond to a range of other stimuli, both attractants, and repellents, and there is crosstalk between the two receptors (table 4.1). For example thermotaxis and pH-taxis in *E. coli* are mediated by Tar and Tsr receptors together, and are examples of so-called precision sensing, as opposed to gradient sensing. The precision sensing means that instead of moving up or down the gradient towards higher/lower value of a certain parameter, bacteria accumulate at the preferred pH or temperature [9, 50, 121]. This is achieved because Tar and Tsr have opposite responses to pH and temperature [9]. Thus bacteria expressing only Tar receptor exhibit attractant response to low and repellent response to high pH, and *vice versa* bacteria expressing Tsr show repellent response to low and attractant response to high pH [9]. pH preference point for wild-type cells, therefore, depends on the relative abundance and methylation level of two receptors. The ratio of Tar to Tsr expression changes throughout the growth curve as a function of cell density thereby changing pH preference point [51]. Additional tuning mechanism is provided by the dependence of the receptor methylation level on the external pH. Thermotaxis is regulated in a similar manner [122].

In addition to sensing extracellular parameters, Tsr receptor is able to sense intracellular changes in Proton-Motive Force (PMF) thereby being a receptor for 'energy-taxis' in addition to Aer [123] receptor, which I will discuss in more details below.

Aer

Aer is one of the low-abundance receptors (table 4.1 and is known as receptor for aerotaxis. Aer mediates a wide range of responses that can be combined by the umbrella term 'energy taxis', that includes aerotaxis, redox taxis, taxis to carbon sources [118, 124]. As discussed previously, Aer, instead of a cytoplasmic ligand-binding domain, has periplasmic sensing domain. Rather than sensing the change in extracellular cues, Aer senses the resulting change in Electron Tranport Chain (ETC). In other words, instead of sensing, for example, oxygen directly it senses the decrease in electron transport that results from hypoxia [118, 124]. Any environmental conditions that alter the flow of electrons through the ETC will elicit a behavioral response in *E. coli* mediated by Aer. That includes inhibitors of electron transport system, electron donors and acceptors, and factors that change the membrane proton motive force [118]. Energy taxis is an example of precision-sensing chemotaxis response: in an aerotaxis capillary assay, different bacterial species form bands at distances from meniscus that correspond to their preferred oxygen concentrations, at which their PMF is maximized [8, 16, 124, 125].

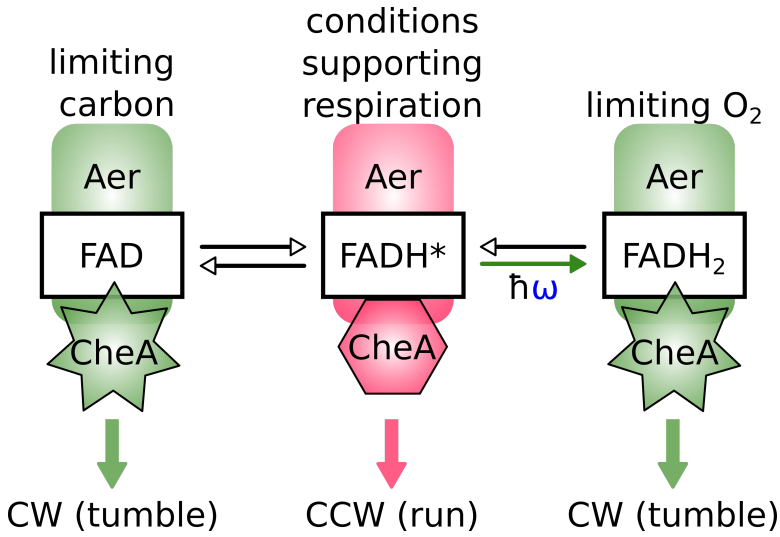

Figure 4.4: 3-state model of the FAD. Aer senses the change in electron transport through the respiratory chain of the cell that causes change of FAD reduction state. Tumbling response to light in respiring E. coli is caused by photoreduction of FADH*. *E. coli* photoresponse depends on FAD reduction state and therefore on the metabolic state of the bacteria

The sensing domain of Aer binds a chromophore, Flavin Adenine Dinucleotide (FAD), as a cofactor. It is the change in FAD redox state in response to perturbation of electron transport that causes a subsequent conformational change in Aer, which in its own turn activates downstream signal transduction through the chemotaxis network and results in a correspondent change in tumble bias [126]. Experimental results of both mutational studies and taxis experiments agree with the three state model of FAD where transition to fully oxidized or reduced forms of FAD results in a CW of flagella motors, and the transition to the semiquinone state results in CCW rotation of flagella motors (running) (fig. 4.4) [118]. At the behavioral level, it means that *E. coli* will be seeking conditions that allow it to support respiration as in the normally functioning electron transport chain FAD is presumed to be in the semiquinone state [118]. It is important to note however that there is no direct experimental evidence supporting three-state FAD model and in fact, FAD can undergo a series of electron and proton transfers to adopt up to 5 different redox states [127].

PMF, electron transport and redox state of the respiration chain are all coupled parameters that can potentially affect FAD redox state [126]. It has been shown that Aer specifically senses redox state of the respiratory enzymes although the exact mechanism is unclear [123].

Aer lacks canonical methylation motifs, which along with other lines of evidence suggests that it adapts through methylation-independent mechanism resulting in significantly slower adaptation kinetics [128].

Tap and Trg

Tap and Trg are two remaining low abundance receptors (table 4.1). Tap stands for taxis associated protein, and Trg stands for taxis to ribose and galactose [95]. As follows from the name Tap mediates positive chemotaxis to dipeptides via periplasmic dipeptide-binding protein and pyrimidines [119, 120]. Similarly Trg interacts with periplasmic ribose- and galactose-binding proteins to mediate positive taxis to these attractants [129]. Both Tap and Trg also mediates repellent taxis in response to phenol [130, 131]. Tap and Trg lack the NWETF motif that recruits the methyltransferase CheR and therefore require the presence of Tsr or Tar for adaptation [132].

Despite being low abundance receptors, Tar, Trg, and Aer, can nevertheless have a significant effect on bacterial motility, as the signal from individual receptor is amplified due to receptor-receptor interaction (5.1).

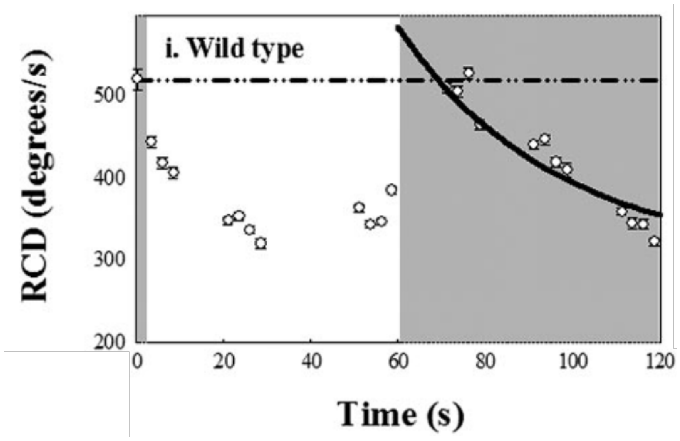

Figure 4.5: Light exposure causes increase in RCD (rate of change in direction) in swimming *E. coli* bacteria. Figure from [1].

4.1.3 What is known about *E. coli* phototaxis

As mentioned in the Introduction (1.2.2), tumbling response to blue light in *E. coli* has been reported in a few previous papers [1, 58, 69]. According to Taylor and co-workers, the minimum power density of blue light (390 - 530 nm) required to cause a response is $\sim 200 - 500 mW/cm^2$ [69]. However, in the most recent paper, Wright *et al.* have shown that blue light illumination of much lower intensity (440 $\pm$ 5 nm, $\sim 7 mW/cm^2$) can cause a tumbling response in *E. coli* (fig. 4.5).

Wright and co-workers have identified two receptors that can independently mediate tumbling response to light, Tar and Aer [1]. The authors have also observed running light response in Tsr-only strain but only occasionally and the response was weak [1]. The role of Tap and Trg receptors in *E. coli* response to light

was not explored [1].

Tar does not have a chromophore, so the mechanism of its photosensitivity is unclear. For example, it has been speculated that Tar senses light indirectly by monitoring some parameter perturbed by absorption of blue photons, e.g. electron transport [1].

As discussed above, the sensing domain of Aer binds a chromophore, the flavin adenine dinucleotide (FAD), as a cofactor. The *E. coli* phototaxis action spectrum is consistent with flavin absorption so it is possible that tumbling response is a result of photo-reduction of the Aer-bound FAD [1]. It has been shown that FAD in Aer is labile and easily removed in denaturing conditions [118] so light might be reducing free FAD in the cytoplasmic pool that exchanges with Aer-bound FAD and causes the response. Finally, it is plausible that Aer is responding to light-induced perturbation of electron transport [1]. However, direct experimental evidence, as well as quantitative characterization of the response, are lacking.

Note, that Tar- and Aer-mediated responses have different adaptation kinetics, consistent with what is known about these receptors. Thus Tar-only strain has a very short-lived response that decays with 0.6 s^{-1} rate. On the contrary, in a strain expressing Aer from a plasmid at the level comparable with that of Tar/Tsr expression in the wild-type strain, the adaptation is slow (characteristic adaptation time is $\sim$ 2 minutes), which reflects its methylation-independent mechanism.

Below I will show my experimental results which reveal the role of all five receptors in *E. coli* response to light.

4.2 Methods

Microbiology

Bacteria were grown for 20-24 hours overnight from a single colony in 1 ml of M9 minimal media supplemented with 4 mg/ml succinate unless noted otherwise (1x M9 salts; 2 μM MgSO4; 0.1 mM CaCl2; 0.5 mM of each Meth, Leu, Thr and His; 100 $\mu g/l$ thiamine; 4 mg/ml succinate) shaking at 265 RPM at 30°C with appropriate antibiotics if necessary (34 $\mu g/l$ of Cm or 100 $\mu g/l$ of Amp). The overnight culture was diluted 50-fold in 1 ml of the same media and grown, shaking at 265 RPM at 30°C for 8-12 hr (to OD600 $\sim$ 0.25-0.3) with appropriate inducers if necessary. The following concentrations of inducers were used for strains with plasmids: 50 μM IPTG for UU1250 + pSB20, 0.7 μM NaSal for UU1250 + pTP1 and 0.8μM NaSal for UU1250 + pPA705.

The over-day culture was harvested by centrifugation (1300 g, 10 min) and gently resuspended in the appropriate volume of motility buffer (70 mM NaCl, 100 mM Tris-Cl pH 7.5, 4 mg/ml succinate, 100 μM

Meth) to reach the final OD of 0.15. Bacteria were placed back in the shaker to oxygenate the media. Methionine was added to the final concentration of 100 μM prior to chamber assembly. Phenol was added to the final concentration of 2.5 mM or 5 mM where noted.

Bacterial strains and plasmids used in this part of the study are shown in the appendix (D.1). All of the strains were derived from the RP437 background. Tap, Aer, and Trg receptors were expressed from the plasmid as the chromosomal expression levels of these receptors are too low to ensure non-zero tumble bias.

2D swimming assay

Slides (3x1 inch, №3010, Thermo) and coverslips (22x22mm, №1, VWR) were sonicated in acetone for ∼15 min, rinsed, then sonicated in KOH for 15 min, rinsed and dried by centrifugation (1000 rpm, 3 min). Cleaning was done on the day of each experiment as we found that storing cleaned slides in the distilled water, even for one day, results in the accumulation of defects on the glass surface. Prior to the experiment slides and coverslips were passivated with BSA to prevent sticking of bacteria. Slides and coverslip were incubated with 2 mg/ml BSA for ∼20 min, then rinsed with a copious amount of water and dried with nitrogen. To assemble the chamber a drop of motility buffer ($5\mu l$) containing *E. coli* cell was placed on a slide and gently covered with a coverslip. Care was taken to prevent a formation of air bubbles. To prevent drift due to evaporation, open sides were sealed with fast-curing epoxy (Devcon, 5 minute epoxy). The distance between the slide and a coverslip is determined by the thickness of the liquid layer of bacterial media and is $\sim 10\mu m$ which roughly corresponds to the objectives depth of field.

Movies of swimming bacteria were recorded at the frame rate of 12 frames per second in the phase contrast mode. The duration of the recording was 30-50 s prior, during and after light exposure. Experiment with each chamber was limited to 30 min due to oxygen depletion (2.3).

Data analysis

Trajectory linking, filtering and run tumble detection was performed as described in Chapter 3.

4.3 Response to light requires receptors, functional CheY, CheR and CheB

Similarly to Wright *et al* I have observed tumbling following by adaptation in response to light exposure in the wild-type *E. coli* strain [1]. The decrease in light intensity caused running response was followed by adaptation as well. Note that I did have to use much higher light intensity, similar to the one reported

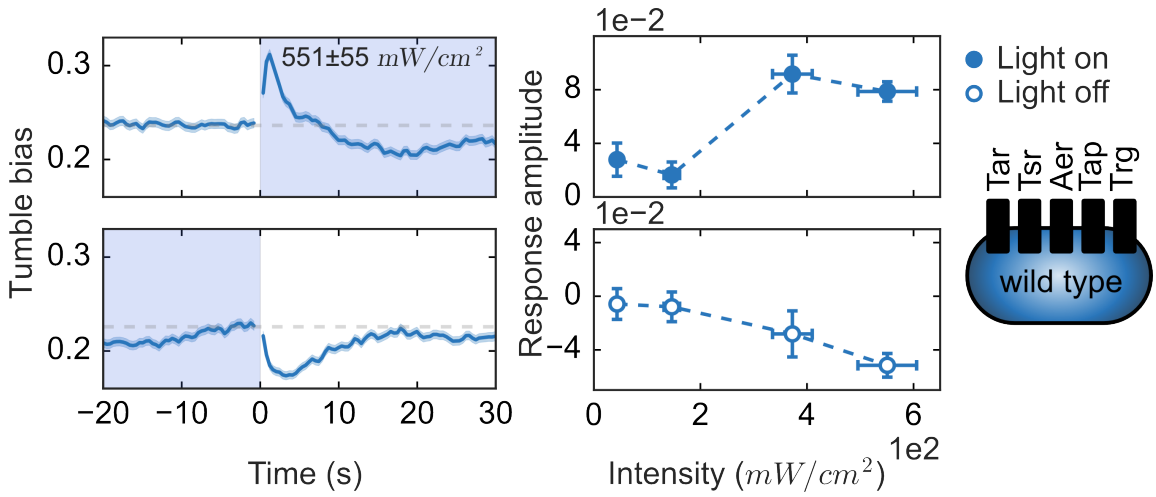

Figure 4.6: Response to light of the wild-type RP437 strain.

by Taylor and Koshland and Taylor and co-workers [58, 69], to see a significant increase in tumble bias compared to Wright and co-workers [1] - more than $300 mW/cm^2$ versus $7 mW/cm^2$. I was able however to reproduce their results at a lower light intensity ($44 mW/cm^2$) when using the same substrates in the growth and motility media - M9 supplemented with 5 mg/ml glycerol and motility buffer with 5 mM lactate (fig. 4.7). I have found that growth conditions had much bigger effect on the light response than motility buffer. I will discuss this phenomenon in more details in the Chapter 7.

To place these results into perspective let's compare the intensity values that I have used with those that bacteria may actually encounter in nature. The intensity of the solar illumination at the surface of Earth is $\sim 140 mW/cm^2$ across the visible spectrum. Intensity in the 10 nm wide blue band is about 1 mW/cm^2 [61]. We do not know what is each individual receptor response to light at different wavelenghts outside of the blue band we used, and, therefore cannot estimate what is the total intensity that receptors experience under solar illumination. Wright *et al* measured response spectrum for the wild-type RP437 strain and showed that bacteria do not exhibit phototaxis response below 400 or above 500 nm [1]. However response spectrum may change when higher intensity of light is used, it might also be that responses mediated by individual receptors has different wavelength sensitivity.

To make sure that at this high light intensity response is still mediated by the components of the chemotactic network we performed control experiments with strains lacking different components of the chemotactic network. We have observed no response to light in either receptorless strain or strain lacking functional *CheY* (4.8). The strain lacking *CheB*, an enzyme responsible for receptor de-methylation, had very high tumble bias and did not show a measurable increase in tumble bias upon light exposure (4.8). In the $\Delta CheB$ strain, receptor methylation level and, therefore, receptor activity is higher than in the wild-

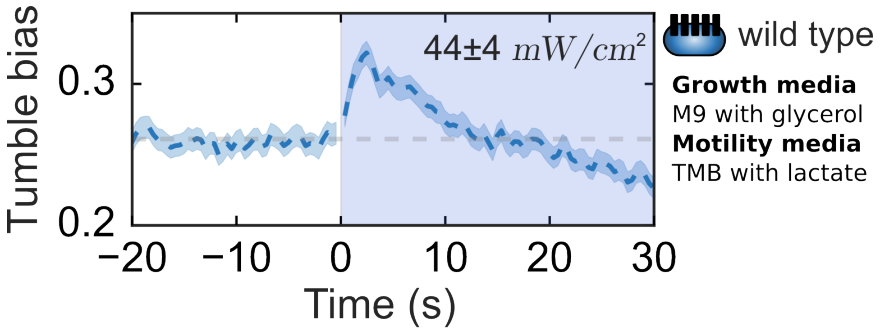

Figure 4.7: Response to light of the wild-type RP437 strain grown in M9 with glycerol, in TMB with lactate.

type, causing a higher probability of clockwise rotation and higher tumble bias (4.8). The strain lacking *CheR*, an enzyme responsible for receptor methylation exhibited an initial sharp increase in tumble bias similarly to wild-type, however, no adaptation was observed, instead tumble bias continued to increase albeit slower (4.8). In the absence of *CheR* strain receptor methylation level and is low and adaptation through demethylation is therefore impossible.

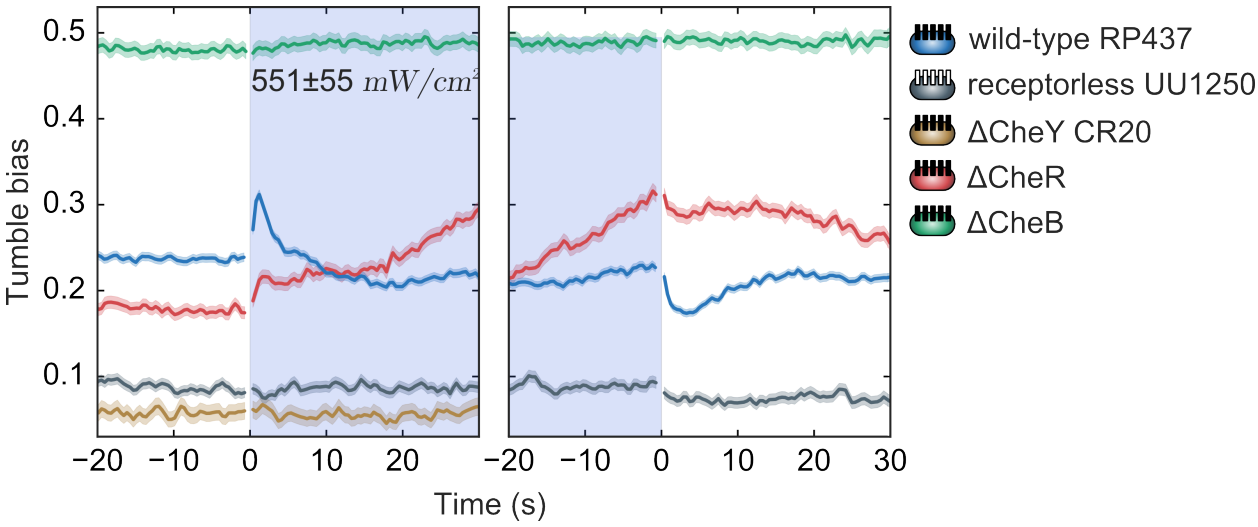

Figure 4.8: Response to light of the *E. coli* mutants lacking different components of the chemotaxis network.

These results suggest that blue light response is indeed mediated by chemotaxis network. Results for receptorless and Δ*CheY* strain confirm that response requires receptor-*CheA* cluster and that blue light does not directly affect the direction of flagellar rotation. The lack of response in Δ*CheB* strain suggests that in wild-type strain tumbling response to light is caused by receptor activation. Finally response in Δ*CheR* strain indicates that the adaptation following the tumbling response we observed in the wild-type strain is mediated by *CheR* protein through the negative feedback loop of the chemotaxis network.

4.4 Role of individual chemoreceptors in blue light response

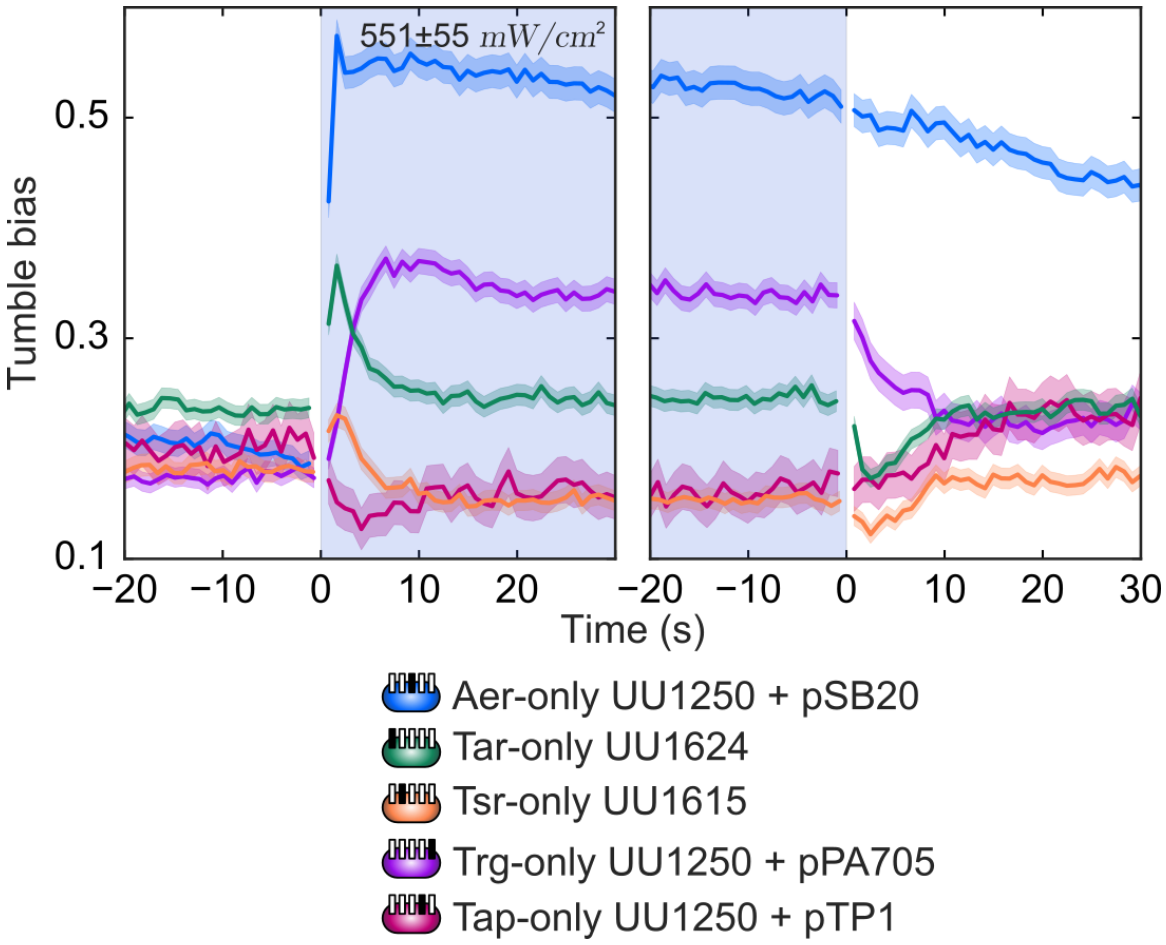

Figure 4.9: Response to light of the *E. coli* strains expressing one type of chemotaxis receptors.

To determine the independent contribution of individual receptors to the light response of the wild-type strain we have measured a light response of the single-receptor *E. coli* mutants. Low copy number receptors Aer, Tap and Trg receptors were expressed from plasmids and induced to reach expression levels similar to those of high-copy number receptor in the wild-type background as indicated by the tumble bias similar to the wild-type strain in the absence of the stimuli. Similarly to Wright *et al* we have observed tumbling responses in Tar-only and Aer-only strains [1] (fig. 4.9). We were able to measure responses mediated by remaining three receptors as well. The Tsr-only strain exhibited weak but consistent tumbling response and the Trg-only strain showed tumbling response with delayed onset.

Originally I was not able to observe any response in Tap-only strain (fig. 4.10). As discussed in the introduction, Tap receptor by itself cannot recruit *CheR* and *CheB* proteins and therefore will have low methylation level and low activity in the receptorless background. Consistently with that Tap-only strain

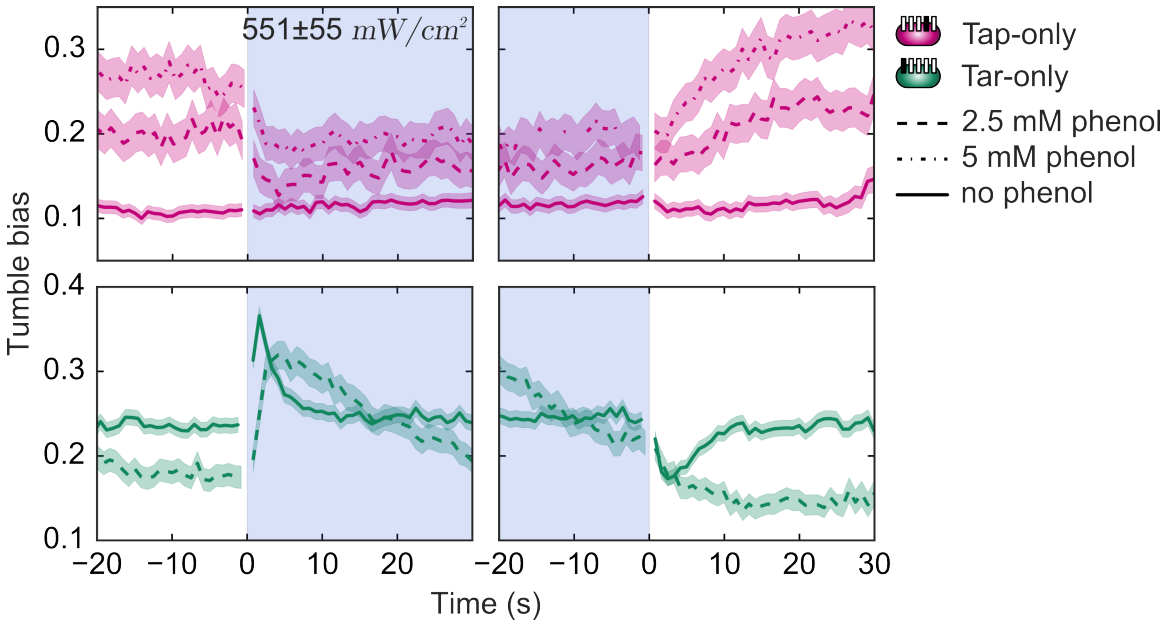

Figure 4.10: Response to light of the Tap-only and Tar-only strains in the presence of phenol.

has significantly lower tumble bias than wild-type strain. The lack of response suggests that, unlike Trg, Tap receptor is not activated by light exposure. We wanted to explore the possibility that Tap receptor may be deactivated by light and mediate running response. To test that idea we performed measurement of light response for Tap-only mutant in the presence of a repellent phenol, which should activate Tap receptors. Indeed Tap-only strain had higher tumble bias in the presence of phenol and tumble bias increased with increasing phenol concentration. Moreover, we observed running responses to light both in 2.5 mM and 5 mM phenol and tumbling response upon light turn off (fig. 4.10). It is important to note that phenol does not absorb in the blue region of the spectrum, which rules out the possibility that Tap responds to light-excited phenol rather than to the light itself. Our results for Tap-only strain suggest that unlike the other four receptors, Tap receptor is deactivated by light exposure and mediates running response. The opposite responses to light mediated by different receptors suggest, that, in principle, bacteria might be able to navigate to specific light intensity, when placed in a light gradient, and their preference will depend on relative receptor abundance.

In all of the single-receptor strains light turn off caused changes in tumble bias in the opposite direction compared to light turn on (fig. 4.9). In the Aer-only strain, at this light intensity, tumble bias was gradually decreasing when light was turned off, which suggests that the effect of light goes beyond just receptor activation, and Aer might be sensing this secondary effect which takes time to recover, rather than light itself. In Tsr-only and Tar-only strains running responses to light turn off had adaptation kinetics similar

to that of responses to light turn on further confirming that adaptation is mediated by negative feedback loop of the chemotaxis network (fig. 4.9, 4.12). In Trg and Tap-only strain responses to light turn off were essentially symmetric to those to light turn on and similarly did not show any adaptation.

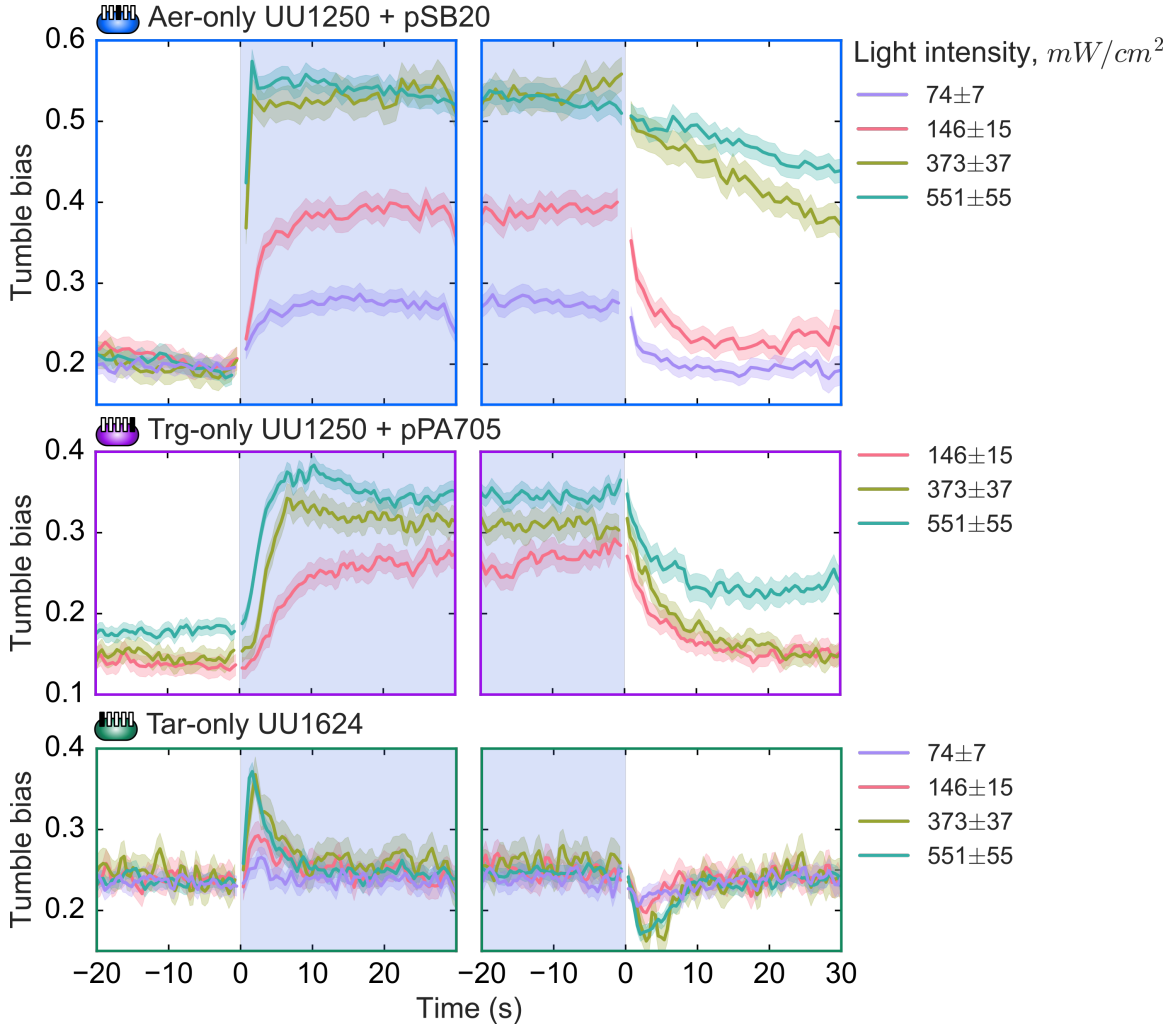

Figure 4.11: Response to light of the Aer-only, Trg-only and Tar-only strains at different light intensities.

I have measured light response at different intensities for Aer, Trg and Tar-only strains. Tumble bias traces for these strains at different light intensities are shown on the figure 4.11. Note that at lower light intensities response to light turn off becomes symmetric to the response to light turn on, which suggest that sensing mechanism might be qualitatively differen at low and high light intensities. In other strains responses to both light turn on and light turn off had the same functional shape at lower light intensities. Response amplitudes, response and adaptation times were calculated as shown on figure 4.12 (upper panel) . There are several trends worth noting 4.12. First of all, amplitude of the response to light exposure increased with intensity and saturated at around 400 mW/cm^2, similarly to wild-type (fig. 4.6). This is in contrast with

the results of Wright *et al* who reported saturation already above the intensity $\sim 10\ mW/cm^2$ [1]. However they increased the intensity by widening the bandwidth around 440 nm from 10 to 50 nm, so the saturation might be due to *E. coli* insensitivity to light at these wavelenghts. Tumble bias at the saturating light intensity that I have measured is comparable to that of the $\Delta CheB$ mutant which implies that saturation happens at the receptor level (fig. 4.8, 4.9).

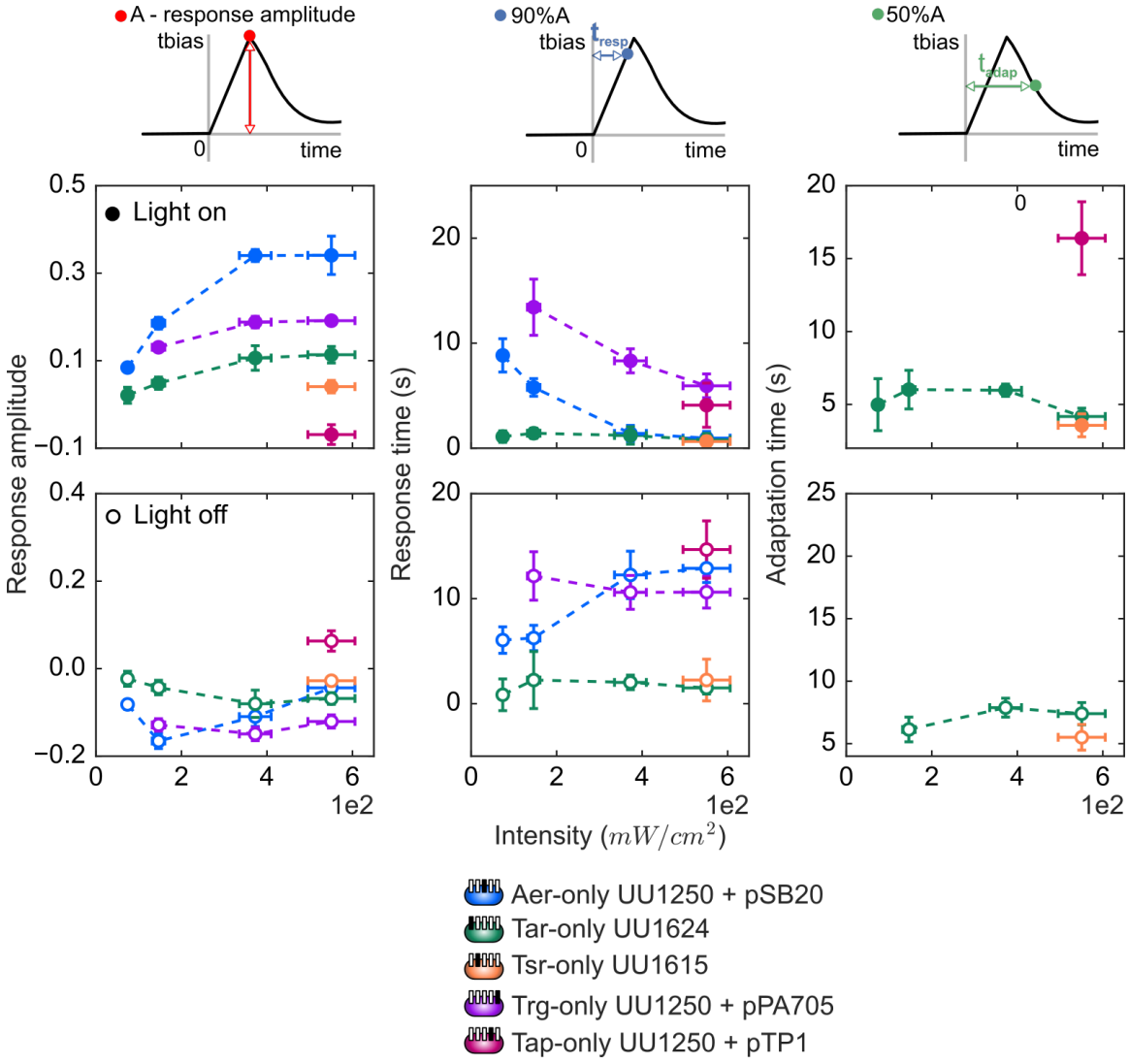

Figure 4.12: Response amplitude, response time and adaptation time for single-receptor strains.

For all practical purposes, light intensity increases and decreases immediately and conformation changes in receptors in response to stimuli happen on subsecond timescale [32]. So changes in tumble bias that take longer than that, indicate that receptors might be responding to the light-induced perturbations of the cellular processes, happening on the longer timescale, rather than to light itself. Response to light exposure was essentially immediate in Tar, Tsr and Aer-only strains at high light intensity, while both Tap and Trg-

only strains demonstrated gradual rather than abrupt response (fig. 4.9). This gradual response kinetics can be a result of averaging abrupt single-cell level responses with varying delays. Alternatively, if tumble bias increases gradually on the single-cell level, then response kinetics might reflect the dynamics of the secondary processes caused by light. Response time to light turn-on in Aer and Trg-only strains decreased with light intensity (fig. 4.12, 4.11). This again might not necessarily reflect the change in the intrinsic response kinetics, but rather higher synchronization of individual cell response. In order to test that single-cell level trap experiments are necessary [81]. Different kinetics of responses mediated by different receptors may reflect different sensing mechanisms: e.g. Tar and Tsr may be responding to light or parameters that change immediately with light intensity, while Tap, Aer, and Trg may be sensing light-induced changes that take longer to take an effect.

Adaptation kinetics to change in illumination conditions that we observe in single receptor mutants is consistent with what is known about the mechanisms of adaptation for different receptors. Both Tar-only and Tsr-only strains reach steady-state tumble bias in less than 10 s after the light has been turned on or off, which is reflective of methylation-dependent adaptation. No dependence on light intensity was observed for Tar and Tsr-only strains (fig. 4.12). Aer receptor adapts through an unknown methylation-independent pathway that also tends to be slower and consequently, we do not observe significant adaptation for Aer-only strain at least within the duration of our experiment. Finally, Tap and Trg cannot adapt through methylation in the absence of Tar or Tsr receptors. Slow adaptation kinetics that we observe both for Tap-only and Trg-only mutants might be due to motor remodelling [133], or, alternatively, it might reflect internal dynamics of the processes perturbed by light.

4.5 Conclusions

My results on the light responses of *E. coli* chemotaxis mutants and single receptor strain strongly suggest that response to light in wild-type strain is mediated by receptors, requires functional *CheY* and adaptation is due to receptor de-methylation. Results for single-receptor mutants *E. coli* strains expressing only one out of five chemotaxis receptors demonstrate that all five receptors are able to independently mediate changes in motility behavior in response to blue light exposure, which is a novel and unexpected result. Therefore, light emerges as the first universal tactic stimulus that affects all five *E. coli* chemotactic receptors. While 4 out 5 receptors mediate tumbling, or repellent response to light, Tap receptor mediates running, or attractant response. I have tested whether, despite its low abundance, Tap receptor contributes to the responses in multiple receptor mutants, where receptor expression levels are similar to the wild-type. I will discuss these

results in the Chapter 5. Measuring phototaxis response in single-receptor strains at different wavelenghts across the visible spectrum may provide some insights about the nature of the photosensitive entity involved in phototaxis.

Chapter 5

Phototaxis response in multiple receptor strains

As discussed in Chapter 4, my results for the single-receptor *E. coli* strains suggest that all chemoreceptors are able to independently mediate light-induced changes in tumble bias. I was interested in measuring the contribution of the low-abundance receptors, Aer, Tap, Trg, to the response of multiple-receptor strains. In general, signalling, mediated by low-abundance receptors, is amplified through an interaction with high-abundance receptors. In this Chapter, I will discuss the higher-order organization of receptors, which forms a structural basis for signal amplification and review models of receptor interaction (section 5.1). Then, I will show my results for multiple-receptor *E. coli* strains and their implications (5.3).

5.1 Background

As I have already mentioned in the Introduction (1), chemotaxis is characterized by the extreme sensitivity; an *E. coli* cell responds to concentration changes as small as ∼3 nM, corresponding to just a few molecules per cell volume [6]. It means that even small changes in the receptor occupancy state, due to ligand binding, can produce noticeable changes in the swimming behavior. Signal amplification in the network is realized through cooperative binding of CheY-P to the flagellar motor [76] and through receptor-receptor interaction, which I will discuss in more details below.

5.1.1 Receptor organization as a structural basis for signal amplification

Two levels of receptor structural organization have been shown experimentally. Cross-linking, in *in vitro* reconstitution and CryoEM studies, show that structural and functional unit of chemotaxis - two heterotrimers of receptor homodimers which bind one CheA homodimer, and two molecules of the coupling protein (fig. 5.1) *CheW* [55, 110, 134, 135]. Trimer contact residues are conserved among all five chemoreceptors. Tar, Tsr, Aer, and Trg have been shown to readily form trimers in cross-linking studies [134, 136]. No signal amplification was shown on this first level of organization. In experiments with isolated mixed-receptor core complexes, reconstituted in Nanodiscs, kinase activity was only partially inhibited, even in saturating

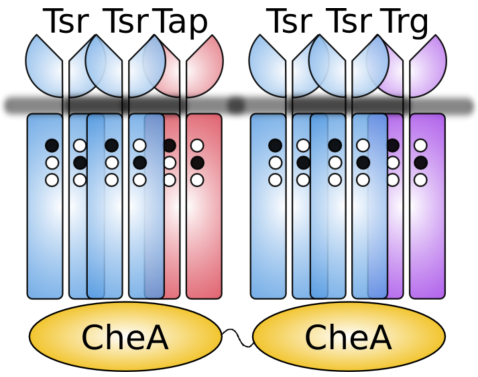

Figure 5.1: The core unit of chemotaxis signalling is two heterotrimers of receptor homodimers with one CheA homodimer. Low abundance receptors can interact with high abundance receptors within one unit.

concentrations of ligand [137]. This is consistent with CryoEM studies that show that only one receptor dimer within a trimer is directly interacting with *CheA* [55]. Kinase inhibition is, therefore, only transmitted through direct interactions of a receptor with the kinase, not through dimer-dimer interaction within the core complex [110].

On the next organizational level, core functional units are organized in hexagonal lattice patches, the largest of which are situated at the cell poles [55, 138]. The lattice forms a structural basis for signal amplification in the chemotaxis network; it was shown that attractant binding to a single receptor can influence up to $\sim$ 35 *CheA* molecules, which requires long-distance interaction between receptors [139]. *CheA* - *CheW* hexagonal rings, which hold the lattice together, are thought to be responsible for signal transmission through the lattice, although the exact molecular mechanism is unknown [110].

Cooperative motor switching and cooperative receptor activation, together, give about 100-fold amplification of the signal [111]. While motor cooperativity is believed to be constant, amplification and sensitivity on receptor level depend on the size of the signalling receptor cluster and relative abundances of different receptors. There has some been mixed evidence on cluster rearrangement due to ligand binding [140, 141]. It was also shown that cluster size depends on growth conditions, with bigger clusters forming under poor nutrient limitation leading to higher sensitivity [111]. Relative receptor abundance changes with bacterial density throughout the growth curve resulting in shifting amino acid preference. Therefore, a cell has several mechanisms that enable it to fine tune its chemotactic sensitivity depending on the environmental conditions.

As shown in table 4.1, receptor abundances differ by several orders of magnitude. Signals from low abundance receptors are amplified through interaction with high abundance receptors through the receptor lattice and can, therefore, still result in chemotaxis response. When all receptors respond to the same stimuli, as is the case for phototaxis, it is not clear how the signals from different receptors will be integrated to produce a response, which was a motivation for the experiments done in this Chapter. I will discuss my

results with multiple receptor mutants below.

5.2 Methods

Experiments and data analysis were performed as described in Chapter 5.

5.3 Results

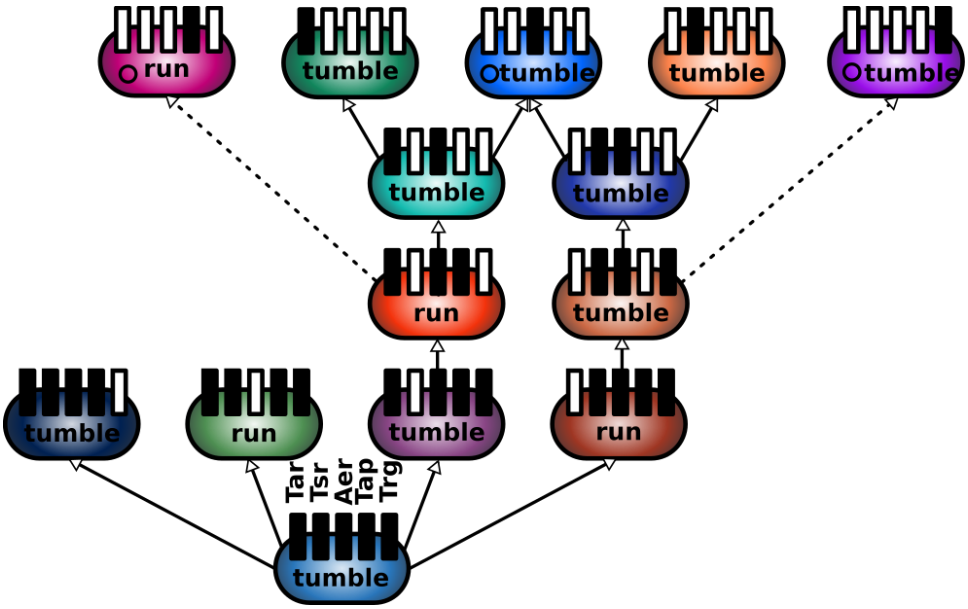

Figure 5.2: *E. coli* receptor mutants used in this study. Response to light is indicated as a run/tumble. Receptors are indicated by black rectangles if present and by white ones if absent, the order corresponds to that shown for wild-type strain. Solid arrows connect mutants that differ from each other by one receptor type. Dotted arrows connect mutants that differ by two receptor types.

All the strains for which I have measured light response, including single-receptor ones with corresponding responses, are shown on the figure 5.2. Expectedly, strains that did not contain Tap receptor, which was shown to mediate running response to light (Chapter 4), exhibited a tumbling response to light (fig. 5.3a, fig. 5.4). The amplitude of the response for those strains increased with the number of receptors mediating a tumbling response (fig. 5.3b). Remember that both Aer and Trg receptors were overexpressed from the plasmid (as well as Tap), so comparing amplitudes of Aer-only and Trg-only strains to those of multiple receptor mutants containing these receptors is not meaningful. Interestingly, response amplitude for two- and three-receptor strains without Tap was higher than for the wild-type strain, which suggests that tumbling response in wild-type might be 'weakened' by a 'running' Tap receptor. Response and adaptation kinetics in

these strains were similar to the Tsr-only strain. Fast adaptation kinetics mean that adaptation is mediated by the demethylation of Tar and Tsr receptors, so the de-activation of Aer and Trg receptors must be due to interaction with Tar and Tsr.

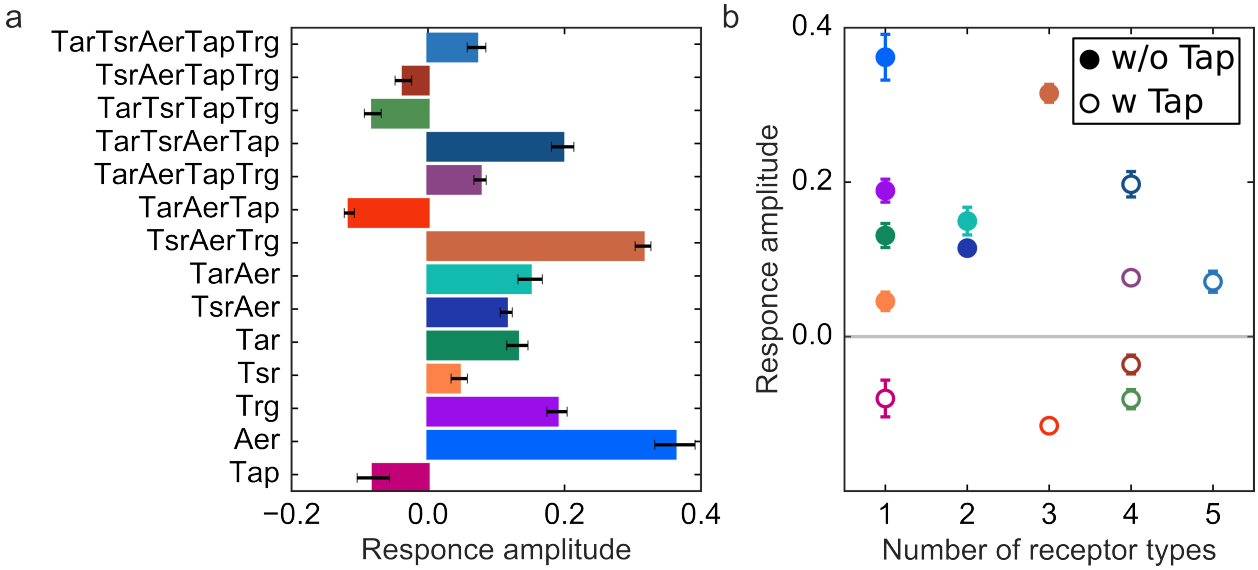

Figure 5.3: Phototaxis response amplitude in *E. coli* strains with different number of receptors.

Tumble bias traces for Tap-containing strains are shown on the figure 5.5a and b. I have found that, despite being a low abundance receptor (fig. 5.5d), Tap can determine the direction of the response in multiple-receptor mutants. In these strains, relative receptor abundance is similar to that of the wild-type strain [117], and therefore, the running response can only be explained by the strong amplification of the Tap-mediated response through receptor-receptor interaction.

In general, the presence of Tap receptor was necessary but not sufficient to observe the running response. Indeed, adding Tsr or Trg receptors to $\Delta Tsr\Delta Trg$ mutant resulted in a drastic switch of the response from running to tumbling (fig. 5.5a, c). This result is especially surprising given that Tsr only mediates a weak tumbling response on its own (fig. 4.9), and Trg is a low-abundance receptor, and further underlines the importance of interactions between receptors in determining the integrated cell-level response. In addition to $\Delta Tsr\Delta Trg$, I have measured running response in ΔAer strain. ΔTar strain showed a combined run + tumble response.

It might be educating to attempt to interpret results for four-receptor strains by comparing them to the wild-type (fig. 5.3). Removing both Aer and Tar from wild-type background causes a response switch from tumbling to running, which makes sense intuitively, as Aer and Tar mediate tumbling responses on their own, and therefore in their absence relative contribution of 'running', Tap receptor increases (fig. 5.3,

fig. 5.5). At the same time, the effect of Trg receptor depends on the background, response amplitude increases upon removal of Trg receptor from wild-type background (fig. 5.3), while removing Trg from the ΔTsr background causes response switch from tumbling to running (fig. 5.5). Similarly, removing Tsr from the wild-type background does not have an effect, while removing it from the ΔTrg strain causes a switch from tumbling to running (fig. 5.5). Rigorous quantitative interpretation of these results requires simulating phototaxis response. The effect of light can be formalized as an external perturbation causing a change in the free energy difference between active and inactive receptor states. The size of the effect for individual receptors can be inferred from single-receptor strains.

In the discussion above, I assumed that the only difference between different strain is the number of receptor types. It might be, however, that knocking out receptors affects the expression of other chemotactic proteins within the same operon. Thus Tar, Tap, *CheR*, *CheB*, *CheY*, and *CheZ* are all in one operon; while Tsr, Aer, and Trg are in separate operons [95].

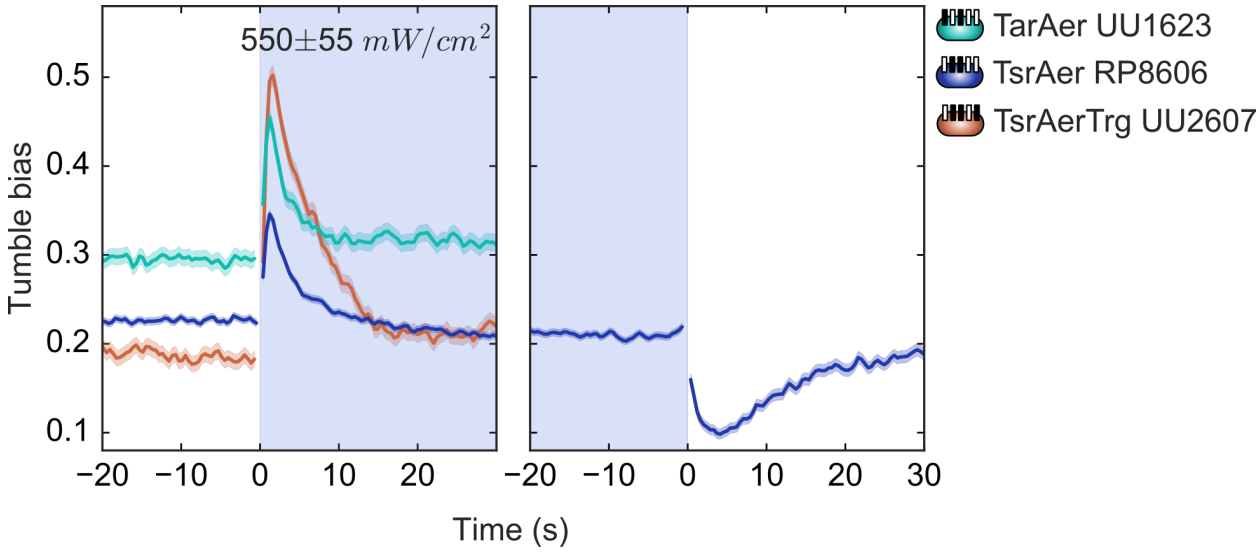

Figure 5.4: *E. coli* strains that do not contain Tap receptors, mediate a tumbling response to light.

5.4 Conclusions

I have found that despite being a low abundance receptor, Tap is capable of determining the direction of light response in multiple receptor mutants. The presence of Tap, was necessary but not sufficient, to observe a running response. My results also suggest that interactions between receptors play an important role in the integrated response. Simulating behavioral output of the chemotaxis network in response to light and fitting it to the experimental data may provide a way to quantify interactions between different types of receptors.

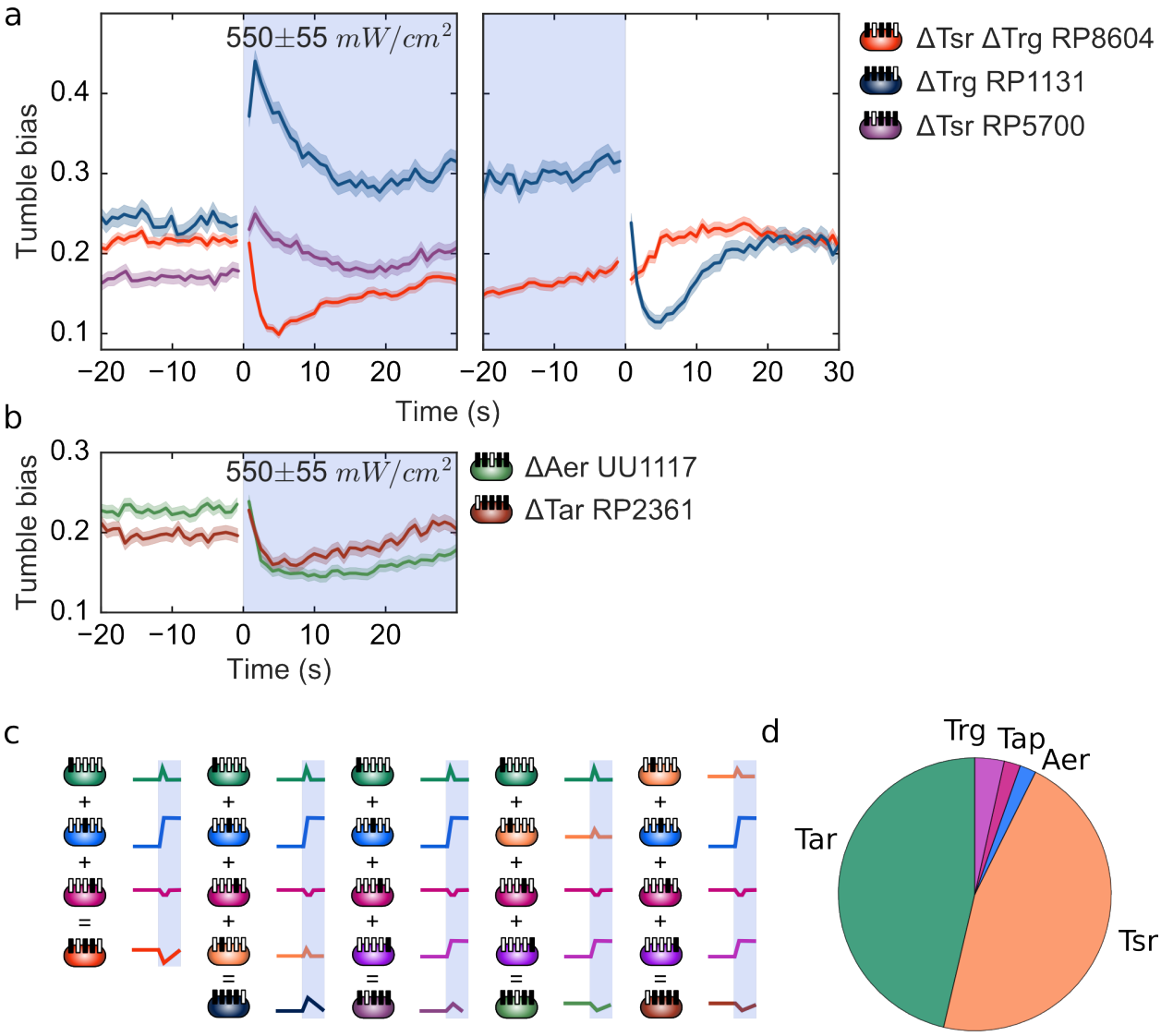

Figure 5.5: Contribution of individual receptors to the response of the multiple-receptor mutants is strongly non-additive. (a) - Tumble bias traces of ΔTrg and ΔTsrΔTrg strains before and during light exposure are indicated by the blue shaded area. (c) - Cartoon showing schematic responses of single receptor strains that contribute to the responses of multiple receptor strains. Direction and kinetics in strains with multiple receptors are different from what you would expect from simple addition and is, therefore, a combined result of individual receptor responses and their interactions. (d) - Pie chart of the relative abundance of different receptor types in the wild-type strain, based on data from [117].

Chapter 6

Effect of blue light on PMF

As discussed in Chapter 4, blue light response in *E. coli* is mediated by chemotactic receptors; and all five receptors are able to mediate light-induced changes in tumble bias. At the same time, to the best of our knowledge, Aer is the only receptor that binds chromophore as a cofactor and, therefore, can be directly photosensitive. This suggests that other receptors might be responding to secondary processes caused by blue light. Wright and co-authors suggested, for example, that the Tar receptor might be sensing perturbation of the electron transport, or Proton-Motive Force (PMF), induced by blue light. So we were interested in exploring whether or not this is a plausible hypothesis. In this chapter I will first introduce electron transport as well as PMF and their role in motility and chemotaxis (6.1). I will then show my experimental results that suggest that light does indeed affect PMF, and finally I will show some data on chemotactic response to chemical PMF disrupters (6.3).

6.1 Background

6.1.1 PMF and electron tranport

The concept of PMF comes from Mitchell's chemiosmotic theory in which electron transport in respiring cells is coupled to the generation of an electrochemical proton gradient which drives the synthesis of ATP [142]. Proton electrochemical potential energy, $\Delta\mu_{H^+}$, has two components: electrical component - membrane potential, $\Delta\psi$, created by charge difference across the membrane, and chemical component created by proton concentration gradient across the membrane. Electrochemical work required to move the mole of protons against electric potential difference, $\Delta\psi$, and concentration gradient, $[H^+]_{in}/[H^+]_{out}$, can be calculated as follows:

$$\Delta\mu_{H^+} = F\Delta\psi + RTln([H^+_{in}]/H^+_{out}), \tag{6.1}$$

where F, Faraday constant, is the total charge per mole of singly charged entities, e.g. protons.

Proton-motive force, Δp, is then just $\Delta\mu_{H^+}/F$:

$$\Delta p = \Delta\psi + RT/F * ln([H^+_{in}]/H^+_{out}) = \Delta\psi - RT/F * \Delta pH/lg(e), \tag{6.2}$$

where ΔpH, is a pH difference across the membrane:

$$\Delta pH = pH_{in} - pH_{out} = -lg([H^+]_{in}) + lg([H^+]_{out}) = -lg([H^+_{in}]/H^+_{out}) \tag{6.3}$$

PMF is generated during respiration by electron and proton translocation across the membrane. First and foremost, PMF is used to generate ATP: energy released when protons are translocated down the concentration gradient is used to drive rotary engine of ATP-synthase which catalyzes the synthesis of ATP from ADP. PMF is also used to energize other processes in the cell such as ion transport and rotation of the flagellar motor, although there are bacteria with sodium-dependent motors as well [77, 142].

6.1.2 Swimming speed as a proxy for PMF

Over the years, a number of studies provided important insights into the mechanism of torque generation by a bacterial flagellar motor, speed-torque relationship, and the role of different structural elements of the motor [39, 77, 143, 144]. For the purpose of this discussion, I would like to focus on one aspect: the flagellar rotation rate is linearly proportional to PMF under both high and low viscous load [145, 146]. The measurements were performed when either bacteria tethered to the glass by the flagella in which case flagellar has to rotate the entire bacterial body (high load), or when a bacterial body is attached to the glass and a bead is attached to a short flagellar stub (low load) [145, 146]. Viscous drag of a full-length flagellum is roughly the same as that of a half-micron diameter bead which suggests that flagellar rotation rate in the free-swimming bacteria should be proportional to PMF as well [77].

A number of parameters contribute to bacterial swimming efficiency: geometric parameters of the helical flagellar bundle, number of flagellar filaments, and size of the cell body [79]. Therefore, relating flagellar rotation velocity to bacterial swimming velocity is non-trivial. With all else being equal, bacterial swimming velocity depends on PMF, and therefore can serve as a proxy measure of PMF.

The more direct way of estimating PMF would be to use a bacterial optical trap as it allows measurement of both body roll and flagella rotation frequencies [80]. However bacteria have to be under anaerobic conditions to prevent damage by IR-light excited triplet oxygen species while in the trap . This is different from the conditions of the 2D assay where bacteria are under aerobic conditions within the duration of the experiment (see section 2.3). As shown by the earlier studies, respiration, aerobic or anaerobic, is essential

for observing phototaxis in *E. coli* [1]. For these reasons as a first approximation, we decided to use changes in swimming velocity upon light exposure in the 2D phototaxis experiments as a qualitative measure of light effect on PMF or electron transport.

6.1.3 PMF and electron transport as chemotactic signals

Given what we know about chemotactic receptors, is it plausible that in addition to ligand-binding, they might be able to respond to cellular level processes such as electron transport or PMF change?

As discussed previously, both Aer and Tsr serve as signal transducers for energy taxis responses [147, 148]. More specifically, Tsr responds to changes in PMF and Aer senses redox state of the respiratory enzymes [123]. In general, both of these parameters are coupled to electron transport although the relationship may differ depending on the type of the Electron Tranport Chain (ETC). For example, an increase in PMF is associated with an increase of electron flow only for the branches of the ETC coupled to proton pumping, and may decrease with increased electron transport through non-coupled branches [45]. This means that Aer and Tsr actually perform an independent assessment of the intracellular energy level or the state of ETC, which potentially allows for more robust and efficient energy taxis.

Tar and Tsr have both been shown to respond to pH changes; pH increase causes Tsr-mediated attractant response and Tar-mediated repellent response [9] According to equation 6.2, PMF depends on the pH difference across the membrane so the change in the extracellular pH will affect PMF and, *vice versa*, electroneutral transfer of the proton during ETC will affect ΔpH. While Tap and Trg receptors have not been implicated in energy-taxis or pH taxis, it is not inconceivable that these receptors are capable of sensing PMF or some other membrane-associated parameter.

6.1.4 PMF disrupters

To test the hypothesis that Trg, Tap, and Tsr respond to changes in PMF caused by the light, we wanted to check whether or not they respond to chemically-induced changes in PMF. While there is a number of ways to chemically change PMF, such as changing pH, the concentration of electron donors and acceptors, and redox potential, we decided to use PMF disrupters because their effect on PMF is fast and PMF disrupters are not known to elicit chemotactic response independently from PMF, unlike, for example, pH.

PMF can be disrupted chemically using respiration uncouplers or respiratory poisons. As follows from the name uncouplers essentially decouple proton transport from producing useful work in the cell such as ATP synthesis or flagellar rotation by allowing protons to enter the cell on the uncoupler rather than through the e.g. ATP-synthase. The addition of uncouplers, therefore, results in the collapse of PMF and increased

rate of electron transport as a higher rate of proton flow causes a higher rate of electron flow [142]. One of the commonly used uncouplers is carbonylcyanide m-chlorophenylhydrazone (CCCP). Th mechanism of action of CCCP and other protonophores, or proton tranlocators, can be described as follows: negatively charged form of the protonophore P^- reacts with a proton H^+ to form a neutral compound PH which diffuses across the membrane and dissociates into H^+ and P^- on the other side of the membrane [149, 150]. Protonophores are able to cross the lipid bilayer both in its negative and charged form [151].

Another type of PMF disrupters, the so called respiratory poisons (e.g. sodium azide), act by inhibiting oxidative phosphorylation. Their addition causes the collapse of PMF and the decrease in electron transport.

6.2 Methods

6.2.1 2D assay with CCCP

Both CCCP and sodium azide have been used in chemotaxis studies to collapse PMF [146, 152], however, in the experiments described below, I used CCCP as it is much less toxic and therefore easier to work with than sodium azide. CCCP only dissolves in organic solvents such as ethanol, methanol, or DMSO. I choose to use methanol for preparing the stock solution because CCCP solubility in methanol is higher than in ethanol (10 mg/ml vs 1 mg/ml), and, therefore, the final concentration of the solvent in the bacterial media can be lower. Furthermore, while both ethanol and methanol are repellents for *E. coli*, threshold sensing concentration is much higher for methanol than for ethanol: 10 - 100 mM *vs* 1 mM as measured by the capillary assay [153].

I used 10 μm CCCP as stimuli which should be enough to collapse PMF according to previous studies [146, 152]. The resulting concentration of methanol in the final media was 0.02 %, or 5 mM, so I also performed control experiments only with methanol to en sure that the response is caused by the addition of CCCP, not methanol. The stock solution was 200 μm CCCP and 0.4 % methanol.

The 2D assays with chemical addition were performed the same way as the 2D phototaxis assays (see appendix C.4 for more details). Bacteria were grown and harvested as described previously. For each experiment baseline movies were recorded with bacteria in TMB only. A chemical, CCCP or methanol, was added right before chamber assembly, and time, passed between the addition of the chemical to bacterial suspension and recording of the first movie, was noted in order to shift the resulting response traces accordingly.

The nature of the 2D assay does not allow us to probe the kinetics of the response right after chemical addition so we can only detect a response in strains that do not exhibit adaptation to the stimuli, such as Aer-only UU1250 + pSB20 and Trg-only UU1250 + pPA705. I also wanted to look at one of the running

strains. As discussed previously, Tap-only strain only responds to light when receptors are activated by repellent phenol. Instead of Tap-only strain, I used the RP8604 strain that mediates the running response to light and does not adapt fully, at least not within 30 s. Aer-only strain was used as a control as it is known to respond to changes in PMF.

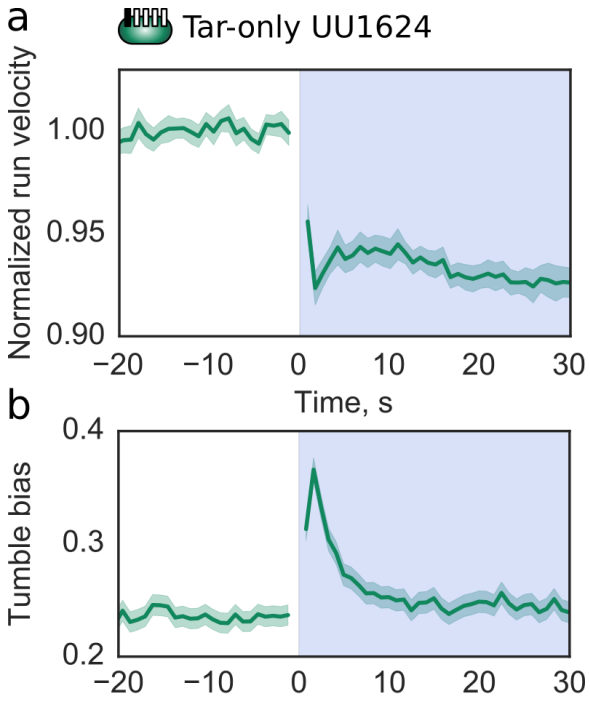

Figure 6.1: (a) Normalized run velocity and (b) tumble bias time traces for Tar-only UU1624 strain.

6.2.2 Data analysis

Swimming velocity from phototaxis assays

Swimming velocity is the velocity during frames that were assigned to runs. Because absolute swimming velocity may differ from experiment to experiment, I wanted to look for trends in relative, or normalized, velocity instead. Time traces of the normalized run velocity were calculated as follows: each individual velocity trace coming from a different movie was divided by the prestimulus velocity calculated in a 20 s window prior to light exposure. Traces for each strain were then shifted to align 'light on' or 'light off' frames and averaged using 10 frames non-overlapping rolling window.

As tumble assignment procedure is not perfect, not all tumbles are detected which is reflected in a sharp decrease in swimming velocity right after light exposure for strains with tumbling response to light (fig. 6.1). I think this is an artifact of data analysis rather than a real effect, because in all non-responding strains, or

those with small response amplitude, the velocity decrease was gradual (see for example velocity traces for the receptorless UU1250 strain on the fig. 6.2). For the strains with tumbling response, excluding those that show no adaptation to light (Aer-only and Trg-only) instead of plotting time traces, velocity analysis was done in the following way: velocities were calculated in a 4 s window after 30 s of light exposure and then 10, 20 and 30 s after the light is turned off for each individual movie. Observation is limited by 30 s to avoid contribution of unexposed bacteria swimming in the field of view (see section 3.3). Velocities calculated in this way for each trace are then normalized to the prestimulus velocity calculated in a 20 s window and averaged across all the traces for a particular strain (fig. 6.3a).

Decrease and recovery of normalized run velocity are calculated as illustrated on 6.3a by averaging datapoints for different strains shown on fig. 6.3a . Velocity decrease, $\Delta\nu_{on}$, is simply average decrease of normalized run velocity after 30 s of light exposure averaged across all strains. Velocity recovery, $\Delta\nu_{off}$, characterizes fraction of $\Delta\nu_{on}$ recovered 30 s after light has been turned off and is calculated as $(\Delta\nu_{on} - \Delta\nu_{off})/\Delta\nu_{on}$.

Data analysis from 2D assays with CCCP

Movies from 2D assays with CCCP and methanol are analyzed the same way as phototaxis movies. Prior to averaging, each trace is shifted by the time passed between the addition of the chemical and recording of the movie corresponding to this trace. Velocity traces are normalized by the average velocity from the movies recorded on the same day in TMB only. For bar plots, tumble bias and velocity in the presence of CCCP or methanol are averaged within first 110 s after addition of the chemical (fig. 6.4b and c).

6.3 Results

6.3.1 Light effect on swimming velocity

I have found that light exposure causes a gradual decrease in swimming velocity for all strains that we have studied (fig. 6.3a). The magnitude of the decrease in normalized swimming velocity after 30 s of light exposure $\Delta\nu_{on}$ depends on the light intensity and varies from 0 at $44\,mW/cm^2$ to about 8% at $550 mW/cm^2$ on average (fig. 6.3b). The decrease in velocity is partially reversible and, therefore, cannot be attributed purely to photodamage (fig. 6.3a). About 50% of the velocity decrease recovers 30 s after the light is turned off at all intensity levels (fig. 6.3c). It is possible that full recovery can be achieved with enough waiting time, however, as discussed previously, (section 3.3) under conditions of our experiment we cannot distinguish between velocity recovery for previously exposed bacteria and velocity increase due to unexposed

bacteria swimming in the field of view more than 30 s after light has been turned off.

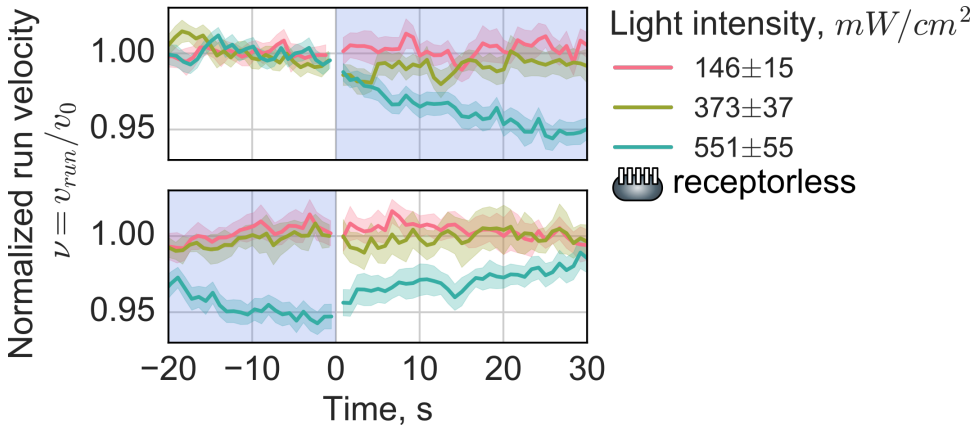

Figure 6.2: Light exposure causes reversible decrease of swimming velocity. Normalized velocity traces are shown for receptorless UU1250 strain. Light intesnity is indicatd by the color, blue shaded area indicates light exposure. Velocity was normalized by its prestimulus value (calculated in a 20 s window before light on) for traces coming from different movies separately and then averaged between traces.

These results are consistent with the hypothesis that blue light perturbs electron transport or affects PMF causing a reversible decrease in swimming velocity. The mechanism of this effect is not clear and our experiments do not provide information that might help to elucidate it. However, we can speculate that light causes photoreduction of the electron carriers, e.g. of Flavin Adenine Dinucleotide (FAD), in the cytoplasmic pool thereby disrupting electron transport. FAD absorbs in blue region and is known to undergo photoconversion between its different redox and protonation states as a co-factor of LOV and BLUF flavoprotein light sensors [127, 154, 155].

6.3.2 Response to chemical PMF disruptors

As discussed above, Tap, Tar and Trg receptors have not been implicated in sensing PMF. Therefore I wanted to test whether these receptors can respond to chemically-induced changes in PMF, and whether the sign of the response will be the same as in the case of light. As expected, I observed tumbling response to the addition of 10 μm CCCP, but not to methanol in Aer-only strain. The adaptation took 150 s which is consistent with the lack of adaptation to light within 30 s for this strain (fig. 6.4). CCCP addition also caused about 20% decrease in running velocity in Aer-only and Trg-only strain, but not in RP8604. No change in tumble bias was observed in either Trg-only or RP8604 strain. Trg-only strain is unable to adapt, as we have shown previously, so it is unlikely that the lack of response is due to adaptation. This result suggests that Trg receptor is unable to sense changes in PMF, however, it does not rule out the possibility that it might respond to decrease in electron transport as uncoupler CCCP collapses PMF causes an increase

in electron flow.

6.4 Conclusions and future directions

In summary, I have shown that light exposure causes a reversible decrease in running velocity which is consistent with the hypothesis that light may be perturbing PMF or electron transport. These results also suggest that Trg receptor does not sense changes in PMF. To test whether it can sense electron transport, sodium azide, which collapses both PMF and electron transport, can be used in place of CCCP. Another alternative is to perform adaptation experiments in the trap which allows seeing the response immediately after the stimuli and therefore makes it possible to test strains with fast adaptation kinetics such as Tar-only UU1624 [81].

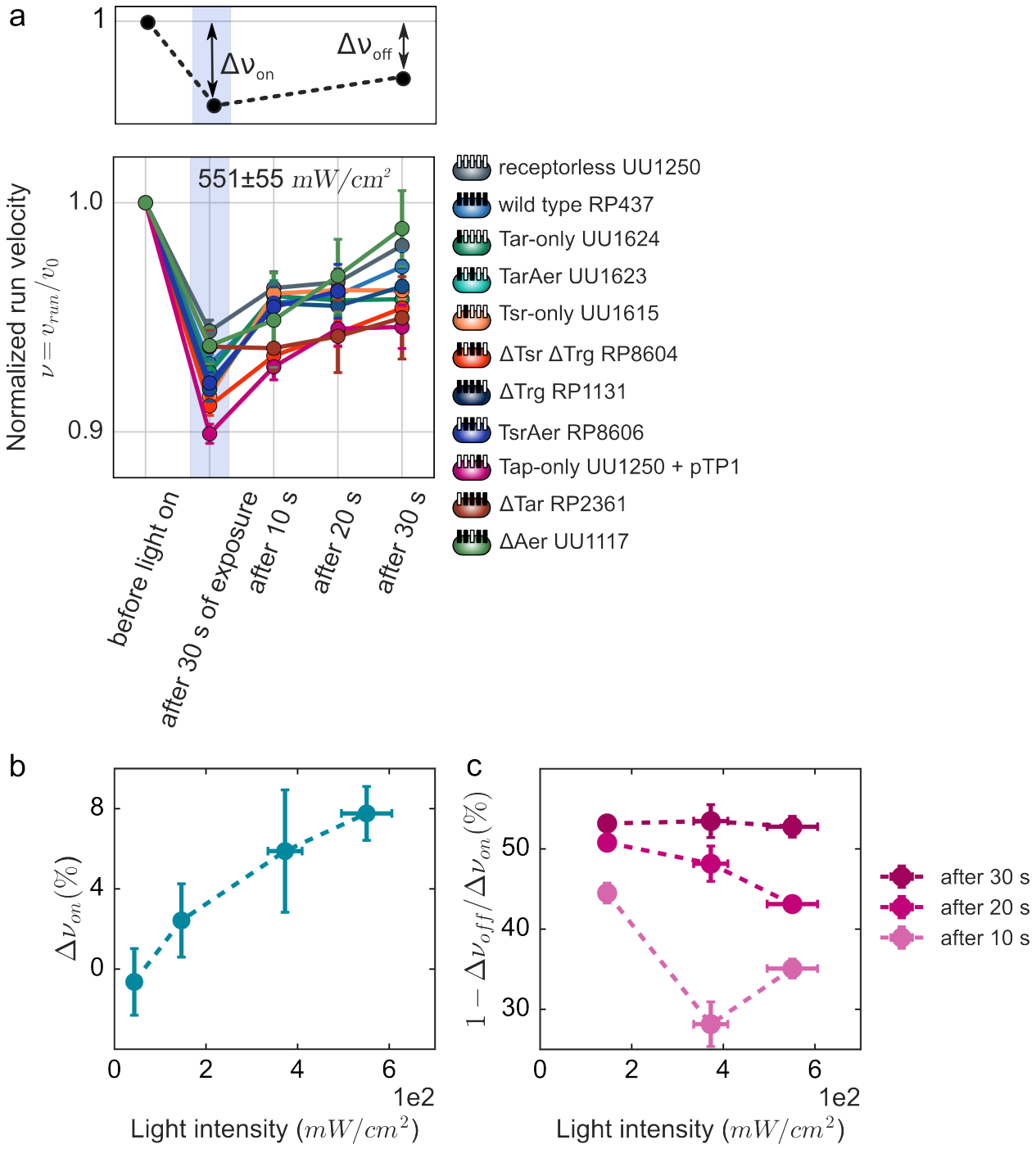

Figure 6.3: Effect of light on run velocity depends on the intensity. (a) Bar plot of the normalized swimming velocity for different *E. coli* strains. Velocity was calculated in a 4 s windows after 30 s of exposure to light, then 10, 20 and 30 s after the light was turned off, and normalized by the prestimulus value (calculated in a 20 s window before light on). Schematic shows how velocity decrease and recovery was calculated. The decrease in normalized run velocity $\Delta\nu_{on}$ was calculated as the difference between prestimulus velocity and velocity after 30 s of light exposure or $1 - \nu_{30s}$. Recovery is calculated as a difference between velocity decrease after 30 s of light exposure $\Delta\nu_o n$ and velocity decrease after 30 s after the light was turned off $\Delta\nu_o ff$. (b) Decrease in velocity *versus* light intensity. (c) Velocity recovery *versus* light intensity.

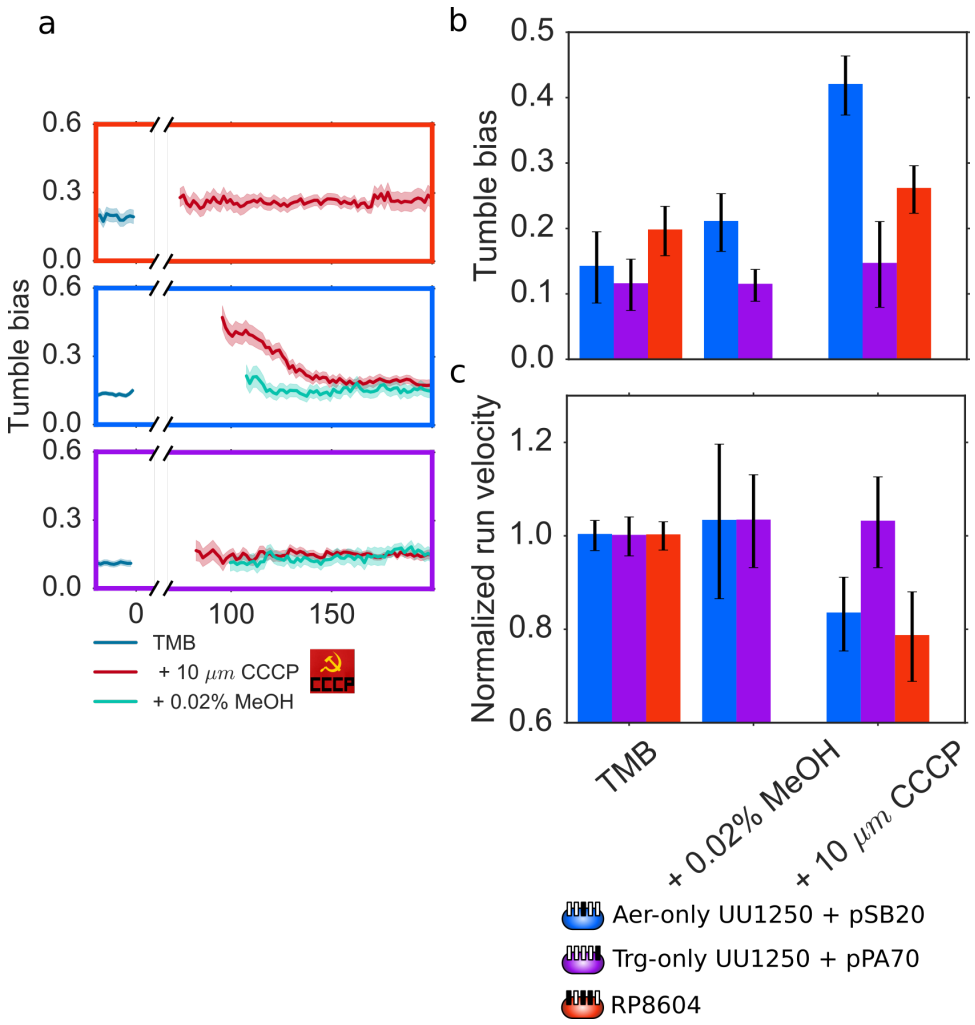

Figure 6.4: Effect of CCCP on the tumble bias and swimming velocity. (a) Tumble bias traces of three *E. coli* strains (indicated by the color) in TMB, in TMB with 0.02% Methanol, and in TMB with 10 μm CCCP and 0.02% Methanol. Traces with CCCP and Methanol were shifted according to the time delay between addition of the chemical and recording of the movie. (b) Bar plot of the tumble bias in different media. Tumble bias in TMB only was calculated as average across full traces, tumble bias in CCCP and Methanol was averaged within first 110 s after addition of the chemical. (b) Bar plot of the normalized run velocity in different media, averaging was performed the same way as in (c).

Chapter 7

Factors affecting blue light response in *E. coli*

As mentioned in Chapter 4, the amplitude of the blue light response for wild-type *E. coli* bacteria grown in M9 minimal media with succinate as a growth substrate turned out to be significantly lower than for those grown with glycerol. I have found that to be the case for several other strains as well, suggesting a coupling between phototaxis and metabolism, which is not all that surprising given the potential effect of light on PMF that I discussed in Chapter 6. In this Chapter, I will first review some relevant background information: metabolism-dependent chemotaxis and examples of translational regulation of chemotaxis (section 7.1). I will then compare light responses for different *E. coli* strains grown with different substrates 7.3. Finally, I will discuss variability of light response I observed, day-to-day and within one experiment, as well as potential causes of such variability.

7.1 Background

As discussed previously in Chapters 1 and 4, chemotaxis in *E. coli* can be both directly dependent on metabolism, as is the case for 'energy-taxis', and can be indirectly affected by the type of growth substrate, growth stage or the density of bacteria. Below I would like to reiterate some point that I have already mentioned before in relation to *E. coli* bacteria specifically.

7.1.1 Metabolism-dependent chemotaxis in *E. coli*

As discussed in Chapter 4 and 6 Tsr and Aer receptors mediate 'energy-taxis' responses in *E. coli* with Tsr sensing change in the PMF and Aer sensing change in the redox state of respiratory enzymes [123]. 'Energy-taxis' is a type of metabolism-dependent chemotaxis, because in order to elicit behavioral response a compound must be metabolized and produce subsequent changes in the ETC [8, 16, 45]. Different carbon sources and electron acceptors require a different set of enzymes [156], as a results, bacteria will only be able to chemotax towards those chemicals in the presence of which they were grown and therefore had a chance to express appropriate enzymes. Exceptions to this are glucose and oxygen: these are, respectively,

the preferred carbon source and electron acceptor for *E. coli* and bacteria always express a set of enzymes required for glucose and oxygen metabolism.

7.1.2 Translational regulation of chemotaxis in *E. coli*

In addition to being directly dependent on metabolism, chemotaxis and motility can be affected by growth conditions, possibly through translational regulation. There are several studied examples of such regulation. The size of the receptor signalling team and, therefore, chemotactic sensitivity increases for bacteria grown under nutrient limitation, potentially to ensure more efficient navigation towards nutrient sources [111]. Relative abundance of different types of receptors changes with bacterial density irrespectively of the growth stage, possibly to enable chemotaxis towards amino acids in the order of preference [51]. And finally, motility and, therefore, the ability to perform chemotaxis depends on growth conditions as well. For example, bacterial motility is impaired during growth on glucose [46], possibly due to downregulation of cAMP [48]. Additionally, bacterial swimming velocity changes throughout growth curve in response to either growth stage or bacterial density [49].

7.2 Methods

Experiments and data analysis were performed as described in Chapter 4. Bacteria were either grown in M9 with succinate and resuspended in TMB with succinate or grown in M9 with glycerol and resuspended in TMB with lactate, unless noticed otherwise.

7.3 Results

7.3.1 Blue light response is affected by the growth substrate

As mentioned in Chapter 4, the tumble bias change in response to light that I observed for wild-type *E. coli* strain RP437 had lower amplitude as compared to results by Wright *et al* [1], which is why I used significantly higher light intensity (550 mW/cm^2 vs 7 mW/cm^2). I was able to reproduce their results at lower light intensity when I used the same substrates in growth and motility media, namely when growing bacteria in M9 with glycerol and resuspending them in TMB with lactate (fig. 4.7). I have also performed experiments with bacteria grown in M9 with succinate or glycerol and resuspended in either TMB with lactate or succinate, and I have found that growth substrate had a larger effect on the response amplitude than carbon source in the motility buffer (fig. 7.1). Kinetics of the response were affected to a lesser extent;

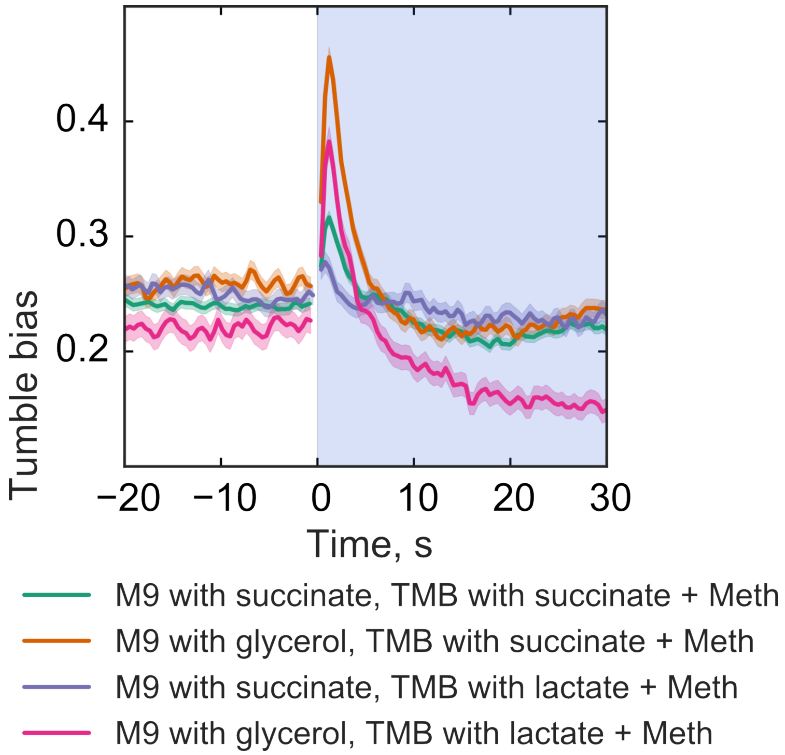

Figure 7.1: Growth substrate has larger effect on the light response than motility media. Light response of wild-type strain RP437 grown in M9 with glycerol or succinate, resuspended in TMB with succinate or lactate.

in all four cases, bacteria exhibited fast response and adaptation kinetics (fig. 4.7).

One might argue that when growing bacteria in succinate and resuspending in TMB with succinate I am not switching the substrates between the growth and motility medias, while in the case of glycerol I am, either to succinate or lactate, which might affect methylation state of energy-taxis receptors if bacteria did not have enough time to adjust to the new substrate. I did, however, perform experiments with several strains grown in M9 with glycerol and resuspended in TMB glycerol, and the results were similar to those I got when bacteria were resuspended in TMB with succinate (data not shown).

I have measured response for the RP347 strain grown in glycerol at different light intensities (fig. 7.2). Similar to results for bacteria grown in succinate (fig. 4.12), I have found that response amplitude increased and response time decreased with light intensity (fig. 7.2). In addition to that, adaptation time slowed down with light intensity.

To investigate the phenomenon further I have measured light response for several other *E. coli* strains grown in M9 with glycerol and resuspended in TMB with succinate. Interestingly, it turned out that two strains that were previously found to exhibit running response to light, ΔAer UU1117 and ΔTar RP2361, when grown in glycerol, responded to light by tumbling (fig. 7.3). For both strains, the initial tumbling

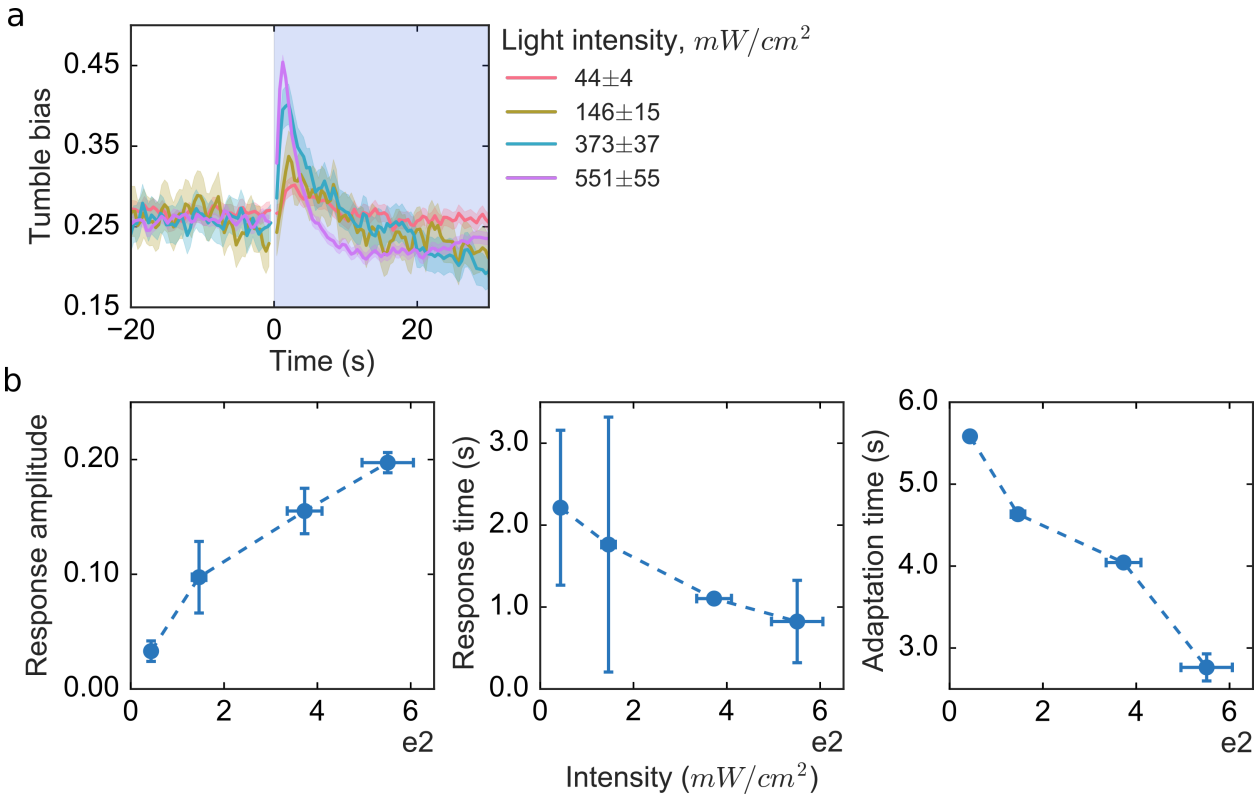

Figure 7.2: Light response of wild-type strain RP437 grown in M9 with glycerol, motility media - TMB with succinate, at different light intensities.

response was followed by undershoot that closely matched tumble traces corresponding to growth in succinate (fig. 7.3a dotted *vs* solid lines). Especially for the Δ*Aer* UU1117 strain, the response trace looks like a combination of tumbling and running responses with different kinetics. This suggests that the difference between responses might be due to stronger tumbling component for bacteria grown in glycerol, which is also consistent with a higher amplitude of response for the wild-type RP437 strain grown in glycerol (fig. 7.1).

I have also looked at some of the single-receptor mutants grown in glycerol. Responses for Tsr-only, Tar-only and TarAer strains were very similar, both when they were grown in glycerol and in succinate, although the response amplitude was slightly higher for the Tsr-only strain when grown in glycerol.

Taken together, these results suggest that type of carbon source in the growth media has a major effect on the amplitude of the tumbling response to light although the mechanism of that effect remains unclear (fig. 7.3b dotted *vs* solid lines). Below I will discuss possible explanations, but at this point these are just speculations as I do not have enough experimental evidence to confirm or completely rule out any of those.

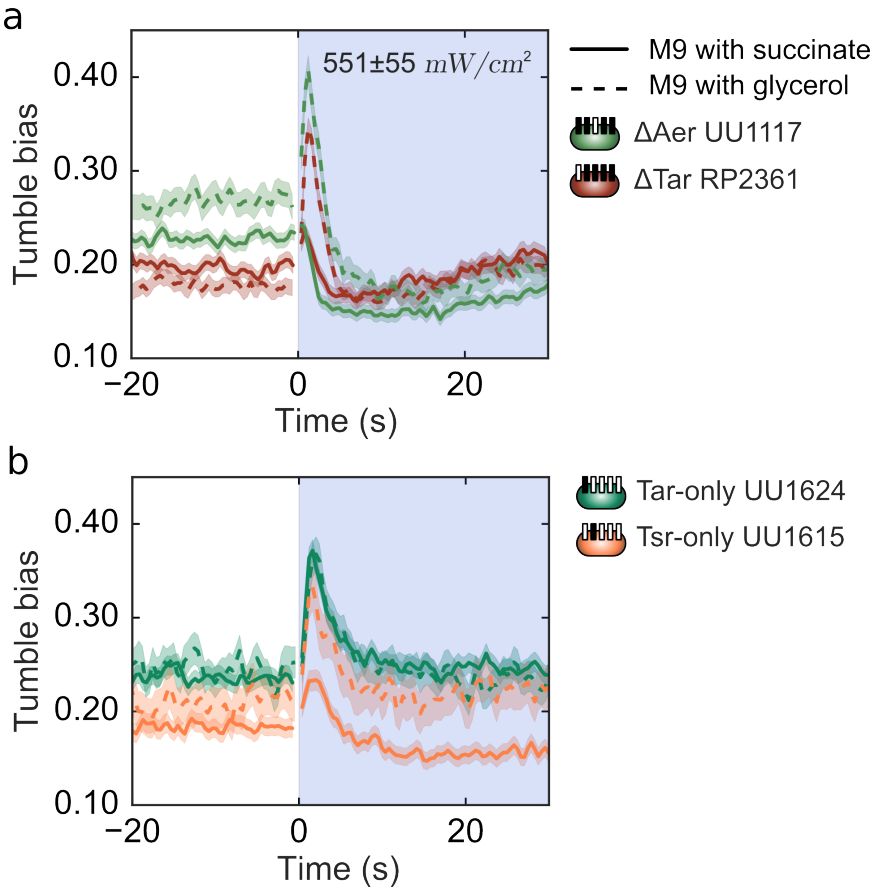

Figure 7.3: Effect of growth substrate on the direction of light response. (a) Strains that respond to light by running, Δ*Aer* UU1117 and Δ*Tar* RP2361, when grown in succinate (solid line) switch their response when grown in glycerol (dotted line). (b) Responses of Tar-only and Tsr-only strains do not depend on growth substrate.

Growth substrate or bacterial density affect receptor abundance?

Can the difference in responses between bacteria grown in different growth substrates be attributed to different density of bacteria rather than growth substrate *per se*? It is possible that relative abundance of different receptor types is different for bacteria grown in different growth substrates. In the study of the stoichiometry of the chemotactic network components, Li and Hazelbauer have found that absolute numbers of receptors and chemotactic proteins can vary significantly depending on the strain and growth media. At the same time, standard deviations of the pairwise ratios between abundances of different components for different strains and growth medias were comparable or modestly larger than those measured for the same strain and growth conditions in independent replicates and varied from 4 to 30% [117]. One caveat is that they measured the total abundance of Tar and Tsr receptors and, therefore, their results would not reflect the change in Tar/Tsr ratio. Moreover, given the signal amplification on the receptor level in the

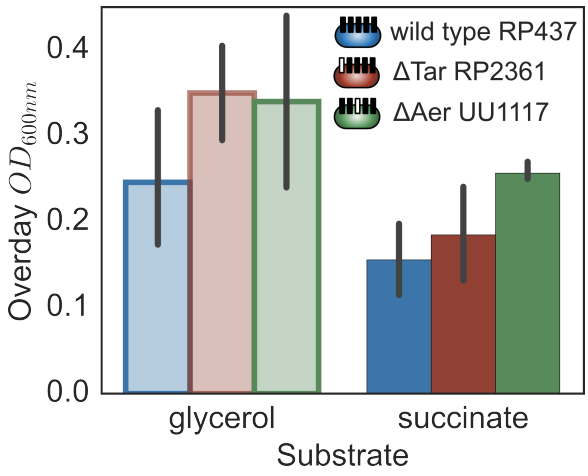

Figure 7.4: Optical density OD_{600nm} of the overday cultures grown in M9 with glycerol and M9 with succinate.

chemotactic network, it is possible that even small changes in relative receptor abundance may produce noticeable changes in the behavioral output [51].

Bacteria reach higher density values when grown in glycerol (fig. 7.4). At the same time, it was shown that Tar/Tsr ratio increases with the density of bacteria [51]. Can higher response amplitude for bacteria grown in glycerol be explained simply by the larger contribution of the Tar receptor? The Tar-mediated response has a higher amplitude than that of Tsr, but only in succinate not in glycerol, so this explanation would not tie up all the loose ends.

Finally, growth conditions may affect steady-state methylation state of individual receptors and therefore their contribution to the integrated response.

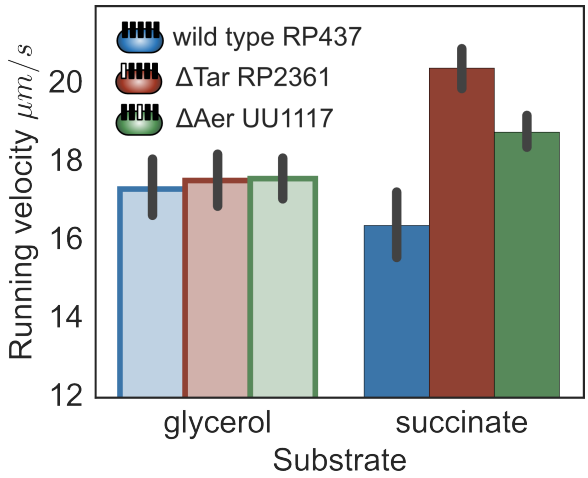

Figure 7.5: Swimming velocity of bacteria grown in M9 with glycerol and M9 with succinate.

Growth substrate *vs* swimming velocity

As reviewed in the Introduction, both the type of growth media and bacterial density may affect bacterial swimming velocity (7.1). In Chapter 6, I have discussed the possibility that the light sensing mechanism is related to the light-induced changes in swimming velocity. Maybe the change in the light response for some mutants can be explained by the differential effect of light on their swimming velocity depending on the growth conditions?

First, I wanted to test whether swimming velocity is actually affected by growth substrate. Swimming velocity was indeed higher in RP2361 ΔTar and UU1117 ΔAer when grown in succinate as compared to glycerol, however, for wild-type RP437 strain there was no significant difference between velocities in two substrates (fig. 7.5). Then I wanted to compare the effect of light on swimming velocity in different growth substrates, so I performed analysis of velocity traces as described in Chapter 6. I have found that, similar to my previous results (fig. 6.3), light caused reversible decrease in swimming velocity for strains grown in glycerol (fig. 7.6a). Velocity decrease was comparable to that for bacteria grown in succinate and proportional to light intensity (fig. 7.6b). In conclusion, these results show that the effect of light on swimming velocity does not depend on the growth substrate.

Growth substrate causes switch in the direction of response?

It is possible that response mediated by one of the receptors switches direction depending on the growth substrate, which would result in the different response for multiple receptor mutants. Based on the results shown in figure 7.3, the only candidates would be the Tap receptor. However, so far I was not able to grow Tap-only strain in M9 with glycerol in order to test this hypothesis.

At this point, I can only speculate about potential mechanism of how growth substrate may affect the direction of the response. Both PMF and electron transport, which, according to my previous results (Chapter 6), may be perturbed by light and sensed by receptors, are coupled to central metabolism, and, therefore, may depend on the type of carbon source in the growth media. The difference between glycerol and succinate is that glycerol is channeled to central metabolism through glycolysis, while succinate is already an intermediate of the TCA cycle. When grown on glycerol, bacteria produce ATP by oxidative phosphorylation during respiration, and by substrate-level phosphorylation during glycolysis. In case of succinate, oxidative phosphorylation is the only source of ATP. Respiration is more energy efficient, as it yields more ATP molecules per unit of carbon source, however it also requires more enzymes [47]. The flux through TCA cycle and respiration is regulated transcriptionally in such a way that in faster growing cells larger fraction of resources is used to produce ribosomes, and consequently the expression of respiration enzymes is reduced

[47]. On glycerol bacteria grow faster than on succinate (see Appendix D.4). It might be that they rely on substrate-level phosphorylation as a source of ATP when grown on glycerol, and, consequently, have lower PMF, which at least partially agrees with my data on swimming velocity (fig. 7.5). Why would change in PMF due to different metabolism affect light response, is unclear to me, but at least there is a connection. One way to test that hypothesis would be to measure light response in bacteria grown on other types of glycolitic, e.g. galactose, and non-glycolitic, e.g. lactate, substrates.

The effect of metabolism

7.3.2 Variability of the response

In addition to differences between light responses for bacteria grown on different substrates, there was variability in the response between independent experiments performed under the same conditions as well as within one experiment. Variability was significantly larger for strains with multiple receptor types, presumably because integrated response is a result of both contributions of individual receptors and interaction between them, which can be affected by the change in relative receptor abundance or tightness of receptor clusters (fig. 7.7). Figure 7.7 shows tumble bias traces (each trace corresponds to one experiment, i.e. is average of the multiple movies recorded from the same experimental chamber) for wild-type RP437 and Δ Tar RP2361 strains, for which I observed the largest variability from experiment to experiment when they were grown in succinate but not in glycerol.

I have tested a number of parameters but was not able to pin down experiment-to-experiment variability to any one specific factor. Instead I have found that a combination of parameters, including plate age, freshness of the growth media, density of the overday culture, have an effect on the response. In figure 7.8, I have plotted response amplitude *versus* the density of the overday culture for the wild-type RP437 and Δ Tar RP2361 strains. The correlation between the two, if any, is weak, especially in the working range of densities that I have used - 0.15 - 0.3.

In general, variability between experiments was larger than between individual traces within one experiment (fig. 7.9a), although for some strains I did observe that response changes throughout the experiment as well (fig. 7.9b).

7.4 Conclusions

I have found that light response in *E. coli* depends on a variety of external factors. This sensitivity may be explained by the fact that the response results from the contribution of all *E. coli* receptors and therefore

may be sensitive to even a small variation in receptor abundance, methylation state, etc. It is also possible that this variability should be considered in the context of the light sensing mechanism. There are additional experiments that may shed more light on the underlying reasons for the response variability: performing measurements with bacteria grown on other substrates in addition to glycerol and succinate, more rigorous studies of the effect of bacterial density, quantifying receptor abundance, and measuring response for the remaining single-receptor mutants grown in glycerol.

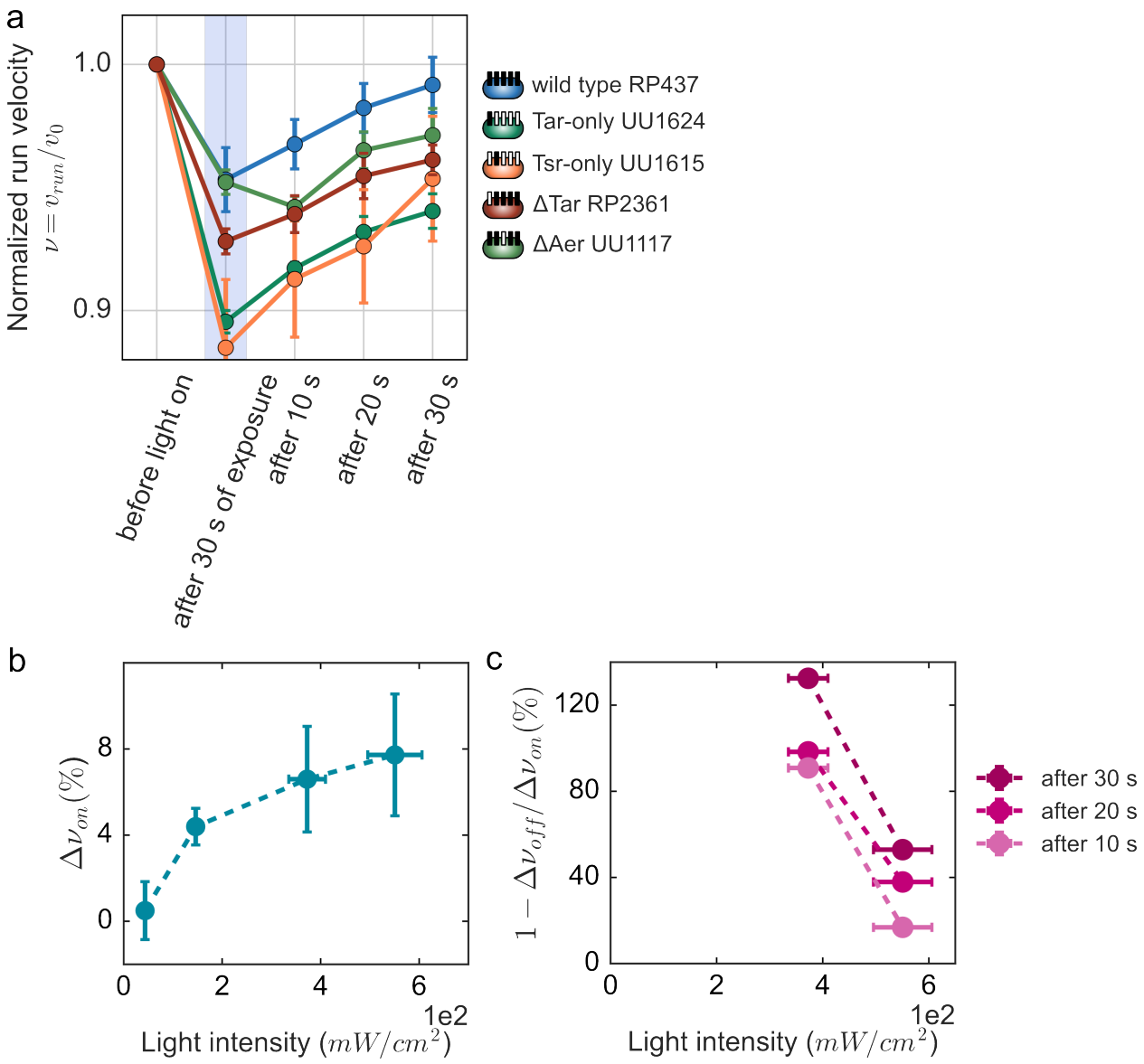

Figure 7.6: Effect of light on swimming velocity of strains grown in M9 with glycerol. (a) Bar plot of the normalized swimming velocity for different *E. coli* strains. Velocity was calculated in 4 s windows after 30 s of exposure to light, then 10, 20 and 30 s after light was turned off, and normalized by the prestimulus value (calculated in a 20 s window before light on). Decrease in and recovery in normalized run velocity was calculated as illustrated on fig. 6.3. (b) Decrease in velocity *versus* light intensity. (c) Velocity recovery *versus* light intensity.

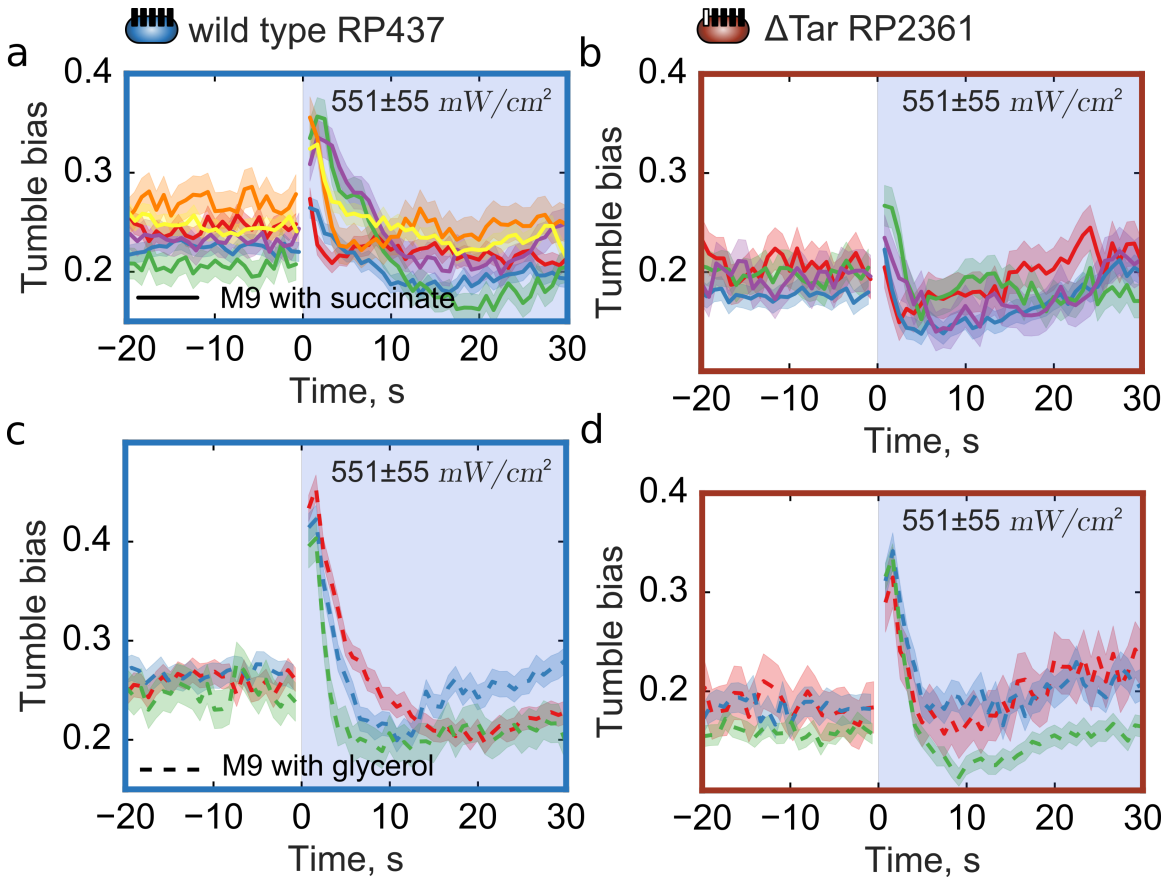

Figure 7.7: Day-to-day variation in the chemotactic response. Trace shown in different colors are averaged across movies taken on the same day. (a) - RP437 wild-type grown in M9 with succinate. (b) - RP2361 ΔTar grown in M9 with succinate. (b) - RP437 wild-type grown in M9 with glycerol. (c) - RP2361 ΔTar grown in M9 with glycerol.

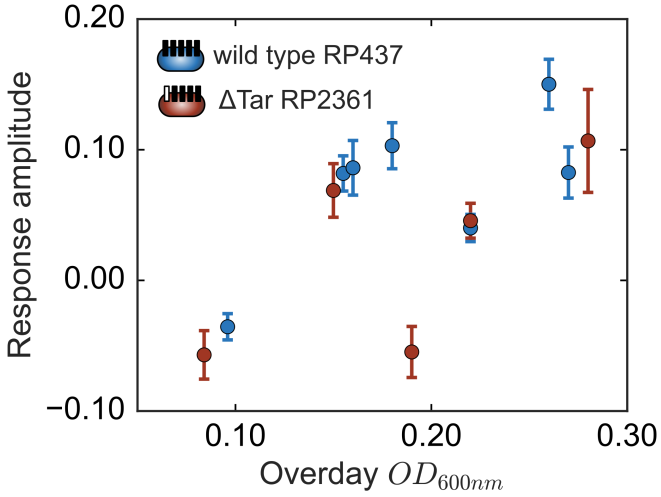

Figure 7.8: Variation of the response amplitude with density of overday bacterial culture used for experiments OD_{600nm}.

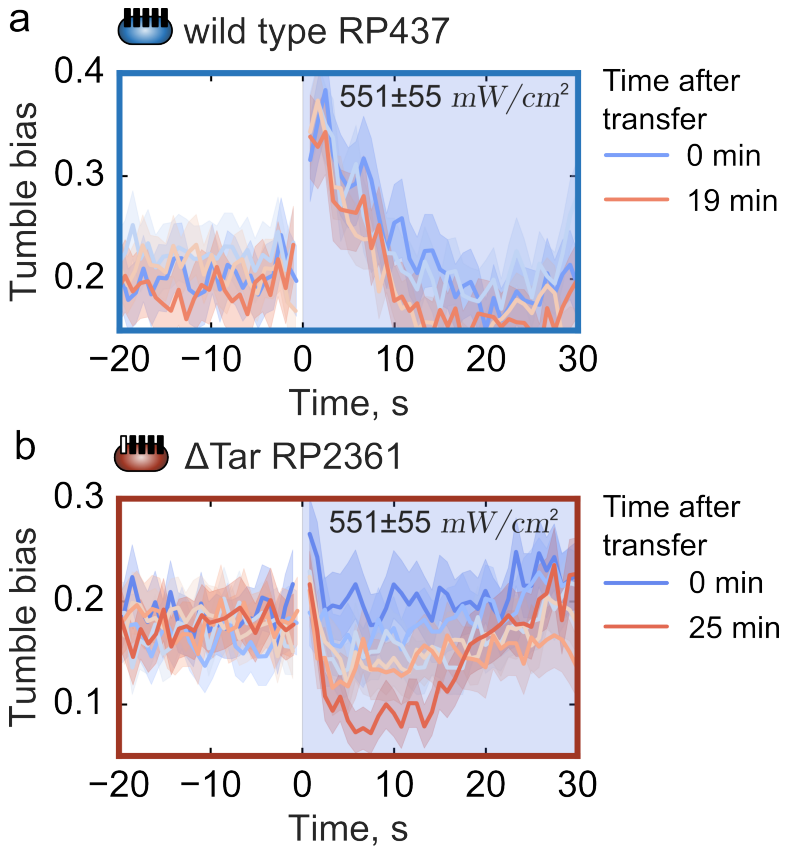

Figure 7.9: Variation in the chemotactic response within one experiments. Each trace corresponds to one movie, color indicates time from the beginning of experiment. (a) - RP437 wild-type grown in M9 with succinate. (b) - RP2361 ΔTar grown in M9 with succinate.

Chapter 8

Future directions

In previous Chapters, I have briefly mentioned potential future experiments that can be done in order to further investigate some of the aspects of phototaxis in *E. coli*. I this Chapter I would like to discuss some alternative projects that can build on the experimental and data analysis tools that I have developed. I will review background information and show my preliminary results on phototaxis in phototrophic bacteria *R. sphaeroides* (8.1). I will also discuss a possibility of using light as a tool for manipulating bacterial density (8.2): I will describe the experimental platform that I have developed and show some preliminary data on the light-driven migration of *E. coli* and *R. sphaeroides*. Finally, I will show my preliminary data on studying phototaxis on the single-cell level using the optical trap instrument (8.3).

8.1 Phototaxis in *Rhodobacter sphaeroides*

As discussed in the Introduction Chapter 1, *E. coli* was chosen as a model phototactic bacteria in order to test the experimental and data analysis tools. It would be interesting, however, to apply the developed methods to studying phototrophic bacteria where phototaxis towards light may confer actual fitness benefits. *Rhodobacter sphaeroides* is an example of phototrophic bacteria which is relatively well studied, however, there have not been many time-resolved studies of its phototaxis behavior. Below I will review what is known about *R. sphaeroides* and its tactic behavior and present some of my preliminary measurements of its phototactic response.

8.1.1 Background

R. sphaeroides is a purple, non-sulphur, photoheterotrophic bacterium living in soil and freshwater habitats. It can perform both aerobic and anaerobic respiration as well as photosynthesis when grown under appropriate conditions [68]. *R. sphaeroides* is propelled by a single rotating flagellum and alternates between runs and stops [63]. During a run, its flagellum rotates CW and pushes the cell forward, during stop flagellum stops rotating altogether [94]. Distribution of run and stop times appears to be exponential on short time

intervals with average stop and run times equal to 0.27 and 1.7 s respectively [63]. Steady-state stop bias in tethered cell assay was found to be 0.15.

R. sphaeroides is much faster than *E. coli* and can swim at speeds up to 80 $\mu m/s$. Similarly to *E. coli*, *R. sphaeroides* changes the fraction of the time it spends in run state under the influence of external stimuli such as light. But unlike*E. coli*, *R. sphaeroides* has been shown to respond much stronger to negative than to positive stimuli [63]. Thus, only a moderate decrease in *R. sphaeroides* stopping bias have been observed in response to the increase in light intensity, possibly because its resting stopping bias is already very low. In response to decrease in light intensity bacteria stop completely and stopping bias reaches 1 [63]. Similar trends have been reported for *R. sphaeroides* response to addition and removal of attractants/repellents [157, 158].

Organization of *R. sphaeroides* chemotaxis signaling pathway is more complex when compared to *E. coli* and still not fully understood [41]. *R. sphaeroides* has three operons encoding complete chemosensory pathways, two of each are essential under laboratory conditions and are expressed at different levels in aerobic *vs* anaerobic conditions [41, 159, 160]. *R. sphaeroides* has nine transmembrane chemoreceptors (MCPs) and four putative cytoplasmic chemoreceptors (transducer-like proteins - Tlps). MCPs localize to the poles of the cell and sense extracellular ligands, Tlps form cluster in a cytoplasm and presumably sense intracellular metabolism [161]. The signals from both tansmembrane and cytoplasmic receptor clusters are combined to determine integrated behavioral output. *R. sphaeroides* has four CheA proteins, six CheY proteins and two CheB proteins [41]. In vitro phosphotransfer experiments have shown that the different CheA proteins can phosphotransfer to different subgroups of response regulators [41]. *R. sphaeroides* does exhibit adaptation, but its mechanism is unclear [43].

Phototaxis in *R. sphaeroides* does not involve a dedicated photosensor, instead, it is triggered by changes in electron transport caused by light exposure [60, 162]. Therefore, phototaxis in *R. sphaeroides* is metabolism-dependent and requires photosynthetic apparatus which forms in phototrophically grown bacteria. Formation of the photosynthetic apparatus in *R. sphaeroides* is regulated by growth conditions, more specifically by oxygen presence and light intensity [163]. When grown aerobically, bacteria do not produce photosynthetic complexes [163]. When oxygen concentration is decreased, photosynthetic complexes are formed even in the absence of light [163]. Therefore, for phototaxis experiments, bacteria should be grown anaerobically and in the presence of light.

Studies of *R. sphaeroides* in the spatial light gradients have shown that bacteria fail to accumulate in the light beam potentially dues to random reorientation at the light-dark interface [62]. This results, however, might be an artifact of a stepwise decrease in light intensity, something that bacteria probably do

not routinely encounter in the wild, where conditions change more gradually.

8.1.2 Methods

Microbiology

The motile strain of *R. sphaeroides* WS8N was generously provided by Judith Armitage [68]. From the frozen stock bacteria were grown on the LB agar plate at 30 ℃until the formation of visible red-colored colonies. Overnight liquid cultures were inoculated from the colony on the agar plate and grown aerobically in 1 ml of Sistrom media at 30 ℃, 265 RPM up to OD of 1.6 for over 24 hours (see Appendix E for more details). The overnight culture was diluted 50x in Sistrom media and grown anaerobically in a sealed transparent cuvette under wide-spectrum illumination up to OD of 0.4 for about 24 hours. For 2D experiments, bacterial culture was diluted down to OD of 0.15 in Sistrom media. Glass preparation, chamber assembly and phototaxis experiment was performed the same way as described in Chapter 4.

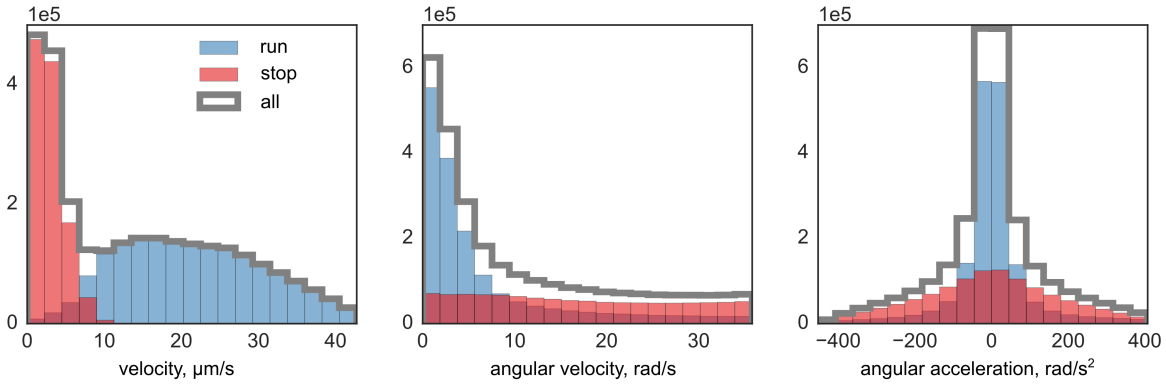

Figure 8.1: Distributions of *R. sphaeroides* motility parameters, velocity, angular velocity and angular acceleration, for stop (red) and run (blue) states.

Data analysis

Detection of bacteria, trajectory linking, calculation of motility parameters and filtering were perfomed the same way as for *E. coli* as described in Chapter 3. For assigning run and stop states I used 2-state HMM model with bacterial velocity as an observable parameter. I have found that this approach gave me the most robust results. Distribution of velocity, angular velocity and angular acceleration for two states is shown on the figure 8.1. As you can see there is a very clear separation between 'run' and 'stop' velocities, which is why using velocity only is enough for reliable assignment of motility states. Example of the trajectory with assigned stops and runs and corresponding time traces of the motility parameters is shown on the figure 8.2. Further analysis was done as previously described (3).

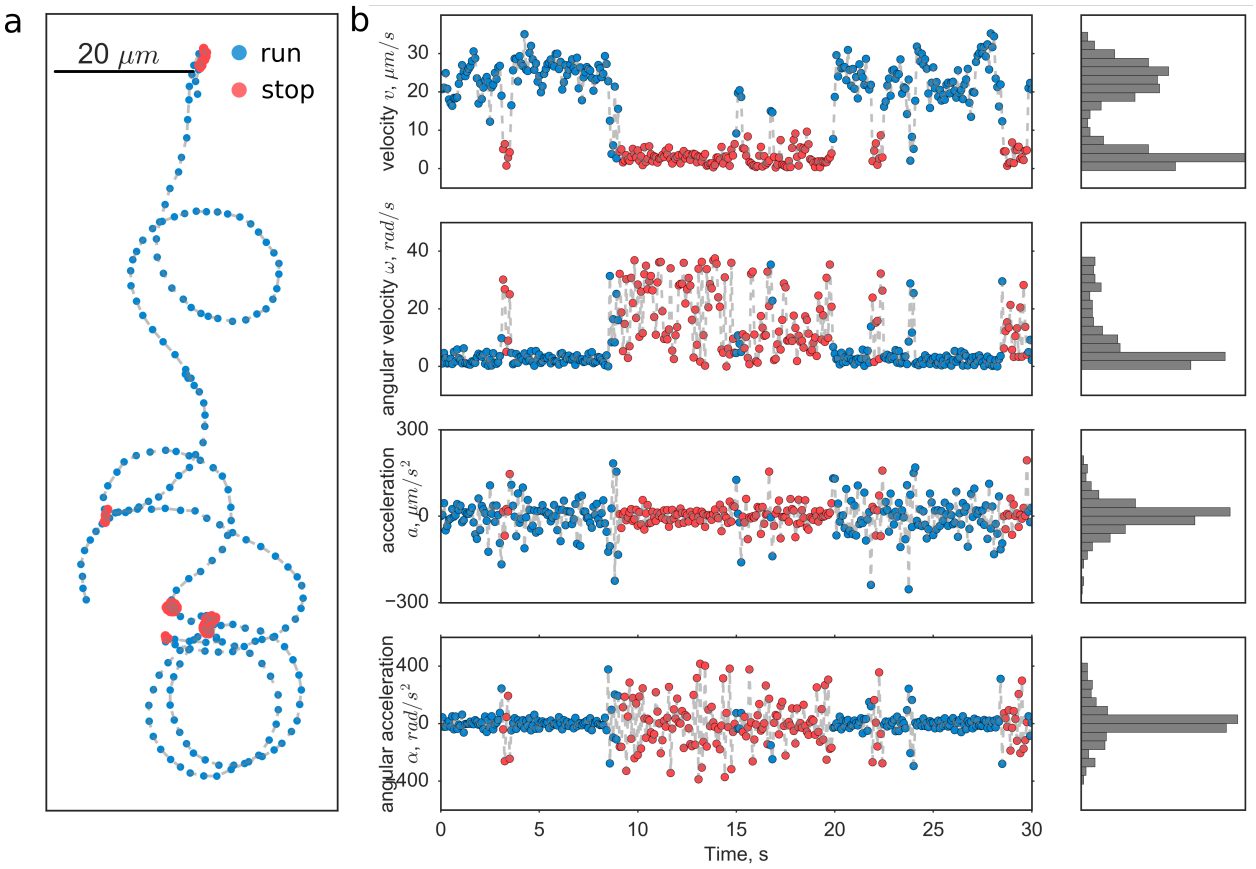

Figure 8.2: An example of analyzed trajectory of WS8N *R. sphaeroides* strain (a) and corresponding time traces of motility parameters (b). Stops are indicated by red, runs - by blue circles.

8.1.3 Preliminary results

Consistently with previous work, I have found that *R. sphaeroides* is indeed faster than *E. coli*, although the distribution of run velocities is very wide (fig. 8.1). Another striking difference is that *R. sphaeroides* tends to have much longer stop intervals compared to *E. coli* tumbles. Average tumble duration was 1.4 s, average run duration - 1.8 s (fig. 8.3), numbers reported for *E. coli* are 0.4 s and 1.5 s respectively [82, 103]. I have found that, similarly to *E. coli*, distributions of run and tumble durations are exponential at short intervals and deviate from exponential at longer intervals (fig. 8.3) [33]. Non-exponential run and tumble distributions suggest that *R. sphaeroides* chemotaxis does not obey simple two-state model which is not surprising given the complexiy of the underlying signalling patways.

I have measured a response of phototrophically grown *R. sphaeroides* to step up and step down in light intensity. Corresponding stop bias and velocity traces are shown on the figure 8.4. I have found that steady-state stop bias was significantly higher than previously reported - 0.4 *vs* 0.15 [63]. The difference might be related to the type of assay employed in each case - free swimming *vs* tethered cell assay. Consistently with

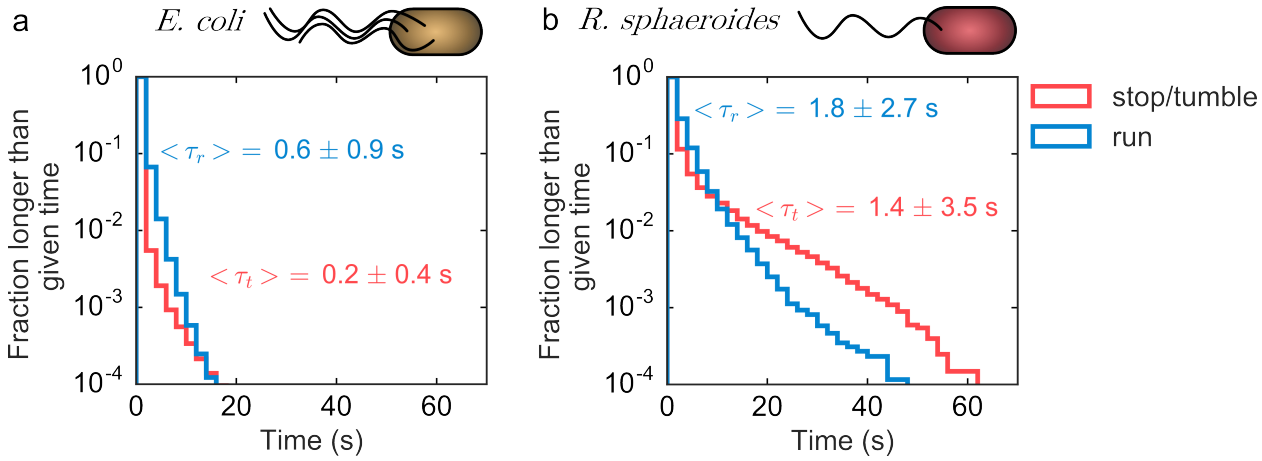

Figure 8.3: Cumulative distributions of run and tumble/stop times in *E. coli* (a) and *R. sphaeroides* (b) with average values and standard deviation shown.

previous results bacteria only responded by a moderate decrease in stop bias to increase in light intensity (fig. 8.4). The response was much more drastic when the light was turned off: bacteria were completely stopped for a few seconds. Adaptation and return to the prestimulus behavior took about 30 s. Note that there were two adaptation phases with fast kinetics right after the response, followed by a phase with slow kinetics. It is impossible to tell from this data though whether the gradual adaptation kinetics results from population averaging or reflects adaptation kinetics of single bacteria [81]. Note that the response was significant already at the light intensity of 150 mW/cm^2. Additionally, the response was evident from velocity traces (velocity was calculated over all states, not just runs). These results suggest that studying phototaxis in *R. sphaeroides* might be more straightforward at least from the analysis point of view.

8.1.4 Future directions

It would be interesting to combine population measurements of *R. sphaeroides* phototaxis with single-cell measurements (see 8.3). It would also be interesting to study the behavior of *R. sphaeroides* in a heterogeneous environment: how they respond to gradients of different steepness and size and under what conditions they are able to effectively navigate towards light gradients (see 8.2). Next obvious step that can be done with 2D assay with homogeneous illumination would be measuring intensity dependence of the response and the effect of growth conditions, e.g. light wavelength and intensity.

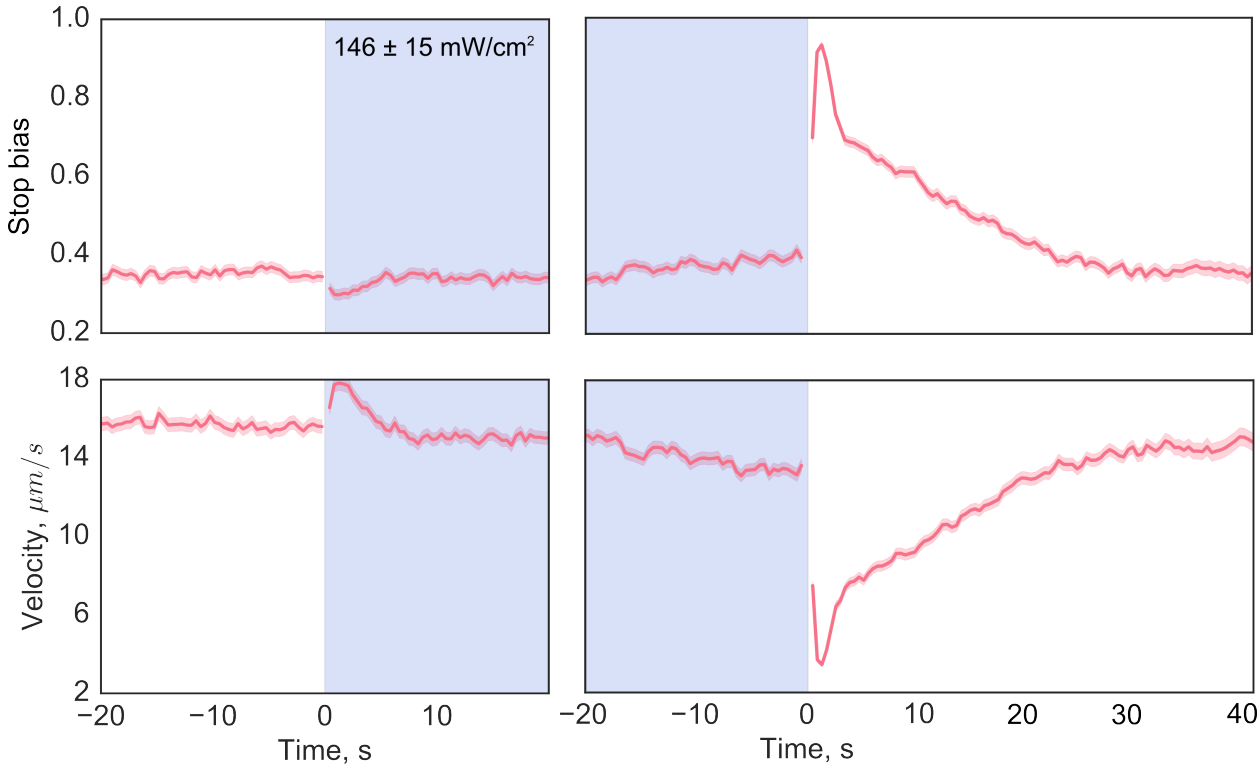

Figure 8.4: Response to blue (440 ± 5 nm) light of *R. sphaeroides* strain WS8N (146 $\pm 15 mW/cm^2$), stop bias and velocity traces.

8.2 Using light to manipulate bacteria

As discussed in Chapter 1, light is especially attractive to use in bacterial studies because it is so easy to control both spatially and temporally. Experiments that I have shown throughout this work make use of the temporal resolution: using light as a stimuli 2D assay allows to measure response and initial adaptation kinetics, which is inaccessible when chemical stimuli are used instead (see for example fig. 6.4). Controlling light in space may enable manipulation of phototactic organisms or provide a way to study their behavior in diverse types of light gradients. In this section, I will first discuss several experimental works that use light to control phototactic organisms, both bacteria, and eukaryotes. I will then describe the experimental setup that allows creating heterogeneous illumination patterns in the microscope sample plane. Finally, I will show some preliminary data on light-driven migration of *E. coli* and *R. sphaeroides*.

8.2.1 Background

There have been a few works that report using light to manipulate phototactic organisms. Steude and co-workers, for example, have used a programmable microarray of organic LEDs (OLEDs) to control the

locomotion of green phototactic algae *Chlamydomonas reinhardtii* [164]. The array of OLEDs was situated directly underneath the chamber with swimming algae. The authors observed accumulation of algae on top of the turned on OLEDs within minutes after they were turned on [164]. Kim *et al* have developed mobile phone operated educational platform, Ludoscope, that enables manipulation and tracking of phototrophic eukaryotes, such as *Euglena gracilis* and *Euglena gracilis* with four independently-controlled directional LEDs [165]. Ozasa and co-workers used LC projector to generate light patterns and study phototactic responses of *Euglena gracilis* and *Chlamydomonas reinhardtii* [166]. Finally, Vizsnyiczai used Spatial Light Modulator (SLM) to control 3D micromotors powered by smooth-swimming *E. coli* bacteria expressing light-driven proton pump [167]. I was interested in taking advantage of bacteria inherent ability to sense and respond to light: if light exposure causes a change in tumble bias it means that population of bacteria will migrate up or down the gradients of light intensity.

8.2.2 Experimental platform for heterogeneous illumination

I have designed an experimental platform that will allow us to study spatiotemporal dynamics of a bacterial population in a heterogenous illumination environment. To create light patterns in the sample plane of the microscope we are using Spatial Light Modulator (SLM), the same technology that is used in the projectors to produce illuminated image. More specifically we use the evaluation module DLP LightCrafter from Texas Instruments. The LightCrafter module includes a light engine and electronic boards. The light engine consists of the DMD chipset; red, green and blue LEDs and optical elements that allow projection of a focused image. Electronic boards control the components of the light engine and interact the LightCrafter and computer it is connected to.

Spatial light modulation in Lightcrafter is performed by a digital micromirror device (DMD). It is an array of 1024 by 768 electrically controlled micromirrors. Each mirror can be in two states. In the on state it sends light from the light source to the projection lens and therefore corresponds to the white pixel in the projected pattern; in the off state it sends light off the light path to the light absorber and therefore corresponds to the dark pixel in the projected pattern [168].

Several characteristics of this setup make it difficult to use for our proposed application. First of all, the optics in the light engine are organized in such a way that the resulting image has 100% offset, that is image shifted relative to the optical axis of the system, which significantly complicates the alignment procedure. Then, the design of the LightCrafter module does not allow us to set the current through the LED lower than 141 mA which results in 40 mW of light power output for blue light. When focused down to the field of view, that will result in a power density of about 1 W/cm^2 if we do not consider losses in the microscope,

which is obviously too high for our purposes. Finally, the maximum response amplitude to the blue light in E. coli was observed at 440 nm, while the LightCrafter blue LED emission maximum is at 460 nm.

For the reasons outlined above, I have replaced the LightCrafter light engine with our own custom-designed optics. We have removed the light engine from LightCrafter with LEDs and projection optics leaving just the control boards and DMD. The current design of the system is shown in fig. 8.5. Light from the blue LED is directed onto the DMD at a 24˚angle and produces a defined light pattern when reflected off the DMD, which is then focused in the image place (fig. 8.5 plane A) and projected on the sample plane of the microscope through the dual side port adapter (fig. 8.5 plane B).

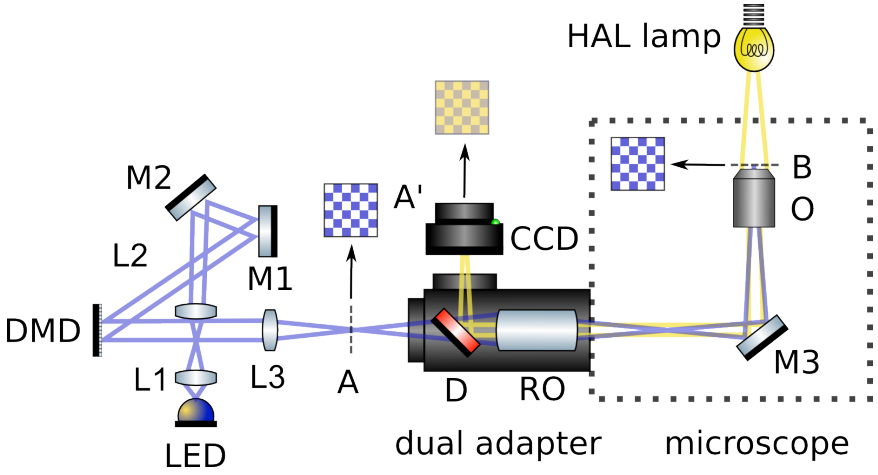

Figure 8.5: The layout of the setup for patterned light applications with the light paths indicated by yellow (wide-range visible light from HAL lamp) and blue (blue LED) lines. Components are labeled as follows: DMD - digital micromirror device; L1, L2, L3 - lenses; M1, M2, M3 - mirrors, D - dichroic mirror, RO - relay optics in the dual adaptor, O - objective, A, A' - image planes, B - sample plane.

8.2.3 Preliminary results: light causes phototactic drift of bacterial populations

E. coli concentrates in the light despite tumbling response

I have collected some preliminary data on how light exposure affects the density of bacteria both for *E. coli* and *R. sphaeroides*. Note, for these experiments I have not used the illumination patterns. Instead I observed change in bacterial density within the area illuminated by the blue light, size of the area is controlled by luminous field stop (2). Results for *E. coli* TsrAer strain RP8606 are shown on the figure 8.6. This strain responds to light by tumbling with fast adaptation (fig. 5.4), which is a classic repellent response, so I expected bacteria to run away from light and bacterial density in the field of view to decrease. However the results was just the opposite. The density of bacteria steadily increased upon light exposure

and reached almost 4 times the original value in less than 10 min (fig. 8.6). *Vice versa*, when light was turned off the density started to decrease. It may be possible to explain this surprising result if we take into account the shape of the light gradient, which, according to simulations, affects the ability of bacteria to follow the gradients [32]. Testing this hypothesis would require simulating populations of phototactic bacteria in 2D in gradients of different sizes.

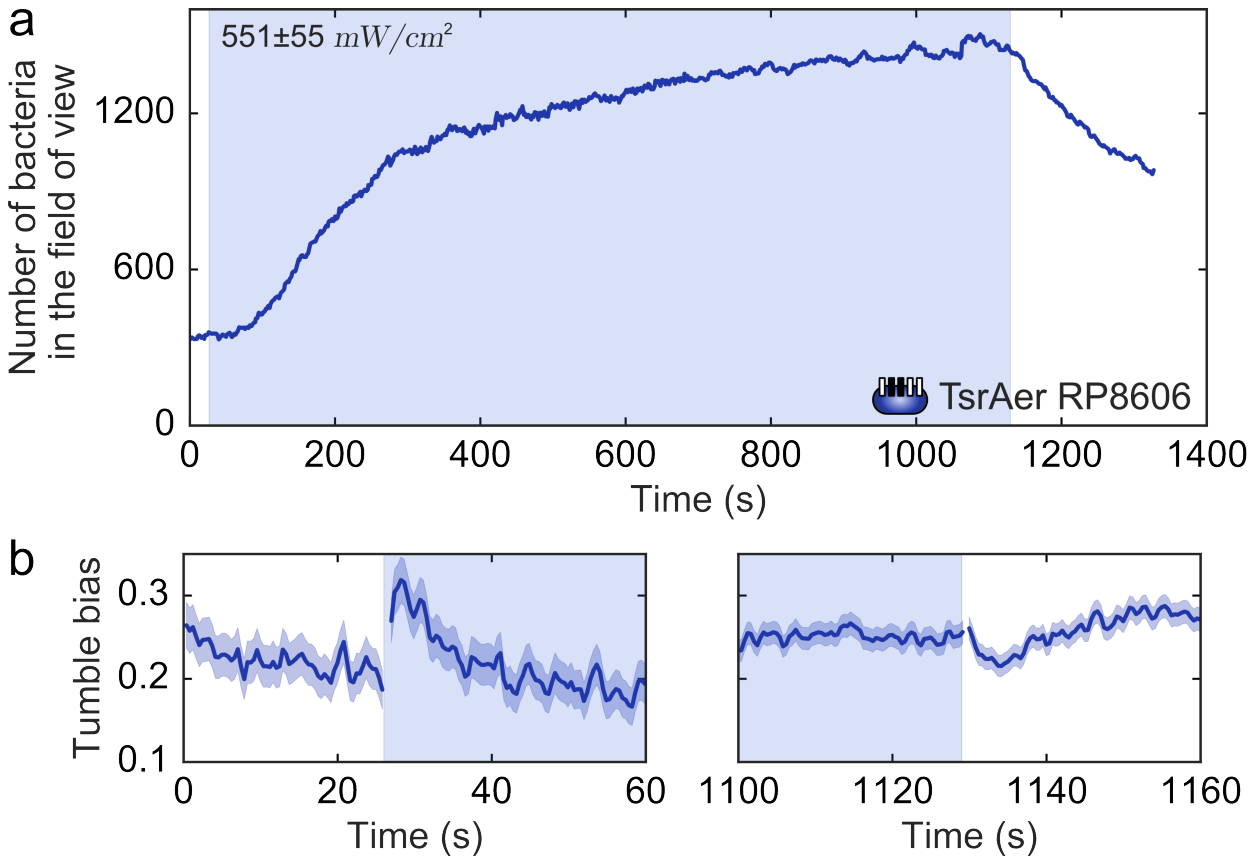

Figure 8.6: Bacteria migrate towards illuminated area despite exhibiting tumbling response to light. Results for TsrAer RP8606 strain. (a) Density versus time. (b) Corresponding tumble bias responses to step up and step down in light intensity.

R. sphaeroides concentrates in the light

Experiments with *R. sphaeroides* were performed with partially closed luminous field stop so that the illuminated area was actually smaller than the field of view (fig. 8.7a). Bacteria were recorded prior, during and after light exposure. Density changes from two different movies are shown on the figure 8.7. As you can see absolute densities in the field of view, inside and outside of the illuminated area increased when the light was turned on ((fig. 8.7b and c upper panels)). To see whether the density inside the illuminated area changed compared to the density outside I divided both densities by the total density in the field of

view. While trends are noisy results for both movies suggest that the density inside the illuminated area increases and the density outside decreases compared to the total density, which means that bacteria tend to swim inside the illuminated area. The increase in absolute densities outside of the illuminated area can be explained by the presence of higher density source of bacteria within the field of view.

8.2.4 Future directions

The next step would be studying the behavior of bacteria in heterogeneous illumination patterns created using the SLM. It may be useful to compare experimental results with a simulation of chemotactic bacteria swimming in 2D.

8.3 Phototaxis on the single-cell level

While technically I do observe single-cell behavior in the 2D assay, I have no guarantee that the trajectories I end up with indeed come from the same bacteria (see section 3.3). True single-cell measurements are necessary to quantify cell-to-cell phenotypic variability in clonal populations. Such measurements are made possible by the method previously developed in the Chemla lab by Min and co-workers, which I will describe in more details below. I will also describe the modifications I have made to the instrument layout to enable light stimulation and show my preliminary data.

8.3.1 Background

As discussed in Chapter 2, although tremendous progress has been made towards elucidating the mechanism of bacterial taxis behavior, current methods have been limited to either short, population-averaged measurements performed on free-swimming cells, or longer-term, precise measurements performed on individual flagellar motors of tethered cells, but not on the behavior of the whole cell. To overcome these limitations, a technique combining optical traps, fluidics, and fluorescence microscopy was developed in the Chemla lab [80]. This technique allows one to track swimming behavior of individual bacterial cells for long durations and measure their response to a variety of external stimuli [80, 81]. Optical traps are used to immobilize a single *E. coli* bacterium by holding each end of the cell; trapped cells can be visualized by brightfield or epi-fluorescence microscopy (fig. 8.8a).

Despite immobilization by the traps, cells display motile behavior, as evidenced by rolling of the cell body during swimming, detected as oscillatory signals by Quadrant Photo Diode (QPD) (fig. 8.8a). Regions of alternating oscillatory and non-oscillatory, or erratic, signals correspond to runs and tumbles of the cell,

respectively [80]. The optical traps act as a bacterial treadmill, maintaining an individual cell stationary for an extended time period while allowing it to run and tumble.

This instrument was used successfully to study the chemotactic response of individual *E. coli* cells to step-up and -down chemical stimuli of various strength [80, 81]. The design of the instrument offers great flexibility in the types of stimuli that are applied and the behavioral responses that are detected. For example, tracking of fluorescently labeled flagella along with the run-tumble swimming state of the cell allowed to characterize the mapping between cell motile behavior and that of the individual flagella [54].

8.3.2 Methods

Instrumentation

To stimulate bacteria with the light, we have added a blue LED to the setup. Output light intensity of the LED is determined by the current from the LED driver (Thorlabs, LEDD1B) which is controlled by the modulating the voltage supplied by the analog output from the Digital Aquisition (DAQ) card and defined using a LabView interface. Blue light is directed towards the sample plane between the two objectives using a dichroic mirror. Light intensity in the sample plane is determined as the light power after the objectives divided by the objective attenuation and by the size of the illuminated area. See Appendix A.3 for more details.

Growing bacteria and preparing samples

Aerobic *E. coli* cultures were grown in Tryptone Broth (TB) at 30°C in the water shaker at 265 RPM. Overnight cultures were harvested at the stationary phase and diluted 100x in TB to start an overday culture. Overday cultures were harvested at the mid-exponential phase by centrifugation, washed, and resuspended in TMB motility buffer containing 70 mM NaCl, 100 mM Tris-Cl, 2% (wt/vol) glucose and 100 μ M methionine to maintain tumble bias [81]. Motility buffer contained oxygen scavenging system (100 $\mu g/ml$ of glucose oxidase and 20 $\mu g/ml$ of catalase) to reduce oxidative damage to the cells by IR excited triplet oxygen [80]. Glucose serves as a substrate for the oxygen scavenging system and as a carbon source for bacteria. Bacteria were placed in the fluidic chambers constructed from cleaned glass coverslips, parafilm spacer, and custom metal frame, as described by Min et al [80].

8.3.3 Preliminary results and future directions

Representative run-tumble binary traces for individual bacteria from one of the experiments are shown on the figure 8.8b. As you can see, bacteria respond to light by a prolonged run, followed by a return

to pre-stimulus tumble behavior. Light intensity used in this experiment was $\sim$3.6 W/cm^2, much higher than the one used in the 2D assay (4). I was not able to detect any response at the intensities below 200 mW/cm^2. The difference between results from 2D and trap assay may be due to the difference in the oxygen concentration between two experiments: in the trap, bacteria are under anaerobic conditions, while in the 2D assay conditions are aerobic at least within first 30 min (2.3). It was shown previously that functioning electron transport chain is required for blue light response and can only be observed for respiring bacteria [58]. In order for bacteria to be able to respire under an anaerobic environment of the trap, they should either be grown anaerobically in the presence of alternative electron acceptor, such as nitrate. Alternatively, bacteria can be grown aerobically and then made anaerobic in the presence of nitrate [58].

Another caveat to these results is that glucose oxidase is a flavoprotein, i.e. it uses FAD as a cofactor. As discussed in Chapter 4 FAD is chromophore which absorbs in the blue region. It is unclear how light would affect glucose oxidase present in the solution but there is no guarantee that the results I observe reflect *E. coli* inherent light response and not interaction with excited Glucose oxidase. The way out may be using the alternative scavenging system - PCA-PCD [169]. I have tested it in the trap and it works reasonably well: I do not observe bacteria slowing down due to oxidative damage.

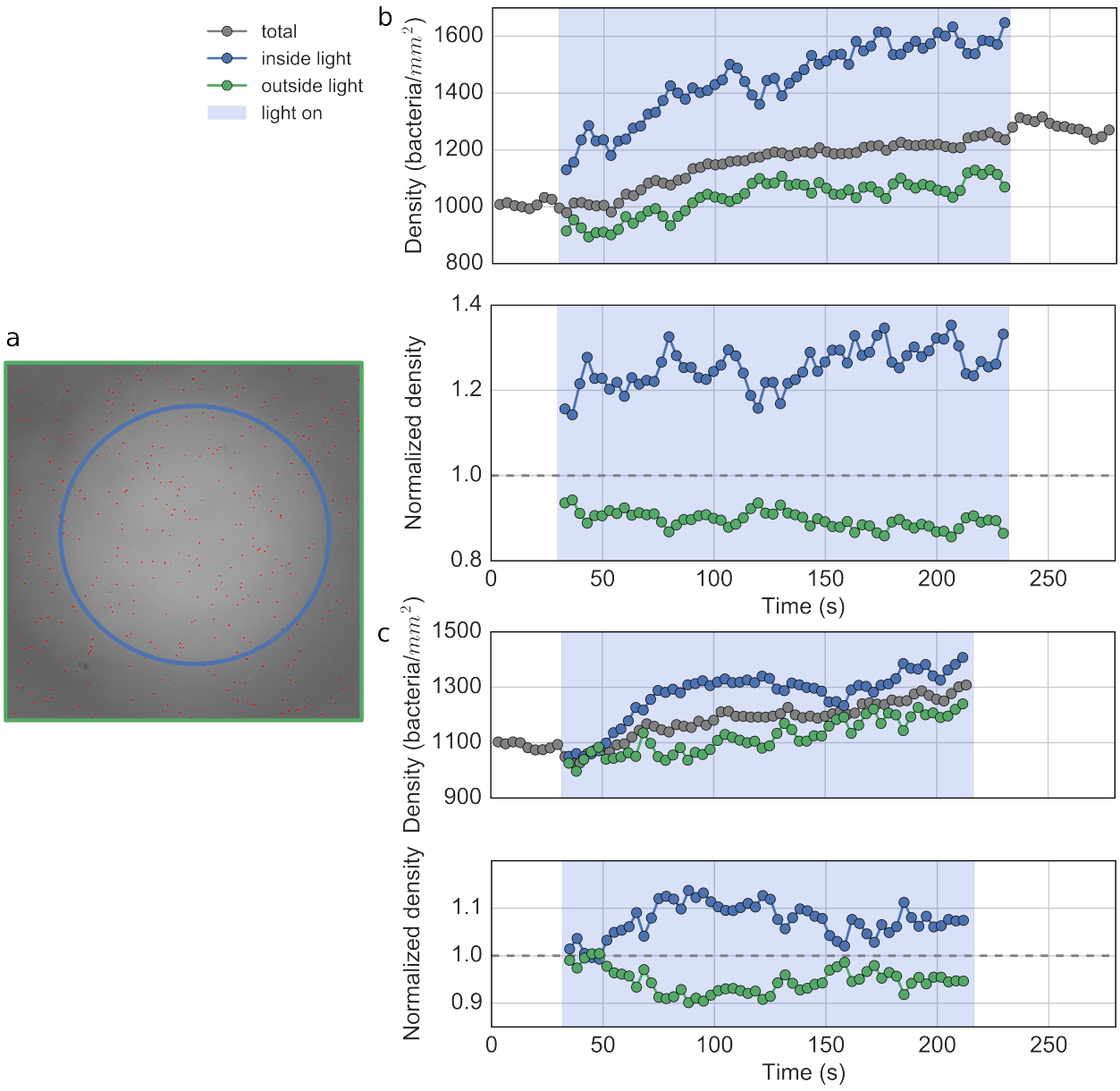

Figure 8.7: *R. sphaeroides* migrate towards illuminated area.(a) Movie frame with outlined illumination patch. (b) Density and normalized density as a function of time, total density is shown in gray, densities inside and outside of the illuminated area in blue and green respectively. Normalized densities are calculated by dividing densities inside and outside by the total density. (c) Same as (b) for a different movie.

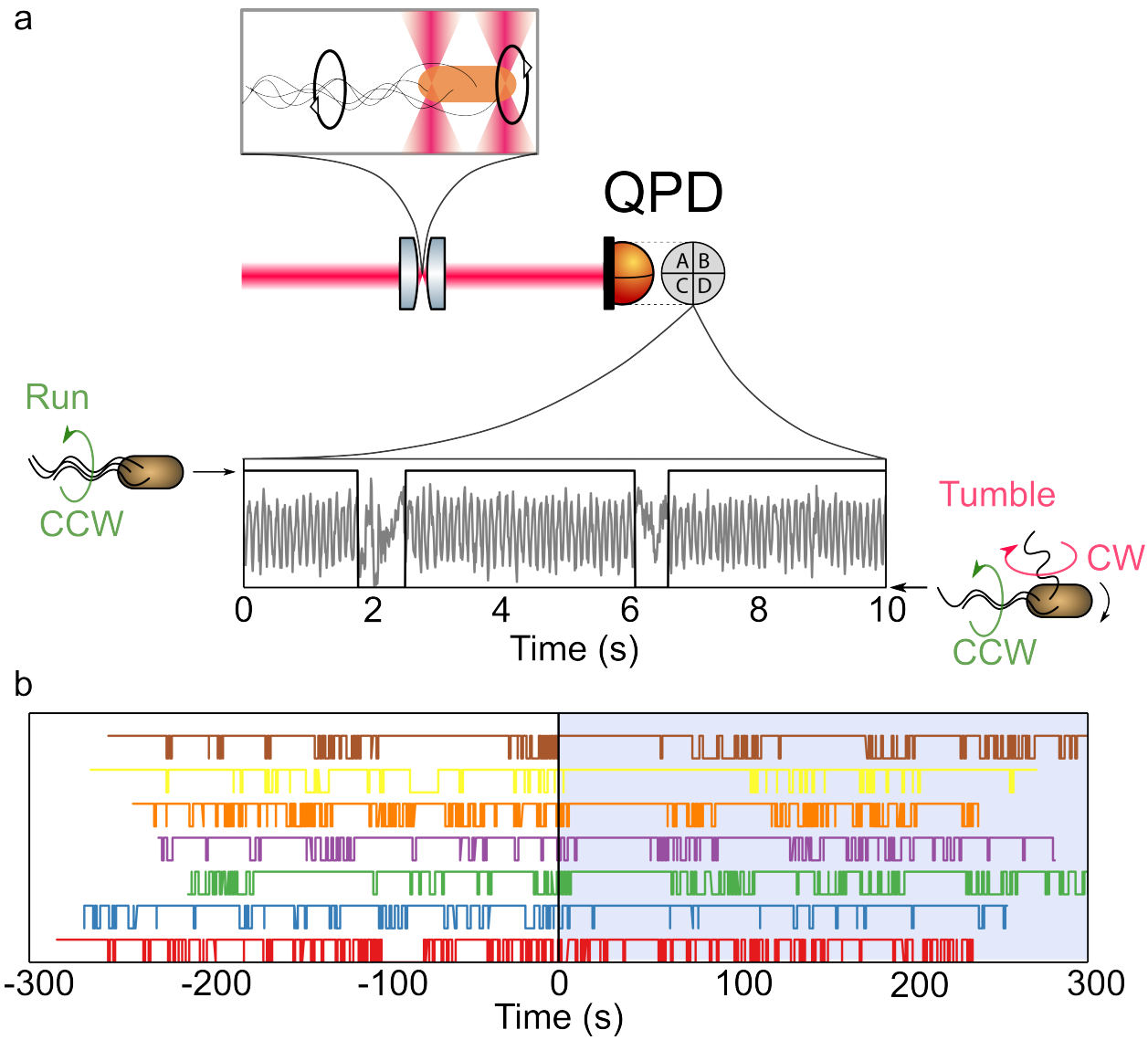

Figure 8.8: (a) Schematic representation of an *E. coli* bacterium (brown cylinder) held by two optical traps (red cones). Representative cell-body rotation signal (gray line) from a trapped cell registered by quadrant photodiode (QPD). Runs and tumbles (black line) are distinguished by using an automated routine. (b) The response of single cells to the blue light exposure. Light intensity was $\sim$3.6 W/cm^2. Binary traces for individual bacteria are offset for clarity. On the binary traces, 1 corresponds to run, 0 to tumble. Blue shaded area indicates light exposure.

Appendix A

Instrumentation

This chapter contains list of components used in microscope-based setup for population level measurements (A.1) as well as description of modification of the optical trap setup that enabled single-cell phototaxis measurements (A.3).

A.1 Instrument components

Table A.1: Optical systems and devices

Type	Part number	Company	Description
Microscope	Axio Observer A1	Zeiss	Inverted optical microscope
Objective	A-Plan 20x/0.45 M27	Zeiss	Suitable for phase contrast
Camera	Grasshopper 3	PointGrey	CMOS sensor
Camera	dmk22buc03	ImagingSource	CCD sensor
Dual adaptor	Dual port adapter 60N	Zeiss	Splits focal plane
SLM	DLP LightCrafter	Texas Instruments	Spatial Light Modulator
DMD	0.3 WVGA chipset	Texas Instruments	Array of micromirrors
HAL Lamp	HAL 12V/100W	Zeiss	Observation light source
Blue LED	M455L3	Thorlabs	Excitation light source

A.2 Controlling LED output

LED needs to be supplied with a constant current that does not exceed 1000 mA, and should be delivered at a forward voltage of 3.2 V. I use LED driver T-cube to provide current to the LED (table A.4). To avoid the damage of the LED I set the maximum possible output current to 1000 mA using the adjustable LED current limit.

According to the description on the Thorlabs website: "The LEDD1B driver can work in three operation modes: constant current mode, trigger mode, and modulation mode. The trigger and modulation modes are

Table A.2: Optical components

Label	Part number	Company	Description
500 nm LP	ET500lp	Chroma	Long-pass filter, transmits wavelengths above 500 nm
L	ACL2520-A	Thorlabs	Aspheric condenser lens
BP	CT440/10bp	Chroma	Band-pass filter, transmits wavelengths in the range of $440 \pm 5nm$
D	500dcxr	Chroma	Long-pass dichroic mirror, transmits wavelengths above 500 nm
ND 0.5	NE05B ND	Thorlabs	Neutral density filter in the microscope slide after LED
ND 1	NE10B ND	Thorlabs	Neutral density filter in the microscope slide after LED

Table A.3: Optomechanics

Name	Part number	Company	Description
Back port adaptor	SM1A23	Thorlabs	Zeiss Axioskop Microscope Lamphouse Port Adapter
Retaining ring	SM1RR	Thorlabs	For 1" lens tubes and mounts
Lens tube	SM1V05	Thorlabs	0.5" Lens Tubes with Rotating Optic Adjustment
Lens tube	SM1L03	Thorlabs	SM1 Lens Tube, 0.3" thread
Lens tube	SM1L05	Thorlabs	SM1 Lens Tube, 0.5" thread
Lens tube	SML10	Thorlabs	SM1 Lens Tube, 1" thread
Slip Ring	SM1RC	Thorlabs	For SM1 Lens Tubes and C-Mount Extension Tubes
Filter holder	SFH2	Thorlabs	Quick-Release Rectangular Filter Holder
Quick-Release adapter	SM1	Thorlabs	For SM1 lens tubes
Lens tube coupler	SM1T10	Thorlabs	External Threads, 1" Long

controlled by an external voltage in the 0 to 5 V range. When in the modulation mode, the LED current output exactly follows the amplitude and waveform of the input signal independent of the knob settings on the top of the T-Cube control unit. In trigger mode the output current switches to the level that has been selected by the knob on the top of module as soon as a threshold voltage is reached. This can be used for pulse width modulation (PWM). The operation mode can be changed by a switch next to the current selector knob." I used LED cube in the modulation mode. Voltage was provided by an analog output from a NI DAQ card (table A.4)

Table A.4: Controllers and Detectors

Name	Part number	Company	Description
T-cube	LEDD1B	Thorlabs	LED driver cube
DAQ card digital inputs	NI PCI-6221 outputs	National Instruments	With analog
T-cube Power supply	TPS001	Thorlabs	15 V, for a Single T-Cube
Power meter	1916C	Newport	Low power, defocused light
Sensor	918D-SL-OD3	Newport	Photodiode sensor for the power meter

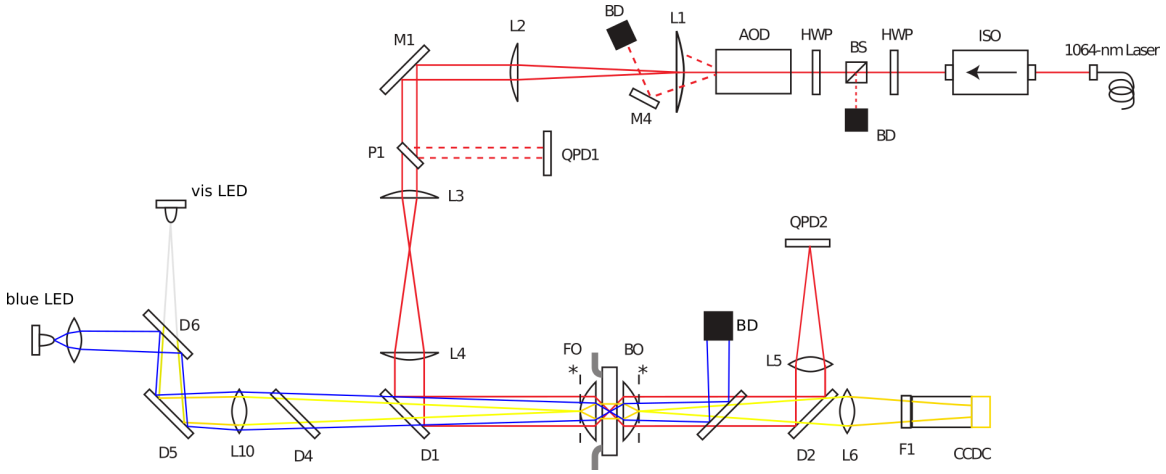

Figure A.1: Instrument layout showing the trapping beam (red), LED illumination path for brightfield imaging (yellow), blue light excitation beam (blue), optical isolator (ISO), half-wave plate (HWP), acousto-optic device (AOD), dichroic mirrors (DM), front and back microscope objectives (FO & BO), quadrant photodiodes (QPD1 & 2), and charge-coupled device cameras (CCDC), lenses (L), mirror (M), dichroic mirror(D) and visible LEDs. See Patrick's thesis for detailed description of the components.

A.3 Phototaxis in the trap

The optical layout of the instrument is shown on the Figure 1 (epi-fluorescent excitation and detection paths are omitted for simplicity). To enable light stimulation I added blue LED to the setup (blue lines on the fig. A.1). To direct the light towards the sample plane I put in the longpass dichroic D6 (500dcxr, Chroma) that passes light above 500 nm and reflects brightfield illumination below 500 nm. D5, which is a 488 nm dichroic (ZT488rdc, Chroma, see Patricks thesis appendix) used for flagella labelling experiments, is switched to a mirror for phototaxis experiments, otherwise you don't get any light from the visible LED in the sample plane.

Blue LED is placed at the same distance from the L10 as visible LED, which can be used with or without the collimation lens assembly. With the collimation lens blue light fills the back focal aperture of the first objective and is focused in the sample plane. Without the collimation lens blue light is focused at the back

focal aperture and is collimated after the objective - fills the objective field of view. The inhomogeneity of the illumination is not important in this case as we only want to illuminate one bacteria in the center of the sample plane. However it is easier to determine the light intensity when the light is focused in the sample plane, and, therefore, illuminated area can be determined from the image.

To determine the light intensity in the sample plane the power of blue light is measured after the objective, divided by the attenuation of the one objective and by the illuminated area. To determine the attenuation of one objective I measured the light power before, P_{before}, and after objectives, P_{after}. Assuming that attenuation in the first and second objective are equal, it can be calculated as $\sqrt{P_{after}/P_{before}}$. CCD camera was calibrated by placing USAF target in the sample plane between the objectives, which gave pixel size of 0.117 μm.

The LED output was controlled the same way as described in section A.2. The only difference is that instead of a DAQ card we used Multifunction Reconfigurable I/O Device with FPGA (Field-programmable gate array). The model we have, NI PCIe-7842R, has 8 analog outputs, that are connected to 2 connector blocks (see appendix A.4 in Patricks thesis). According to reference label for the connector block (SCB-68 quick reference label NI 7811R/7831R), pins 14 and 48 provide analog output ground and analog output signal correspondingly for analog output 7, AO7, that was previously unused. AO7 was connected to the T-cube with a bnc cable and LabView code was modified to enable the control of the

Appendix B

Data analysis

B.0.1 Detecting bacteria

To detect bacteria each frame of the movie is background-subtracted, converted to grayscale, dilated using elliptical kernel and then converted to binary. Contours are detected in binary frame using the command from the openCV package:

```
_, contours, _ = cv2.findContours(frame_bin, cv2.RETR_TREE, cv2.CHAIN_APPROX_NONE).
```

Contours' size, or the total number of pixels in the contour, should be larger than 5 and smaller than 250 pixels.

Linking trajectories

I use the following commmand for linking trajectories:

```
traj = trackpy.link_df(coords, search_range = 45(fpspixsize), adaptive_stop =
10, adaptive_step = 0.98, memory = 1),
```

where coords is Pandas dataframe with x, y and frame number. I use the adaptive search option. If in a particular frame there are too many candidates within the search range (the default limit is 30) I allow reducing search range in small steps until there are few enough candidates and the linking becomes possible. This alsmost never happens at the densities that I use, but this option avoids halting the calculation.

Filtering trajectories

Filtering is described in Chapter 3. For some combination of strains and experimental conditions, e.g. Tap-only UU1250 + pTP1 strain in TMB with phenol, cluster corresponding to slow or stuck trajectories, contains more trajectories than the one with normally-swimming bacteria (fig. 3.3). In that case I use the different procedure for finding the center of the custer corresponding to normrlly-swimming bacteria. Instead of simply finding the coordinates of the maximum of the distribution, in such cases I use k-means clustering algorithm from `scikit-learn` Python package to find the centers of the clusters [108] and then

pick the cluster corresponding to the higher swimming velocity.

Assigning tumbles

Procedure used to assign tumble states is described in Chapter 3. The parameters of the HMM model are set as follows:

`HMMmodel = hmmlearn.hmm.GaussianHMM(n_components = 3, covariance_type = 'diag', n_iter = 1000).fit(X, lengths).`

Here `X` is a stacked array of normalized velocities, accelerations and angular accelerations. Sequences of parameters corresponding to different trajectories follow each other, and information about lengths of different trajectories is contained in the parameter `lenghts`. I used diagonal covariance matrix as it assumes that variables, in my case normalized velocities, accelerations and angular accelerations, are independent. I also tried using Gaussian mixture model (`sklearn.mixture.GaussianMixture()`) and Bayesian Gaussian mixture with Dirichlet emissions (`sklearn.mixture.BayesianGaussianMixture()`). I found that both Bayesian mixture model and HMM model gave good results but eventually decided to use HMM, as it takes into account the temporal component of the data.

Appendix C

Protocols

C.1 Culturing bacteria

Bacteria for chemotaxis experiments should be grown overnight from a agar plate inoculate until they reach stationary phase and then overday until the reach exponential phase. Exponential phase is considered to be optimal for carrying chemotaxis experiments because it corresponds to highest swimming speed as shown for bacteria grown in TB [83].

Agar plate culture

- Set the incubator temperature to 37℃. Temperature may vary for different bacterial species, but that is what we use for *E. coli*.
- Put the LB agar plate with the appropriate antibiotic in the incubator $\sim$ 20 min prior to streaking to remove condensate. LB plates with antibiotics should not be older than a month.
- Sign the plate with the content of the agar (antibiotics), strain name, date and time, your initials.
- Place the vial with the frozen stock of the strain from -80℃ freezer on the ice.
- With a sterilized toothpick, scrape a piece of the frozen sample, and touch the edge of the agar plate.
- Streak the plate with streaking needle to dilute the initial drop so that you can get single colonies. Change the needle between streaks.
- Grow the plate in the incubator until the colony size reaches 1 mm. Time will vary depending on the strain and antibiotics used.
- Keep track of how old is the plate. Do not do experiments with plates older than 2 weeks.

Overnight culture

- Pick a bacterial colony from a plate (less than 2 weeks old) using sreaking loop.
- Put the colony in the 15 ml falcon tube with 1 ml of growth media and appropriate antibiotics (standard concentrations are 34 $\mu g/l$ of Cm or 100 $\mu g/l$ of Amp) by stirring the media with the loop vigorously.
- Place the tube in the shaker and grow until the culture reaches stationary phase, ∼15 hours for bacteria grown in TB and ∼ 24 hours for bacteria grown in M9 minimal media. Shaker should be set to 30℃ and 265 RPM for chemotaxis experiments.

Overday culture

- Measure the OD of the overnight culture.
- Dilute 1:50 when using minimal media or 1:100 if using TB in the growth media with appropriate induders.
- Grow till the culture reaches exponential phase.

C.2 Media and buffers

TMB Motility buffer

Bacteria were harvested by resuspending them in the motility buffer. The composition of the buffer was adapted from Trap Motility Buffer used by Min *et al* [80]. Instead of glucose which was used as a substrate for oxygen scavenging system I use succinate, glycerol or lactate as energy source for bacteria. To prepare 42 ml of the TMB with succinate, mix the following ingredients.

- 4.2 ml of 1 M TrisHCl pH 7.5
- 3 ml of 1 M NaCl
- 840 μl of 200 mg/ml sodium succinate $C_4H_4O_4Na_2 \cdot 6\,H_2O$

Sterile filtter. Add 1μl of 2 mM Meth to 19 μl of bacterial culture in TMB prior to the experiment. Final composition: 100 mM TrisHCl, 70 mM NaCl, 0.4 % succinate (4 mg/ml), 0.1 mM Meth. Fresh batch should be made at least every two months.

M9 minimal media

As discused in section 2.3 for the purpose of the project bacteria were grown in the media with defined composition - M9 minimal media. Basic components of M9 media are salts. Carbon source, vitamins and essential amino acids are added as necessary. RP437 strain on *E. coli* is auxotrophic for the following amino acids: Leu, Meth, His, Thr and needs vitamin thiamine (see RP437 genotype on *E. coli* Genetic Resources at Yale CGSC). Depending on the experiments glycerol, glucose or succinate can be used as carbon sources. For the experiments discussed in this work I used 0.4% succinate [170] or 0.5% glycerol [1].

Prepare the following stock solutions.

- 5x concentrate of M9 salts, autoclaved (see below)
- 10 mg/ml thiamine (Cold Spring Harbor Protocols), sterile filtered
- 200 mg/ml of succinate, glycerol or glucose. Succinate solution can be autoclaved, glycerol and glucose should be sterile filtered.
- 50 mM amino acid solutions (Meth, Leu, Thr, His), sterile filtered
- 1 M $MgSO_4$, autoclaved
- 50 mM $CaCl_2$, autoclaved

To prepare 200 ml of the M9 with succinate, mix the following ingredients.

- 40 ml of 5x M9 salts
- 2 ml of 10 mg/ml thiamine
- 4 ml of 200 mg/ml sodium succinate $C_4H_4O_4Na_2 \cdot 6\,H_2O$
- 2 ml of each 50 mM Meth, 50 mM Leu, 50 mM Thr and 50 mM His

Adjust volume to 200 ml and sterile filter. Store at 4℃. Watch for change of color: when media becomes yellowish, make a new batch. After the media is older than one month, use with caution. If the OD value is lower than usual for overnight or overday culture after standard growth time, make a new batch. Note that $CaCl_2$ and $MgSO_4$ are added to the media right before growing bacteria to minimize precipitation: per 1 ml of the media add 2 μl of 1 M $MgSO_4$ and 2 μl of 50 mM $CaCl_2$.

Final composition: 1x M9 salts, 0.1 mg/ml thiamine, 0.5 mM Meth, 0.5 mM Leu, 0.5 mM Thr, 0.5 mM His, 0.1 mM $CaCl_2$, 2 mM $MGSO_4$, 0.4% succinate.

5x M9 salts

Stock solution of salts for preparing M9 minimal media. Sodium phosphate and potassium phosphate are present in M9 as buffering agents. Ammonium chloride provides a source of nitrogen for cells. Sodium chloride provides essential ions and osmotic support. Per 1 liter of the final solution mix the following ingredients:

- 64 g of $Na_2HPO_4 \cdot 7\,H_2O$
- 15 g of KH_2PO_4
- 2.5 g of NaCl
- 5 g of NH_4Cl

Dissolve in 1 liter of water. Autoclave.

C.3 Transformation

Protocol for one-step preparation and transformation of competents cells, adapted from [171].

Materials

- LB with 20 mM (0.36%) glucose (1800 μl per transformation)
- TSS buffer (see below) (100 μl per transformation)
- Agar plates with appropriate antibiotics, 2 for each transformation
- Overnight LB culture of the strain for transformation grown at 37℃

Preparation

- Pre-cool centrifuge to 4℃
- Prepare ice-water bath with a rack
- Cool falcon tubes on ice, 3 per each transformation
- Cool TSS and water on ice
- Warm selection plates
- Set incubator temperature to 37℃

Protocol

1. Grow 2 ml overday culture by diluting overnight culture 100x in LB, incubate at 37℃until OD is about 0.3-0.4 for about 2.5 hours.

2. Spin down cells at 1000 RCF for 10 min at 4℃in ice-cold falcon tubes. Discard supernatant, resuspend cells quickly without pipetting up and down in 200 μl (1/10th of original volume) of 1x TSS. Mix gently on ice for ∼2 min.

3. Add 100 μl of competens cells and $\sim 2\mu l$ of plasmid (8 - 40 ng per transformation) to falcon tube. Add 100 μl of competens cells and $\sim 2\mu l$ of water to a different tube for negative control. Label tubes correspondingly.

4. Mix gently on ice for $\sim$ 3 min. Incubate on ice for 30 min.

5. Add 900 μl of LB with 20 mM glucose to each falcon tube and incubate in the shaker for 30 min at 37℃to allow the expression of antibiotic resistance gene.

6. Label plates and put the in the incubator.

7. Prepare glass spreader by bending Pasteur pipettes with Bunsen burner. Sterilize by dipping in ethanol and burning it off with the flame. Cool down by touching the side of the agar.

8. Pipette 200 μl of the culture on the warm agar plate and spread evenly with the spreader. Repeat for negative control.

9. Incubate overnight at 37 ℃.

10. Transformation worked if you got colonies on the plate with bacterial culture, to which you added the plasmid, but not on the negative control plate.

Transformation and storage solution (TSS)

Prepare the following:

- 50% PEG 3350: add 5 g PEG and 10 ml H_2O, sterile filter.
- DMSO
- LB with 50 mM $MgCl_2$: add 39.5 ml of LB and 0.5 ml of 4 M $MgCl_2$.

Add 4 ml of 50% PEG, 1 ml DMSO, 15 ml of LB with 50 mM $MgCl_2$, adjust pH to 6.5.

C.4 2D assay with epoxy-sealed coverslip chamber

Clean the slides and coverslips on the day of the experiment. When cleaned coverslips are stored dry, they absorb lint from the air. When coverslips are stored in the distilled water even for one day they absorb some deposits from water, which reduces imaging quality and complicates bacteria detection.

- Sonicate for 15 min in acetone, rinse with water
- Sonicate for 15 min in acetone, rinse with water
- Sonicate for 15 min in 1M KOH, rinse with water and leave in water before spin-drying.
- Spin-dry at 1000 RPM for 3 min.

About half an hour before the experiment passivate slides and coverslips with BSA to minimize sticking of bacteria.

- Put $7\mu l$ of 2 mg/ml BSA on the slide and cover with coverslip.
- Mark with sharpie the area that was passivated on the side of the slide.
- Store in a pipette tip box with a layer of water in the bottom to prevent overdrying.

Prepare bacteria.

- Harvest the overday bacterial culture by spinning down at 1300 RCF for 10 min, resuspend in TMB to the final OD of 0.15-0.17.
- Bacterial culture should be well aerated so put bacteria back in the shaker before you're ready to assemble the chamber.

Prepare the chamber with bacteria. As we are not using a spacer, the volume of the culture determines the distance between the slide and the coverslip which should be comparable to the objective's depth of field in order for all bacteria to appear in focus. For example for 22x22 mm coverslip, 5 ul of liquid are enough to create 10-12 um layer of water between slide and a coverlip. Calculate the volume needed depending on the dimensions of the coverslip and objective.

- Wash slides and coverslips with copious amounts of water, holding the passivated surface up.
- Dry using nitrogen line or spin dry.

- Mix 19 ul of the bacterial culture and 1 μl of 2 mM Meth (Methionine in the buffer along with carbon source keeps bacteria energized). Use wide-orifice tips whenenever handling motile bacteria.
- Put 5 ul of the culture on the slide and gently cover with coverslip avoiding formation of bubbles.
- Mix 2-component epoxy (Devcon, 5 minute epoxy) and carefully apply to the edge of the coverslip to seal the chamber. Avoid moving the coverslip as it will create shear stress and damage bacteria. Sealing is necessary to prevent drying and drift and drying.
- If using the chamber before complete drying of the epoxy be careful not to run the objective into epoxy.

If 2D assay is done for measuring response to chemicals, last part of the protocol is slightly altered.

- Mix the epoxy several minutes prior to adding the chemical to let it thicken. This is done to minimize the drift during the experiment.
- Prepare pipettes with volumes set, and a timer.
- Mix bacterial culture with chemical of interest and start the timer.
- Assemble the chamber as described above.
- Stop the timer when recording of the first movie is started. Note the time, it will be used to shift the resulting response trace.

Appendix D

Strains and Plasmids

This appendix includes information about bacterial strains and plasmids used during the work on this thesis project.

All strains used in this work were derived from the wild-type chemotaxis strain RP437, with the exception of alternative wild-type MG1655 and its ΔTsr derivative (table **??**). Majority of the strains were derived by chromosomal deletion of one or more receptor genes.

D.1 Strains

Strains used in this work are shown in table D.1.

D.2 Plasmids

All plasmids used in this work are shown in the table D.2. The following concentrations of inducers were used for strains with plasmids: 50 μM IPTG for UU1250 + pSB20, 0.7 μM NaSal for UU1250 + pTP1 and 0.8 μM NaSal for UU1250 + pPA705.

D.3 Constructing plasmid pTP1

Plasmid pTP1 was constructed from plasmid pKG117 by subcloning wild-type tap gene between NdeI(CATATG)-BamHI(GGATCC) restriction sites. Synthesis and subcloning was performed by Genscript. The map of plasmid pKG116, the parent vector for pKG117 is shown on the figure D.1.

Table D.1: Strains used in this work

Strain	Genotype	Comments	Source
RP437		Wild-type chemotaxis strain	Christopher Rao [172]
MG1655		Wild-type chemotaxis strain	Matt Copeland
JW4318-1	Δtsr	ΔTsr strain, derived from MG1655	Yale Stock Center
ΔR	$\Delta cheR$		Christopher Rao
ΔB	$\Delta cheB$		Christopher Rao
CR20	CheY::FRT	Runner	Christopher Rao
PS2001	$\Delta cheBcheYcheZ$ (Kan^R)	CheY*, pMS164 plasmid	Philippe Cluzel
UU1250	$\Delta(tar-tap)\Delta tsr\Delta aer\Delta trg$	Receptorless strain	John S. Parkinson
UU1615	$\Delta aer\Delta tar\Delta tap\Delta trg$	Tsr-only strain	John S. Parkinson
UU1624	$\Delta aer\Delta tsr\Delta tap\Delta trg$	Tar-only strain	John S. Parkinson
UU1250 + pSB20	$\Delta(tar-tap)\Delta tsr\Delta aer\Delta trg$	Aer-only strain, pSB20 plasmid	John S. Parkinson
UU1250 + pKG117	$\Delta(tar-tap)\Delta tsr\Delta aer\Delta trg$	Aer-only strain pKG117 plasmid	John S. Parkinson
UU1250 + pPA705	$\Delta(tar-tap)\Delta tsr\Delta aer\Delta trg$	Trg-only strain pPA705 plasmid	This work John S. Parkinson
TP6	$\Delta(tar-tap)\Delta tsr\Delta aer\Delta trg$	Tap-only strain, pTP1 plasmid	This work
UU1623	$\Delta tsr\Delta tap\Delta trg$	Aer-Tar strain	John S. Parkinson
RP8606	$\Delta tar\Delta tap\Delta trg$	Aer-Tsr strain	John S. Parkinson
RP8604	$\Delta tsr\Delta trg$	Tar-Aer-Tap strain	John S. Parkinson
UU2607	$\Delta tar\Delta tap$	Tsr-Aer-Trg strain	John S. Parkinson
RP1131	trg::Tn10	ΔTrg strain	John S. Parkinson
UU1117	Δaer	ΔAer strain	John S. Parkinson
RP5700	Δtsr	ΔTsr strain	John S. Parkinson
RP2361	Δtar	ΔTar strain	John S. Parkinson

Table D.2: Plasmids used in this work

Plasmid	Parent plasmid	Genotype	Comments	Source
pMS164		CheYD13K, Cm^R	IPTG-inducible constitutively active version of CheY	Philippe Cluzel [173]
pSB20	pCJ30	Aer, Amp^R	IPTG-inducible wild-type Aer	John S. Parkinson [1] John S. Parkinson [1]
pPA705	pACYC184	Trg, Cm^R	NaSal-inducible wild-type Trg	John S. Parkinson [134] John S. Parkinson [134]
pKG117	pKG116	Aer, Cm^R	NaSal-inducible wild-type Aer	John S. Parkinson [1] John S. Parkinson [1]
pTP1	pKG117	Tap, Cm^R	NaSal-inducible wild-type Tap	This work This work

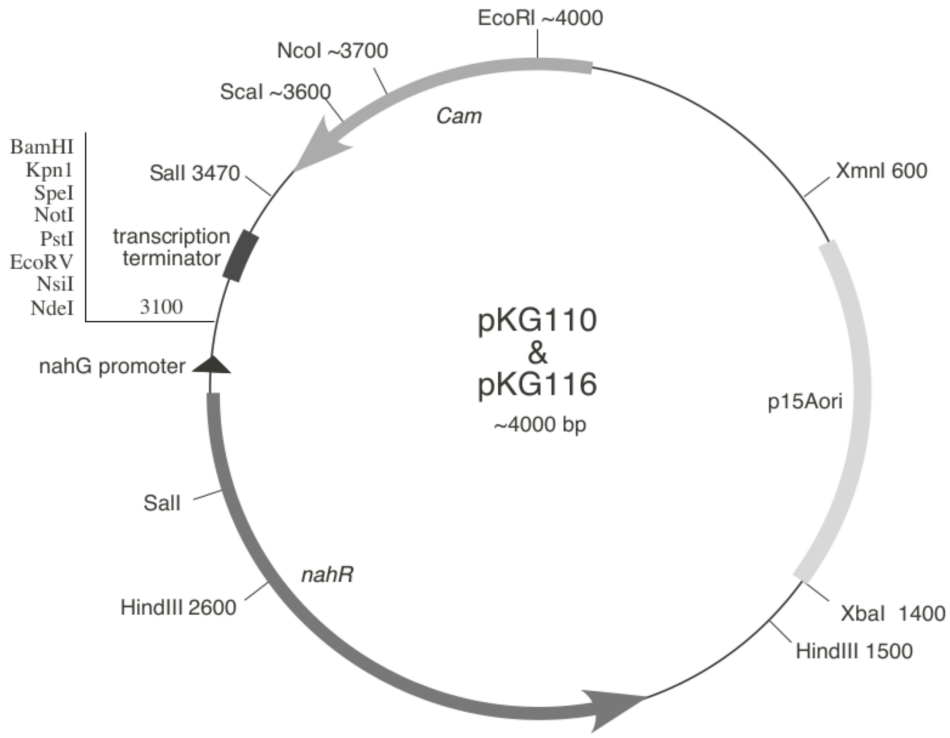

Figure D.1: The map of pKG116 plasmid, parent vector for pKG117, provided by John Parkinson.

Amino acid dequence of the Tap protein

Sequence was obtained from Uniprot database.

MFNRIRISTTLFLILILCGILQIGSNGMSFWAFRDDLQRLNQVEQSNQQRAALAQTRAVM
LQASTALNKAGTLTALSYPADDIKTLMTTARASLTQSTTLFKSFMAMTAGNEHVRGLQKE
TEKSFARWHNDLEHQATWLESNQLSDFLTAPVQGSQNAFDVNFEAWQLEINHVLEAASAQ
SQRNYQISALVFISMIIVAAIYISSALWWTRKMIVQPLAIIGSHFDSIAAGNLARPIAVY
GRNEITAIFASLKTMQQALRGTVSDVRKGSQEMHIGIAEIVAGNNDLSSRTEQQAASLAQ
TAASMEQLTATVGQNADNARQASELAKNAATTAQAGGVQVSTMTHTMQEIATSSQKIGDI
ISVIDGIAFQTNILALNAAVEAARAGEQGRGFAVVAGEVRNLASRSAQAAKEIKGLIEES
VNRVQQGSKLVNNAAATMIDIVSSVTRVNDIMGEIASASEEQQRGIEQVAQAVSQMDQVT
QQNASLVEEAAVATEQLANQADHLSSRVAVFTLEEHEVARHESVQLQIAPVVS

DNA sequence of the tap gene after Genscript optimization

1 catatgttca atcgtattcg tattagcacc accctgtttc tgatcctgat cctgtgcggc
61 atcctgcaaa tcggtagcaa cggtatgagc ttctgggcgt ttcgtgacga tctgcagcgt
121 ctgaaccagg ttgagcaaag caaccagcaa cgtgcggcgc tggcgcagac ccgtgcggtg
181 atgctgcaag cgagcaccgc gctgaacaaa gcgggtaccc tgaccgcgct gagctacccg
241 gcggacgata tcaaaaccct gatgaccacc gcgcgtgcga gcctgaccca gagcaccacc
301 ctgttcaaga gctttatggc gatgaccgcg ggtaacgagc acgttcgtgg cctgcagaag
361 gaaaccgaga agagcttcgc gcgttggcac aacgacctgg agcaccaggc gacctggctg
421 gaaagcaacc aactgagcga ctttctgacc gcgccggttc agggtagcca aaacgcgttc
481 gatgtgaact ttgaggcgtg gcagctggaa atcaaccatg ttctggaagc ggcgagcgcg
541 cagagccaac gtaactacca aatcagcgcg ctggttttca ttagcatgat cattgtggcg
601 gcgatctata ttagcagcgc gctgtggtgg acccgtaaaa tgattgttca gccgctggcg
661 atcattggca gccactttga tagcattgcg gcgggtaacc tggcgcgtcc gattgcggtg
721 tatggccgta acgaaatcac cgcgattttt gcgagcctga agaccatgca gcaagcgctg
781 cgtggtaccg tgagcgacgt tcgtaaaggt agccaggaga tgcacatcgg cattgcggaa
841 atcgttgcgg gtaacaacga tctgagcagc cgtaccgagc agcaagcggc gagcctggcg
901 cagaccgcgg cgagcatgga acaactgacc gcgaccgtgg gtcagaacgc ggataacgcg
961 cgtcaagcga gcgagctggc gaagaacgcg gcgaccaccg cgcaggcggg tggcgtgcaa
1021 gttagcacca tgacccacac catgcaggaa atcgcgacca gcagccaaaa aattggcgac

1081 atcattagcg ttatcgatgg tattgcgttc cagaccaaca ttctggcgct gaacgcggcg

1141 gtggaggcgg cgcgtgcggg tgaacaaggt cgtggctttg cggtggttgc gggtgaggtt

1201 cgtaacctgg cgagccgtag cgcgcaagcg gcgaaggaaa tcaaaggcct gattgaggaa

1261 agcgtgaacc gtgttcagca aggtagcaag ctggtgaaca acgcggcggc gaccatgatc

1321 gacattgtga gcagcgttac ccgtgtgaac gatatcatgg gcgagattgc gagcgcgagc

1381 gaggaacagc aacgtggtat cgaacaggtt gcgcaagcgg tgagccagat ggaccaagtt

1441 acccagcaaa acgcgagcct ggttgaggaa gcggcggtgg cgaccgagca gctggcgaac

1501 caagcggatc acctgagcag ccgtgtggcg gtttttaccc tggaagagca cgaagtggcg

1561 cgtcacgaga gcgttcaact gcagattgcg ccggttgtga gctaaggatc c

Sequence of the pTP1 plasmid

ORIGIN

1 catatgttca atcgtattcg tattagcacc accctgtttc tgatcctgat cctgtgcggc

61 atcctgcaaa tcggtagcaa cggtatgagc ttctgggcgt ttcgtgacga tctgcagcgt

121 ctgaaccagg ttgagcaaag caaccagcaa cgtgcggcgc tggcgcagac ccgtgcggtg

181 atgctgcaag cgagcaccgc gctgaacaaa gcgggtaccc tgaccgcgct gagctacccg

241 gcggacgata tcaaaaccct gatgaccacc gcgcgtgcga gcctgaccca gagcaccacc

301 ctgttcaaga gctttatggc gatgaccgcg ggtaacgagc acgttcgtgg cctgcagaag

361 gaaaccgaga agagcttcgc gcgttggcac aacgacctgg agcaccaggc gacctggctg

421 gaaagcaacc aactgagcga ctttctgacc gcgccggttc agggtagcca aaacgcgttc

481 gatgtgaact ttgaggcgtg gcagctggaa atcaaccatg ttctggaagc ggcgagcgcg

541 cagagccaac gtaactacca aatcagcgcg ctggttttca ttagcatgat cattgtggcg

601 gcgatctata ttagcagcgc gctgtggtgg acccgtaaaa tgattgttca gccgctggcg

661 atcattggca gccactttga tagcattgcg gcgggtaacc tggcgcgtcc gattgcggtg

721 tatggccgta acgaaatcac cgcgattttt gcgagcctga agaccatgca gcaagcgctg

781 cgtggtaccg tgagcgacgt tcgtaaaggt agccaggaga tgcacatcgg cattgcggaa

841 atcgttgcgg gtaacaacga tctgagcagc cgtaccgagc agcaagcggc gagcctggcg

901 cagaccgcgg cgagcatgga acaactgacc gcgaccgtgg gtcagaacgc ggataacgcg

961 cgtcaagcga gcgagctggc gaagaacgcg gcgaccaccg cgcaggcggg tggcgtgcaa

1021 gttagcacca tgacccacac catgcaggaa atcgcgacca gcagccaaaa aattggcgac

1081 atcattagcg ttatcgatgg tattgcgttc cagaccaaca ttctggcgct gaacgcggcg

1141 gtggaggcgg cgcgtgcggg tgaacaaggt cgtggctttg cggtggttgc gggtgaggtt

1201 cgtaacctgg cgagccgtag cgcgcaagcg gcgaaggaaa tcaaaggcct gattgaggaa

1261 agcgtgaacc gtgttcagca aggtagcaag ctggtgaaca acgcggcggc gaccatgatc

1321 gacattgtga gcagcgttac ccgtgtgaac gatatcatgg gcgagattgc gagcgcgagc

1381 gaggaacagc aacgtggtat cgaacaggtt gcgcaagcgg tgagccagat ggaccaagtt

1441 acccagcaaa acgcgagcct ggttgaggaa gcggcggtgg cgaccgagca gctggcgaac

1501 caagcggatc acctgagcag ccgtgtggcg gtttttaccc tggaagagca cgaagtggcg

1561 cgtcacgaga gcgttcaact gcagattgcg ccggttgtga gctaaggatc cgcggataaa

1621 taagtaacga tccggtccag taatgacctc agaactccat ctggatttgt tcagaacgct

1681 cggttgccgc cgggcgtttt ttattggtga gaatcgcagc aacttgtcgc gccaatcgag

1741 ccatgtcgtc gtcaacgacc ccccattcaa gaacagcaag cagcattgag aactttggaa

1801 tccagtccct cttccacctg ctgaccggat cagcagtccc cggaacatcg tagctgacgc

1861 cttcgcgttg ctcagttgtc caaccccgga aacgggaaaa agcaagtttt ccccgctccc

1921 ggcgtttcaa taactgaaaa ccatactatt tcacagttta aatcacatta aacgacagta

1981 atccccgttg atttgtgcgc caacacagat ccgtcgaccg ggtcgaattt gctttcgaat

2041 ttctgccatt catccgctta ttatcactta ttcaggcgta gcaaccaggc gtttaagggc

2101 accaataact gccttaaaaa aattacgccc cgccctgcca ctcatcgcag tactgttgta

2161 attcattaag cattctgccg acatggaagc catcacaaac ggcatgatga acctgaatcg

2221 ccagcggcat cagcaccttg tcgccttgcg tataatattt gcccatggtg aaaacggggg

2281 cgaagaagtt gtccatattg gccacgttta aatcaaaact ggtgaaactc acccagggat

2341 tggctgagac gaaaaacata ttctcaataa acccttttagg gaaataggcc aggttttcac

2401 cgtaacacgc cacatcttgc gaatatatgt gtagaaactg ccggaaatcg tcgtggtatt

2461 cactccagag cgatgaaaac gtttcagttt gctcatggaa aacggtgtaa caagggtgaa

2521 cactatccca tatcaccagc tcaccgtctt tcattgccat acggaattcc ggatgagcat

2581 tcatcaggcg ggcaagaatg tgaataaagg ccggataaaa cttgtgctta tttttcttta

2641 cggtctttaa aaaggccgta atatccagct gaacggtctg gttataggta cattgagcaa

2701 ctgactgaaa tgcctcaaaa tgttctttac gatgccattg ggatatatca acggtggtat

2761 atccagtgat ttttttctcc attttagctt ccttagctcc tgaaaatctc gataactcaa

2821 aaaatacgcc cggtagtgat cttatttcat tatggtgaaa gttggaacct cttacgtgcc

2881 gatcaacgtc tcattttcgc caaaagttgg cccagggctt cccggtatca acagggacac

2941 caggatttat ttattctgcg aagtgatctt ccgtcacagg tatttattcg gcgcaaagtg

3001 cgtcgggtga tgctgccaac ttactgattt agtgtatgat ggtgtttttg aggtgctcca

3061 gtggcttctg tttctatcag ctgtccctcc tgttcagcta ctgacggggt ggtgcgtaac

3121 ggcaaaagca ccgccggaca tcagcgctag cggagtgtat actggcttac tatgttggca

3181 ctgatgaggg tgtcagtgaa gtgcttcatg tggcaggaga aaaaaggctg caccggtgcg

3241 tcagcagaat atgtgataca ggatatattc cgcttcctcg ctcactgact cgctacgctc

3301 ggtcgttcga ctgcggcgag cggaaatggc ttacgaacgg ggcggagatt tcctggaaga

3361 tgccaggaag atacttaaca gggaagtgag agggccgcgg caaagccgtt tttccatagg

3421 ctccgccccc ctgacaagca tcacgaaatc tgacgctcaa atcagtggtg gcgaaacccg

3481 acaggactat aaagatacca ggcgtttccc cctggcggct ccctcgtgcg ctctcctgtt

3541 cctgcctttc ggtttaccgg tgtcattccg ctgttatggc cgcgtttgtc tcattccacg

3601 cctgacactc agttccgggt aggcagttcg ctccaagctg gactgtatgc acgaacccccc

3661 cgttcagtcc gaccgctgcg ccttatccgg taactatcgt cttgagtcca acccggaaag

3721 acatgcaaaa gcaccactgg cagcagccac tggtaattga tttagaggag ttagtcttga

3781 agtcatgcgc cggttaaggc taaactgaaa ggacaagttt tggtgactgc gctcctccaa

3841 gccagttacc tcggttcaaa gagttggtag ctcagagaac cttcgaaaaa ccgccctgca

3901 aggcggtttt ttcgttttca gagcaagaga ttacgcgcag accaaaacga tctcaagaag

3961 atcatcttat taatcagata aaatatttct agatttcagt gcaatttatc tcttcaaatg

4021 tagcacctga agtcagcccc atacgatata agttgtaatt ctcatgtttg acagcttatc

4081 atcgatcccg caagaggccc ggcagtaccg gcataaccaa gcctatgcct acagcatcca

4141 gggtgacggt gccgaggatg acgatgagcg cattgttaga tttcatacac ggtgcctgac

4201 tgcgttagca atttaactgt gataaactac cgcattaaag cttcttgcga aacagctctc

4261 gaccaggttt atactggtcg tgcagatgaa agcagttttt gccgaggtcg attccgacca

4321 gcgccatatc gctcatagtg atggtctccg aattataaac accctgcgaa agcgtagcct

4381 acgcagggtg tcgggtgctc atcccattac ccgttttccc atctcttaac ttaaggggggg

4441 aacggtgtcc tgtctttcat ggggctcgtt cactgctaac ttacctgctt ccctgtctgt

4501 caattctctc tatcctgcga tcccgcgaag aaccaaaaaa gctcgacaga gggcgcggtc

4561 attttaggtc gggcggatcg gcgccgccgg ctcggctggt gtgccgcaca gcaccgccta

4621 cgtgagctgc cagttgatga acttccccccg ttgccagcta gggcgcaagc gggctgtata

4681 agatcactgc ccatcacatt gatcggctcg gatttttttct caatccgtaa acaggtcaaa

4741 catcagttgc cgcaaccaaa tattggctag gtccttgtgg tacttcgcat gccagaacat

4801 gttgatggct atttcaggca agacgactgg gtgcggcaag gcgcttaggc cgaagggctc

4861 cacgcagcag tcggctaaac gtatcggcac agtggcgagc agatcggtgc gctggaggat

4921 gtggccaacg gcggcgaagt gcggcacttc cagacggatg tcgcgccgga tgccgacccg

```
4981 tgtcatgtac gtgtccacct cgccgtggcc ggtgccagcg gcgatgacac gcacgtggcc
5041 gtaggaacag aagcgctcca gagtcagggg ttcgcgggtg actggatggt ccttgcgaca
5101 taggcacacg tagtgattct ggagcagccg gcgctgaaag aagccagttt gcagattggg
5161 aagcaggccc acggccaagt ccacggttcc gttctgcaag gcctgcatca ggctcatcga
5221 actgtcgcgc accgtactga tcacgcaatt gggggcctgg tgagccagca catccatcag
5281 ccgcggcatg aagtagatct cgccaatgtc ggtcatggcc agggtgaagg tacgctcgct
5341 ggtcagcgga tcgaagcttt catggtgctg tagggcgttg cgcagtgcgt gcatggccga
5401 agtgacgggc tcggccagat gcgcggcata gggtgtgggt tccattccct gatgtgtgcg
5461 cacgaagagt gggtcctgta gcgaggtgcg caggcgtttc agcgcattgc tcacggcagg
5521 ctgggtcagg cccaggttct ccgcagtgat agagacgcgt ctgtcgacca gcaactggtt
5581 gaacaccacc agcaggttta aatccaggtc acgcagttcc atggggcctc gcttgggtta
5641 ttgctggtgc ccggccgggc gcaatattca tgttgatgat ttattatata tcgagtggtg
5701 tatttatcaa tattgtttgc tccgttatcg ttattaacaa gtcatcaata atgccataag
5761 gagtac
```

D.4 Growth curves

As described in section D.4 bacteria should be harvested in the exponential stage of growth. It is reasonable to assume that strains with the same genetic background will grow roughly at the same rate. To verify that I grew overday cultures of strains from table D.1 in 24-well plates (Thermo Fisher Scientific-Nunclon Delta) in the plate reader. Measurements of the OD were performed every 10 min with 9 reads per well. Plate was shaking for 430 s out of 600 s of the kinetic cycle at 218 RPM with the amplitude 3 mm. Temperature was set to 30 ℃. Indeed, as you can see on figure D.2 while there is some variation in the OD of the stationary phase, growth time till the exponential phase for bacteria grown in both M9 with succinate and TB is roughly the same. At the same time there is quiet a bit of variation between growth curves for bacteria grown in M9 with glycerol.

However specific growth times and OD values measued by the plate reader cannot serve as a reliable indicator of growth in the shaker due to difference in access to oxygen. As shown on figure D.3 wild-type strain RP437 grows faster and to the higher OD values in the shaker than in the plate reader in all three media.

I have measured overday growth curves for several more strains grown in the shaker to verify that I can use wild-type growth curve as a guide for growing other strains (fig. D.4). Similarly to the results from plate

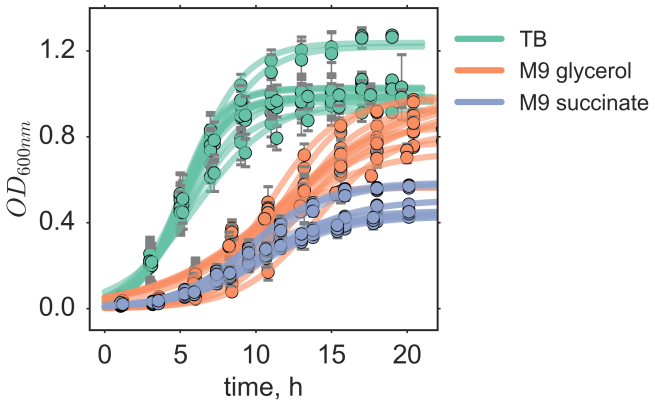

Figure D.2: Overday growth curves for strains without plasmids from table D.1 in TB, M9 with glycerol and M9 with succinate, grown in the shaker as indicated by the color.

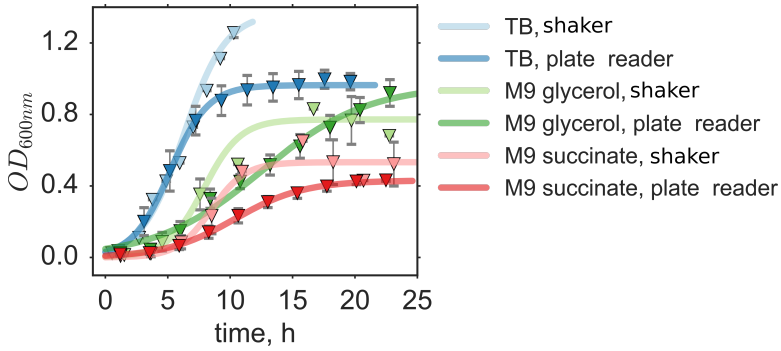

Figure D.3: Overday growth curves for wild-type chemotaxis strain of *E. coli* RP437 in TB, M9 with glycerol and M9 with succinate, grown in plate reader or in the shaker as indicated by the color. OD values have been adjusted to account for the difference in path lengths.

reader growth curves in succinate are close to each other, in glycerol however receptorless strain UU1250 has a much longer lag time. Based on these growth curves I have been growing bacteria in succinate overnight for 20-24 hours up to the OD values of 0.6 to 0.8, and overday for 8-9 hours up to the OD values of 0.25-0.3.

Bacteria usually grow slower in the presence of antibiotic or inducer so I measured growth curves for strains containing plasmids as well (fig. D.5. Based on these growth curves I have been growing strains with plasmids overnight in succinate for $\sim$ 24 hours up to OD of 0.6-0.7 and overday for 9-12 hours depending on the strain up to OD values of 0.2-0.3.

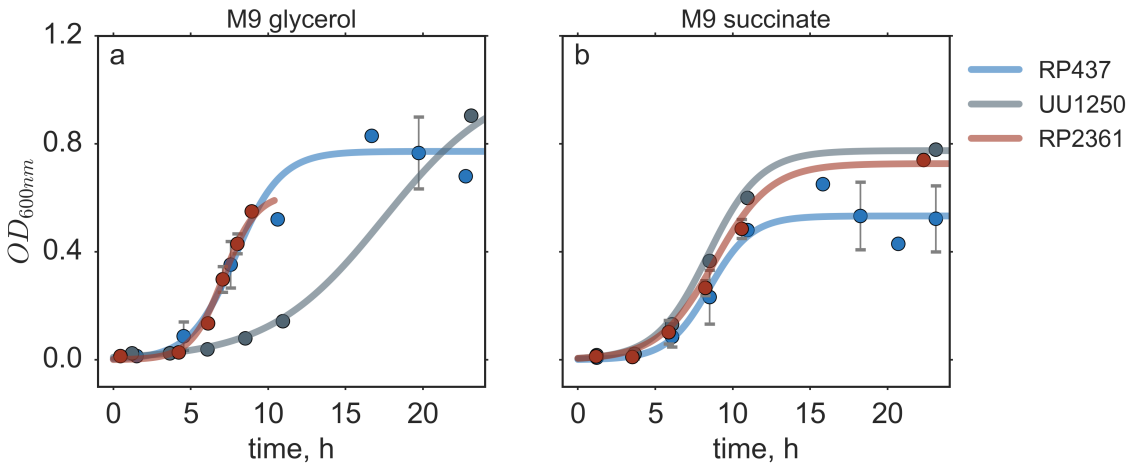

Figure D.4: Overday Growth curves for UU1250 + pSB20 Aer-only, UU1250 + pPA705 Trg-only and UU1250 + pTP1 Tap-only strains in M9 with glycerol (a) and M9 with succinate (b) in the presence of , grown in the shaker.

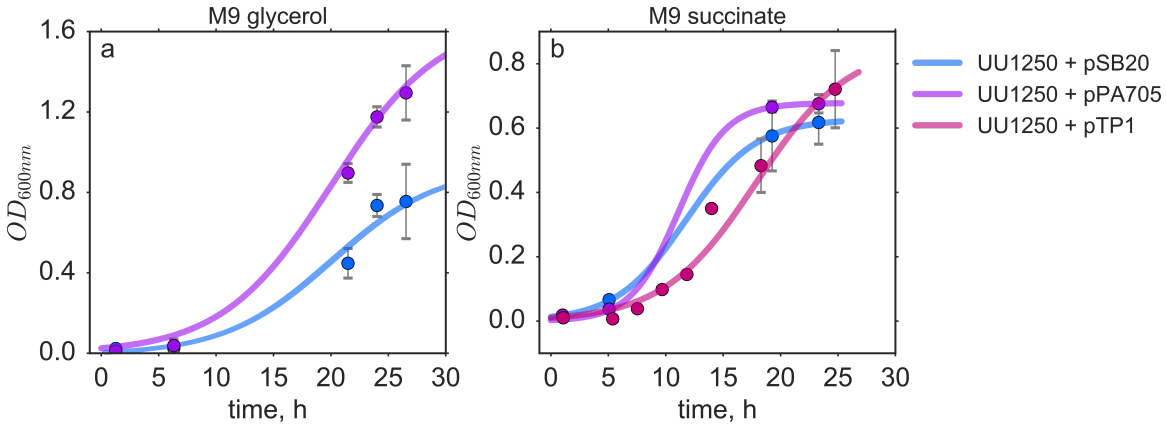

Figure D.5: Growth curves for receptorless strains in M9 with glycerol (a) and M9 with succinate (b), grown in the shaker.

Appendix E

Working with *Rhodobacter sphaeroides*

E.1 Protocols

E.1.1 Growth media

10x Sistrom Medium

Sistrom medium composition: 200 mM K_2HPO, 36.4 mM NH_4Cl, 340 mM Succinic acid, 6.7 mM L-Glutamic acid, 2.5 mM L-Aspartic acid, 85 mM NaCl, 10.5 mM Nitrilotriacetic acid, 12 mM $MgSO_4$, 2.3 mM $CaCl_2 \cdot 2\,H_2O$, 0.07 mM $FeSO_4$, 1.6 μM $(NH_4)_6Mo_7O_{24} \cdot 4\,H_2O$.

Per 1 liter of medium weigh the following ingredients:

- 34.8 g of K_2HPO_4 or 27.2 g of KH_2PO_4
- 34.8 g of K_2HPO_4 or 27.2 g of KH_2PO_4
- 1.95 g of NH_4Cl or 5.0 g $(NH_4)SO_4$
- 40.0 g of Succinic Acid
- 1.0 g of L-Glutamic Acid
- 0.4 g of L-Aspartic Acid
- 5.0 g of NaCl
- 2.0 g Nitrilotriacetic Acid
- 1.44 g of $MgSO_4$ or 2.44 g of $MgCl_2 \cdot 6\,H_2O$ or 3.0 g of $MgSO_4 \cdot 7\,H_2O$
- 0.334 g of $CaCl_2 \cdot 2\,H_2O$
- 0.020 g of $FeSO_4 \cdot 7\,H_2O$
- 0.002 g of $(NH_4)_6Mo_7O_{24} \cdot 4\,H_2O$ or 0.2 ml of 1 % solution of $(NH_4)_6Mo_7O_{24} \cdot 4\,H_2O$

Adjust the volume to 1 liter. Autoclave and store at 4C.

10000x Trace Elements Solution

Trace Element solution composition: 38 mM EDTA, 18 mM $ZnSO_4 \cdot 7\,H_2O$, 9mM $FeSO_4 \cdot 7\,H_2O$, 1.5 mM $CuSO_4 \cdot 5\,H_2O$, 0.9 mM $Co(NO_3)_2 \cdot 6\,H_2$, 1.8 mM H_3BO_3.

To prepare 100 ml of element solution weigh the following ingredients:

- 1.765 g of EDTA
- 10.95 g of $ZnSO_4 \cdot 7\,H_2O$
- 5.0 g of $FeSO_4 \cdot 7\,H_2O$
- 0.392 g of $CuSO_4 \cdot 5\,H_2O$
- 0.248 g of $Co(NO_3)_2 \cdot 6\,H_2O$
- 0.114 g of H_3BO_3

Dissolve in 100 ml of milliQ water. Sterilize by filtration. Store at room temperature in a dark bottle or in a bottle covered with foil.

1000x Vitamin Solution

To prepare 100 ml of Vitamin solution weigh the following ingredients:

- 1 g of Nicotinic Acid
- 0.5 g of Thiamin*HCl
- 0.01 g of Biotin

Dissolve in 100 ml of milliQ water. Sterilize by filtration. Store at 4C.

Sistrom Medium with vitamins and trace elements for growing *R.sphaeroides*

- Add 100 ml of 10x Sistrom medium and 900 ml of milliQ water.
- Adjust the pH to 7.0 and autoclave.
- After the mixture has cooled down to touch add 1 ml of 1000x Vitamin solution and 100 l of the 10000x Trace Elements solution.
- Store at 4°C.

E.1.2 Culturing *R. sphaeroides*

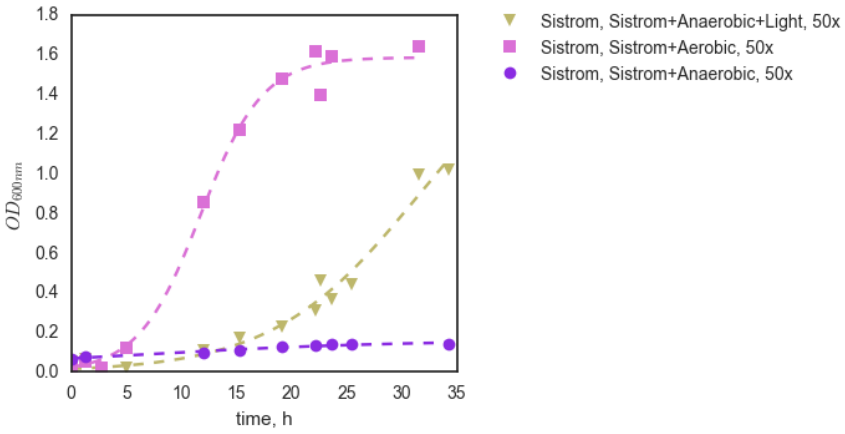

Figure E.1: Growth curves for *R. sphaeroides*.

Agar Plate Culture

- Streak LB or Sistrom plate with *R.sphaeroides* -80 °C stock using standard protocol (see Agar Plate Culture for *E.coli*)
- Plate should be grown at 30 °C.
- Note that it takes about 41 hours for bacteria to form big enough colonies on LB plate.

Aerobic culture

Aerobic culture is grown the same way as for *E. coli* (see D.4) in Sistrom media at 30° C. Overnight culture takes over 24 hours. Overday culture - about 10 (fig. E.1).

Phototrophic culture

To grow phototrophic culture, bacteria are first grown aerobically overnight. Than overnight culture is diluted and grown anaerobically under light illumination.

- Grow overnight culture of *R. sphaeroides* in 1 ml of Sistrom media from the colony on Agar plate at 30° C, 265 rpm.
- Dilute overnight culture 50x in Sistrom media to get about 2 ml of the solution.
- Transfer diluted bacterial culture into the spectophotometer cuvette, which should be filled with solution.

- Seal the cuvette with silly putty (Toysmith Original Silly Putty Pack #104-48) and close with the plastic lid to prevent oxygen access.
- Grow bacteria under wide spectrum visible light. We used 5W LED lamp placed about 10 cm away from the cuvette.

Representative growth curve for the phototrophic culture is shown on the figure E.1. Bacteria in the sealed cuvette without light do not show significant growth (fig. E.1) suggesting that our method of cuvette sealing indeed prevents oxygen access.

List of Terms

Amp Ampicillin. 101

BLUF blue light sensor using FAD. 67

BSA Bovine Serum Albumin. 22, 23, 105

CCCP carbonylcyanide m-chlorophenylhydrazone. 64

CCW counterclockwise rotation of the flagella. 35

Cm Chloramphenicol. 101

CW clockwise rotation of the flagella. 35

DAQ Digital Aquisition. 92

ETC Electron Tranport Chain. 45, 63, 71

FAD Flavin Adenine Dinucleotide. 45, 66, 67

HAMP domain present in Histidine kinases, Adenylyl kinases, Methyl-accepting chemotaxis proteins and Phosphatases. 43

LB Luria-Bertani Broth. 8, 104

LOV Light Oxygen Voltage protein sensors. 67

MSD Mean Square Displacement. 33, 35

OD Optical Density. 101, 102, 113

PEG Polyethylene glycol. 104

PMF Proton-Motive Force. 44, 61

QPD Quadrant Photo Diode. 91

RCD Rate of Change in Direction. 35–37, 39

RCF Relative Centrifugar Force. 104, 105

RPM Revolutions per minute. 101, 105, 113

SLM Spatial Light Modulator. 88

TB Tryptone Broth. 92, 100, 101, 113, 114

TMB Trap Motility Buffer. 101, 105

TSS Transformation and storage solution. 103, 104

References

[1] Stuart Wright, Bharat Walia, John S. Parkinson, and Shahid Khan. Differential activation of Escherichia coli chemoreceptors by blue-light stimuli. *Journal of Bacteriology*, 188(11):3962–3971, jun 2006. 1, 10, 11, 17, 18, 21, 47, 48, 49, 50, 52, 55, 66, 75, 108, 115

[2] H C Berg and E M Purcell. Physics of chemoreception. *Biophysical journal*, 20(2):193–219, nov 1977. 2, 5

[3] Howard C Berg. Motile Behavior of Bacteria. *Physics Today*, 53(1):24, 2000. 2, 3

[4] James G. Mitchell and Kazuhiro Kogure. Bacterial motility: Links to the environment and a driving force for microbial physics. *FEMS Microbiology Ecology*, 55(1):3–16, 2006. 2, 6, 7, 8

[5] Kristin Wuichet and Igor B Zhulin. Origins and diversification of a complex signal transduction system in prokaryotes. *Science signaling*, 3(128):50, jan 2010. 3, 4, 6, 7

[6] Hanbin Mao, Paul S Cremer, and Michael D Manson. A sensitive, versatile microfluidic assay for bacterial chemotaxis. *Proceedings of the National Academy of Sciences of the United States of America*, 100(9):5449–54, apr 2003. 3, 58

[7] Eli Paster and William S Ryu. The thermal impulse response of Escherichia coli. *Proceedings of the National Academy of Sciences of the United States of America*, 105(14):5373–7, apr 2008. 3

[8] Barry L Taylor, Igor B Zhulin, and Mark S. Johnson. Aerotaxis and other energy-sensing behavior in bacteria. *Annual review of microbiology*, 53:103–128, 1999. 4, 8, 45, 74

[9] Yiling Yang and Victor Sourjik. Opposite responses by different chemoreceptors set a tunable preference point in Escherichia coli pH taxis. *Molecular microbiology*, 86(6):1482–9, dec 2012. 3, 8, 43, 45, 66

[10] Melinda D Baker, Peter M Wolanin, and Jeffry B Stock. Signal transduction in bacterial chemotaxis. *BioEssays : news and reviews in molecular, cellular and developmental biology*, 28(1):9–22, jan 2006. 3

[11] Victor Sourjik and Ned S Wingreen. Responding to chemical gradients: bacterial chemotaxis. *Current opinion in cell biology*, 24(2):262–268, dec 2011. 3

[12] George O Toole, Heidi B Kaplan, and Roberto Kolter. Biofilm Formation as microbial development. *Annu. Rev. Microbiol.*, 54:49–79, 2000. 4

[13] Reed M. Stubbendieck, Carol Vargas-Bautista, and Paul D. Straight. Bacterial communities: Interactions to scale. *Frontiers in Microbiology*, 7(AUG):1–19, 2016. 4

[14] Hongyue Dang and Charles R Lovell. Microbial surface colonization and biofilm development in marine environments. 80(1):91–138, 2016. 4

[15] Manoshi S Datta, Elzbieta Sliwerska, Jeff Gore, Martin Polz, and Otto X Cordero. Microbial interactions lead to rapid micro-scale successions on model marine particles. *Nature Communications*, 7(May):11965, 2016. 4

[16] Gladys Alexandre, Suzanne Greer-Phillips, and Igor B Zhulin. Ecological role of energy taxis in microorganisms. *FEMS microbiology reviews*, 28(1):113–26, 2004. 4, 8, 45, 74

[17] S. Park. Motion to Form a Quorum. *Science*, 301(5630):188–188, jul 2003. 4

[18] Nikhil Mittal, Elena O Budrene, Michael P Brenner, and Alexander Van Oudenaarden. Motility of Escherichia coli cells in clusters formed by chemotactic aggregation. *Proceedings of the National Academy of Sciences of the United States of America*, 100(23):13259–63, nov 2003.

[19] Derek L Englert, Michael D Manson, and Arul Jayaraman. Flow-based microfluidic device for quantifying bacterial chemotaxis in stable, competing gradients. *Applied and environmental microbiology*, 75(13):4557–64, jul 2009.

[20] Manjunath Hegde, Derek L Englert, Shanna Schrock, William B Cohn, Christian Vogt, Thomas K Wood, Michael D Manson, and Arul Jayaraman. Chemotaxis to the quorum-sensing signal AI-2 requires the Tsr chemoreceptor and the periplasmic LsrB AI-2-binding protein. *Journal of bacteriology*, 193(3):768–73, feb 2011.

[21] Leanid Laganenka, Remy Colin, and Victor Sourjik. Chemotaxis towards autoinducer 2 mediates autoaggregation in Escherichia coli. *Nature Communications*, 7:12984, 2016. 4

[22] Jacqueline Humphries, Liyang Xiong, Jintao Liu, Heidi A Arjes, Lev Tsimring, Jacqueline Humphries, Liyang Xiong, Jintao Liu, Arthur Prindle, Fang Yuan, Heidi A Arjes, and Lev Tsimring. Species-Independent Attraction to Biofilms through Electrical Signaling Article Species-Independent Attraction to Biofilms through Electrical Signaling. pages 200–209, 2017. 4

[23] F Matthäus, M Jagodic, and J Dobnikar. E. coli superdiffusion and chemotaxis-search strategy, precision, and motility. *Biophysical journal*, 97(4):946–57, aug 2009. 4, 5, 6, 32

[24] Roman Stocker and Justin R Seymour. Ecology and physics of bacterial chemotaxis in the ocean. *Microbiology and Molecular Biology Reviews*, 76(4):792–812, 2012. 6, 7, 8

[25] Nicholas W Frankel, William Pontius, Yann S Dufour, and Junjiajia Long. Adaptability of non-genetic diversity in bacterial chemotaxis. *eLife*, pages 1–30, 2014. 4, 6

[26] Deborah S Millikan and Edward G Ruby. Activator in Vibrio fischeri , Is Required for Motility and Symbiotic Light-Organ Colonization FlrA , a 54 -Dependent Transcriptional Activator in Vibrio fischeri , Is Required for Motility and Symbiotic Light-Organ Colonization. *Society*, 185(12):3547–3557, 2003. 5

[27] Sandra De Weert, Hans Vermeiren, Ine H M Mulders, Irene Kuiper, Nico Hendrickx, V Guido, Jos Vanderleyden, René De Mot, Ben J J Lugtenberg, Sandra de Weert, Hans Vermeiren, Ine H M Mulders, Irene Kuiper, Nico Hendrickx, Guido V Bloemberg, Jos Vanderleyden, René De Mot, and Ben J J Lugtenberg. Flagella-Driven Chemotaxis Towards Exudate Components Is an Important Trait for Tomato Root Colonization by Pseudomonas fluorescens. *Molecular plant-microbe interactions : MPMI*, 15(11):1173–1180, 2002. 5

[28] M. S. Pittman, M. Goodwin, and D. J. Kelly. Chemotaxis in the human gastric pathogen Helicobacter pylori: Different roles for CheW and the three CheV paralogues, and evidence for CheV2 phosphorylation. *Microbiology*, 147(9):2493–2504, 2001. 5

[29] S. P. Strong, B. Freedman, William Bialek, and R. Koberle. Adaptation and optimal chemotactic strategy for E. coli. *Physical Review E*, 57(4):4604–4617, 1998. 5

[30] Burton W Andrews, Tau-Mu Yi, and Pablo a Iglesias. Optimal noise filtering in the chemotactic response of Escherichia coli. *PLoS computational biology*, 2(11):e154, nov 2006. 5

[31] James G Mitchell. The energetics and scaling of search strategies in bacteria. *The American naturalist*, 160(6):727–740, 2002. 6

[32] Nikita Vladimirov, Linda Løvdok, Dirk Lebiedz, and Victor Sourjik. Dependence of bacterial chemotaxis on gradient shape and adaptation rate. *PLoS Computational Biology*, 4(12):e1000242, dec 2008. 6, 34, 42, 55, 94

[33] Elena Korobkova, Thierry Emonet, Jose Vilar, Thomas Shimizu, and Philippe Cluzel. From molecular noise to behavioral variability in a single bacterium. *Nature*, 428(13):12005–8, mar 2004. 6, 14, 89

[34] Thierry Emonet and Philippe Cluzel. Relationship between cellular response and behavioral variability in bacterial chemotaxis. *Proceedings of the National Academy of Sciences of the United States of America*, 105(9):3304–9, mar 2008. 6

[35] Adam James Waite, Nicholas W. Frankel, Yann S. Dufour, Jessica Johnston, and Thierry Emonet. Non-genetic diversity modulates population performance. *Molecular systems biology*, pages 1–14, 2016. 6, 9, 14

[36] Yann S. Dufour, Sébastien Gillet, Nicholas W. Frankel, Douglas B. Weibel, and Thierry Emonet. Direct Correlation between Motile Behavior and Protein Abundance in Single Cells. *PLOS Computational Biology*, 12(9):e1005041, sep 2016. 6, 14, 27, 29, 30, 34, 36

[37] Judith P Armitage and Schmitt Rudiger. Bacterial chemotaxis : Rhodobacter sphaeroides and Sinorhizobium meliloti - variations on a theme? *Microbiology*, 143(6):3671–3682, 1997. 6, 7

[38] Roman Stocker, Justin R Seymour, Azadeh Samadani, Dana E Hunt, and Martin F Polz. Rapid chemotactic response enables marine bacteria to exploit ephemeral microscale nutrient patches. *Proceedings of the National Academy of Sciences of the United States of America*, 105(11):4209–4214, 2008. 6, 7, 16

[39] Howard C. Berg. *E. coli in Motion*. Springer, 2003. 7, 15, 65

[40] Jon L Hobman, Charles W Penn, and Mark J Pallen. Laboratory strains of Escherichia coli: model citizens or deceitful delinquents growing old disgracefully? *Molecular microbiology*, 64(4):881–5, may 2007. 7

[41] George H Wadhams and Judith P Armitage. Making sense of it all: bacterial chemotaxis. *Nature reviews. Molecular cell biology*, 5(December):1024–1037, 2004. 7, 87

[42] Christopher V. Rao, John R. Kirby, and Adam P. Arkin. Design and diversity in bacterial chemotaxis: A comparative study in Escherichia coli and Bacillus subtilis. *PLoS Biology*, 2(2):239–253, 2004. 7

[43] Victor Sourjik and Judith P Armitage. Spatial organization in bacterial chemotaxis. *The EMBO journal*, 29(16):2724–33, aug 2010. 7, 87

[44] Diana Clausznitzer, Gabriele Micali, Silke Neumann, Victor Sourjik, and Robert G. Endres. Predicting Chemical Environments of Bacteria from Receptor Signaling. *PLoS Computational Biology*, 10(10):e1003870, 2014. 7

[45] Barry L. Taylor and Igor B. Zhulin. In search of higher energy: metabolism-dependent behaviour in bacteria. *Molecular Microbiology*, 28(4):683–690, mar 2002. 8, 66, 74

[46] J Adler and Bonnie Templeton. The Effect of Environmental Conditions on the Motility of Escherichia coli. *Journal of General Microbiology*, 46(2):175–184, 1967. 8, 75

[47] Victor Chubukov, Luca Gerosa, Karl Kochanowski, and Uwe Sauer. Coordination of microbial metabolism. *Nature Publishing Group*, 12(5):327–340, 2014. 8, 80, 81

[48] J Dobrogosz and B Hamilton. The role of cyclic AMP in chemotaxis in Escherichia coli. *Biochemical and biophysical research communications*, 42(2):202–207, 1971. 8, 75

[49] Alex Boehm, Matthias Kaiser, Hui Li, Christian Spangler, Christoph Alexander Kasper, Martin Ackermann, Volkhard Kaever, Victor Sourjik, Volker Roth, and Urs Jenal. Second messenger-mediated adjustment of bacterial swimming velocity. *Cell*, 141(1):107–116, 2010. 8, 75

[50] Hanna Salman and Albert Libchaber. A concentration-dependent switch in the bacterial response to temperature. *Nature cell biology*, 9(9):1098–100, sep 2007. 8, 45

[51] Yevgeniy Kalinin, Silke Neumann, Victor Sourjik, and Mingming Wu. Responses of Escherichia coli bacteria to two opposing chemoattractant gradients depend on the chemoreceptor ratio. *Journal of bacteriology*, 192(7):1796–800, apr 2010. 8, 44, 45, 75, 79

[52] S. M. Block, J. E. Segall, and H. C. Berg. Adaptation kinetics in bacterial chemotaxis. *Journal of Bacteriology*, 154(1):312–323, 1983. 8, 26

[53] Daqi Yu, Xiaomin Ma, Yuhai Tu, and Luhua Lai. Both piston-like and rotational motions are present in bacterial chemoreceptor signaling. *Scientific reports*, 5:8640, 2015. 9, 44

[54] PJ Mears, Santosh Koirala, CV Rao, Ido Golding, and YR Chemla. Escherichia coli swimming is robust against variations in flagellar number. *Elife*, pages 1–18, 2014. 9, 35, 96

[55] A. Briegel, X. Li, A. M. Bilwes, K. T. Hughes, G. J. Jensen, and B. R. Crane. Bacterial chemoreceptor arrays are hexagonally packed trimers of receptor dimers networked by rings of kinase and coupling proteins. *Proceedings of the National Academy of Sciences*, 109(10):3766–3771, 2012. 9, 58, 59

[56] C. Keith Cassidy, Benjamin A. Himes, Frances J. Alvarez, Jun Ma, Gongpu Zhao, Juan R. Perilla, Klaus Schulten, and Peijun Zhang. CryoEM and computer simulations reveal a novel kinase conformational switch in bacterial chemotaxis signaling. *eLife*, 4(NOVEMBER2015):1–20, 2015. 44

[57] Ivan Gushchin, Igor Melnikov, Vitaliy Polovinkin, and Others. Mechanism of transmembrane signaling by sensor histidine kinases. *Sience*, 6345(May), 2017. 9, 44

[58] B L Taylor, J B Miller, H M Warrick, and D E Koshland. Electron acceptor taxis and blue light effect on bacterial chemotaxis. *Journal of bacteriology*, 140(2):567–73, nov 1979. 9, 10, 11, 21, 47, 50, 97

[59] Donat-P Häder. Photosensory behavior in procaryotes. *Microbiological reviews*, 51(1):1–21, mar 1987. 10

[60] Judith P Armitage and Klaas J Hellingwerf. Light-induced behavioral responses ('phototaxis') in prokaryotes. *Photosynthesis research*, 76(1-3):145–55, jan 2003. 10, 87

[61] Erin B Purcell and Sean Crosson. Photoregulation in prokaryotes. *Current opinion in microbiology*, 11(2):168–78, apr 2008. 10, 50

[62] MJ Sackett and JP Armitage. Photoresponses of the purple nonsulfur bacteria Rhodospirillum centenum and Rhodobacter sphaeroides. *J Bacteriol*, 179(21), 1997. 10, 17, 87

[63] R M Berry and J P Armitage. Response kinetics of tethered Rhodobacter sphaeroides to changes in light intensity. *Biophysical journal*, 78(3):1207–1215, mar 2000. 10, 17, 86, 87, 89

[64] J S Choi, Y H Chung, Y J Moon, C Kim, M Watanabe, P S Song, C O Joe, L Bogorad, and Y M Park. Photomovement of the gliding cyanobacterium Synechocystis sp. PCC 6803. *Photochemistry and photobiology*, 70(1):95–102, jul 1999. 10

[65] Devaki Bhaya. Light matters: phototaxis and signal transduction in unicellular cyanobacteria. *Molecular microbiology*, 53(3):745–54, aug 2004. 10, 16

[66] RosannaManWah Chau, Tristan Ursell, Shuo Wang, KerwynCasey Huang, and Devaki Bhaya. Maintenance of Motility Bias during Cyanobacterial Phototaxis. *Biophysical Journal*, 108(7):1623–1632, 2015. 10

[67] Rosanna Man Wah Chau, Devaki Bhaya, and Kerwyn Casey Huang. Emergent Phototactic Responses of Cyanobacteria under Complex Light Regimes. *mBio*, 8(2):1–15, 2017. 10, 16

[68] Steven L. Porter, David A. Wilkinson, Elaine D. Byles, George H. Wadhams, Stephen Taylor, Nigel J. Saunders, and Judith P. Armitage. Genome sequence of Rhodobacter sphaeroides strain WS8N. *Journal of Bacteriology*, 193(15):4027–4028, 2011. 10, 86, 88

[69] Barry L Taylor and D E Koshland. Intrinsic and extrinsic light responses of Salmonella typhimurium and Escherichia coli. *Journal of bacteriology*, 123(2):557–69, aug 1975. 10, 11, 21, 47, 50

[70] H Yang, H Inokuchi, and J Adler. Phototaxis away from blue light by an Escherichia coli mutant accumulating protoporphyrin IX. *Proceedings of the National Academy of Sciences of the United States of America*, 92(16):7332–6, aug 1995. 10, 11

[71] Douglas B Weibel, Willow R Diluzio, and George M Whitesides. Microfabrication meets microbiology. *Nature reviews. Microbiology*, 5(3):209–18, mar 2007. 11, 15, 22

[72] Tanvir Ahmed, Thomas S Shimizu, and Roman Stocker. Microfluidics for bacterial chemotaxis. *Integrative biology : quantitative biosciences from nano to macro*, 2(11-12):604–29, nov 2010. 11, 15, 16

[73] H C Berg and D a Brown. Chemotaxis in Escherichia coli analysed by three-dimensional tracking. *Nature*, 239(5374):500–504, 1972. 13, 14

[74] SH Larsen, RW Reader, EN Kort, WW Tso, and J Adler. Change in direction of flagellar rotation is the basis of the chemotactic response in Escherichia coli. *Nature*, 249(452):74–77, 1974. 13, 26

[75] H C Berg and P M Tedesco. Transient response to chemotactic stimuli in Escherichia coli. *Proceedings of the National Academy of Sciences of the United States of America*, 72(8):3235–9, aug 1975. 13

[76] P. Cluzel. An Ultrasensitive Bacterial Motor Revealed by Monitoring Signaling Proteins in Single Cells. *Science*, 287(5458):1652–1655, mar 2000. 14, 43, 58

[77] Yoshiyuki Sowa and Richard M. Berry. Bacterial flagellar motor. *Quarterly Reviews of Biophysics*, 41(02):103–132, 2008. 14, 43, 65

[78] Ryan Boschert, Frederick R. Adler, and David F. Blair. Loose coupling in the bacterial flagellar motor. *Proceedings of the National Academy of Sciences*, 112(15):201419955, 2015. 14

[79] Suddhashil Chattopadhyay, Radu Moldovan, Chuck Yeung, and X L Wu. Swimming efficiency of bacterium Escherichia coli. *Proceedings of the National Academy of Sciences of the United States of America*, 103(37):13712–13717, 2006. 14, 65

[80] Taejin L Min, Patrick J Mears, Lon M Chubiz, Christopher V Rao, Ido Golding, and Yann R Chemla. High-resolution, long-term characterization of bacterial motility using optical tweezers. *Nature methods*, 6(11):831–5, nov 2009. 14, 15, 16, 27, 65, 95, 96, 107

[81] Taejin L. Min, Patrick J. Mears, Ido Golding, and Yann R. Chemla. Chemotactic adaptation kinetics of individual Escherichia coli cells. *Proceedings of the National Academy of Sciences*, 109(25):1–6, jun 2012. 14, 56, 71, 90, 95, 96

[82] U Alon, L Camarena, M G Surette, B Aguera y Arcas, Y Liu, S Leibler, and J B Stock. Response regulator output in bacterial chemotaxis. *The EMBO journal*, 17(15):4238–48, aug 1998. 14, 26, 31, 89

[83] J F Staropoli and U Alon. Computerized analysis of chemotaxis at different stages of bacterial growth. *Biophysical journal*, 78(1):513–9, jan 2000. 106

[84] Jun Xie, Shahid Khan, and Mubarak Shah. Automatic tracking of Escherichia coli bacteria. *Medical image computing and computer-assisted intervention : MICCAI ... International Conference on Medical Image Computing and Computer-Assisted Intervention*, 11(Pt 1):824–32, jan 2008. 14

[85] P. D. Frymier, R. M. Ford, H. C. Berg, and P. T. Cummings. Three-dimensional tracking of motile bacteria near a solid planar surface. *Proceedings of the National Academy of Sciences*, 92(13):6195–6199, 1995. 14

[86] K M Taute, S Gude, S J Tans, and T S Shimizu. High-throughput 3D tracking of bacteria on a standard phase contrast microscope. *Nat Commun*, 6(May):8776, 2015. 14

[87] SM Block, JE Segall, and HC Berg. Impulse responses in bacterial chemotaxis. *Cell*, 31(November):215–226, 1982. 14

[88] J Adler. A method for measuring chemotaxis and use of the method to determine optimum conditions for chemotaxis by Escherichia coli. *Journal of general microbiology*, 74:77–91, 1973. 14, 16

[89] S Khan, F Castellano, J L Spudich, J a McCray, R S Goody, G P Reid, and D R Trentham. Excitatory signaling in bacterial probed by caged chemoeffectors. *Biophysical journal*, 65(6):2368–82, dec 1993. 15, 27, 35

[90] S Khan, J L Spudich, J a McCray, and D R Trentham. Chemotactic signal integration in bacteria. *Proceedings of the National Academy of Sciences of the United States of America*, 92(21):9757–61, oct 1995. 27

[91] Jan F Jikeli, Luis Alvarez, Benjamin M Friedrich, Laurence G Wilson, René Pascal, Remy Colin, Magdalena Pichlo, Andreas Rennhack, Christoph Brenker, and U Benjamin Kaupp. Sperm navigation along helical paths in 3D chemoattractant landscapes. *Nature communications*, 6:7985, 2015. 15, 16

[92] GCR Ellis-Davies. Caged compounds: photorelease technology for control of cellular chemistry and physiology. *Nature methods*, 4(8):619–628, 2007. 15

[93] John M Walker. *CHEMOTAXIS: METHODS AND PROTOCOLS*. 2009. 15

[94] Wouter D Hoff, Michael A Van Der Horst, Clara B Nudel, and Klaas J Hellingwerf. Prokaryotic Phototaxis. 571:25–49, 2009. 16, 86

[95] Ingrid M Keseler, Amanda Mackie, Martin Peralta-gil, Alberto Santos-zavaleta, Anamika Kothari, Markus Krummenacker, Mario Latendresse, Luis Mun, Alexander G Shearer, Quang Ong, Suzanne Paley, Imke Schro, Pallavi Subhraveti, Mike Travers, Deepika Weerasinghe, Verena Weiss, Julio Colladovides, Robert P Gunsalus, Ian Paulsen, and Peter D Karp. EcoCyc : fusing model organism databases with systems biology. 41(November 2012):605–612, 2013. 21, 44, 45, 47, 62

[96] David Jordan, Seppe Kuehn, Eleni Katifori, and Stanislas Leibler. Behavioral diversity in microbes and low-dimensional phenotypic spaces. *Proceedings of the National Academy of Sciences of the United States of America*, 110(34):14018–23, aug 2013. 22

[97] Dmitry a. Markov, Elizabeth M. Lillie, Shawn P. Garbett, and Lisa J. McCawley. Variation in diffusion of gases through PDMS due to plasma surface treatment and storage conditions. *Biomedical Microdevices*, 16:91–96, 2014. 22

[98] Hitoshi Shiku, Takeshi Saito, Ching-Chou Wu, Tomoyuki Yasukawa, Masaki Yokoo, Hiroyuki Abe, Tomokazu Matsue, and Hiroshi Yamada. Oxygen Permeability of Surface-modified Poly(dimethylsiloxane) Characterized by Scanning Electrochemical Microscopy. *Chemistry Letters*, 35(2):234–235, 2006. 23

[99] Mark C M van Loosdrecht, Willem Norde, Johannes Lyklema, and Alexander J B Zehnder. Hydrophobic and electrostatic parameters in bacterial adhesion - Dedicated to Werner Stumm for his 65th birthday. *Aquatic Sciences*, 52:103–114, 1990. 23

[100] John O'Brien, Ian Wilson, Terry Orton, and François Pognan. Investigation of the Alamar Blue (resazurin) fluorescent dye for the assessment of mammalian cell cytotoxicity. *European Journal of Biochemistry*, 267(17):5421–5426, 2000. 23

[101] Yann R Chemla. *Biological Applications of the SQUID Microscope*. PhD thesis, 2001.

[102] Dimitar Karakashev, Danka Galabova, and Ivan Simeonov. A simple and rapid test for differentiation of aerobic from anaerobic bacteria. *World Journal of Microbiology and Biotechnology*, 19(3):233–238, 2003. 23

[103] L. Turner, W. S. Ryu, and H. C. Berg. Real-Time Imaging of Fluorescent Flagellar Filaments. *Journal of Bacteriology*, 182(10):2793–2801, may 2000. 24, 89

[104] Eric Lauga, Willow R. DiLuzio, George M. Whitesides, and Howard A. Stone. Swimming in Circles: Motion of Bacteria near Solid Boundaries. *Biophysical Journal*, 90(2):400–412, 2006. 27

[105] Laurence Lemelle, Jean François Palierne, Elodie Chatre, and Christophe Place. Counterclockwise circular motion of bacteria swimming at the air-liquid interface. *Journal of Bacteriology*, 192(23):6307–6308, 2010. 27

[106] G. Bradski. Open Source Computer Vision Library. *Dr. Dobb's Journal of Software Tools*, 2000. 28

[107] Dan Allan, Thomas A Caswell, Nathan Keim, Franois Boulogne, Rebecca W Perry, and Leonardo Uieda. trackpy: Trackpy v0.3.0, oct 2014. 28

[108] F. Pedregosa, G. Varoquaux, A. Gramfort, V. Michel, B. Thirion, O. Grisel, M. Blondel, P. Prettenhofer, R. Weiss, V. Dubourg, J. Vanderplas, A. Passos, D. Cournapeau, M. Brucher, M. Perrot, and E. Duchesnay. Scikit-learn: Machine learning in python. *Journal of Machine Learning Research*, 12:2825–2830, 2011. 30, 104

[109] Silke Neumann, Karin Grosse, and Victor Sourjik. Chemotactic signaling via carbohydrate phosphotransferase systems in Escherichia coli. *Proceedings of the National Academy of Sciences of the United States of America*, 109(30):12159–12164, jul 2012. 40

[110] John S. Parkinson, Gerald L. Hazelbauer, and Joseph J. Falke. Signaling and sensory adaptation in Escherichia coli chemoreceptors: 2015 update. *Trends in Microbiology*, pages 1–10, 2015. 42, 58, 59

[111] Victor Sourjik and Ned S Wingreen. Responding to chemical gradients: bacterial chemotaxis. *Current opinion in cell biology*, 24(2):262–8, apr 2012. 42, 59, 75

[112] Junhua Yuan and Howard C. Berg. Ultrasensitivity of an adaptive bacterial motor. *Journal of Molecular Biology*, 425(10):1760–1764, 2013. 43

[113] Victor Sourjik. Receptor clustering and signal processing in E. coli chemotaxis. *Trends in microbiology*, 12(12):569–76, dec 2004. 43, 44

[114] Gerald L Hazelbauer, Joseph J Falke, and John S Parkinson. Bacterial chemoreceptors: high-performance signaling in networked arrays. *Trends in biochemical sciences*, 33(1):9–19, jan 2008. 43, 44

[115] Alexander N. Barnakov, Ludmila A. Barnakova, and Gerald L. Hazelbauer. Efficient adaptational demethylation of chemoreceptors requires the same enzyme-docking site as efficient methylation. *PNAS*, 96(September):10667–10672, 1999. 44

[116] Jiongru Wu, Jiayin Li, Guoyong Li, David G Long, and Robert M Weis. The Receptor Binding Site for the Methyltransferase of Bacterial Chemotaxis Is Distinct from the Sites of Methylation . *Biochemistry*, pages 4984–4993, 1996. 44

[117] Mingshan Li and Gerald L Hazelbauer. Cellular Stoichiometry of the Components of the Chemotaxis Signaling Complex. 186(12):3687–3694, 2004. 61, 63, 78

[118] Barry L Taylor, Anuradha Rebbapragada, and Mark S Johnson. The FAD-PAS domain as a sensor for behavioral responses in Escherichia coli. *Antioxidants & Redox Signalling*, 3(5), 2001. 45, 46, 48

[119] M D Manson, V Blank, G Brade, and C F Higgins. Peptide chemotaxis in E. coli involves the Tap signal transducer and the dipeptide permease. *Nature*, 321(6067):253–6, 1986. 47

[120] Xianxian Liu and Rebecca E. Parales. Chemotaxis of Escherichia coli to pyrimidines: A new role for the signal transducer tap. *Journal of Bacteriology*, 190(3):972–979, 2008. 44, 47

[121] Mahmut Demir, Carine Douarche, Anna Yoney, Albert Libchaber, and Hanna Salman. Effects of population density and chemical environment on the behavior of Escherichia coli in shallow temperature gradients. *Physical biology*, 8(6):063001, dec 2011. 45

[122] Y. Meir A. Paulick, W.S. Ryu, V. Jakovljevic, N.S. Wingreen and V. Sourjik. Mechanism of bidirectional thermotaxis in E. coli. In *BLAST XIV conference proceedings*, page 18, 2017. 45

[123] Jessica C Edwards, Mark S Johnson, and Barry L Taylor. Differentiation between electron transport sensing and proton motive force sensing by the Aer and Tsr receptors for aerotaxis. *Molecular microbiology*, 62(3):823–37, nov 2006. 45, 46, 66, 74

[124] Barry L Taylor, Anuradha Rebbapragada, and Mark S Johnson. The FAD-PAS domain as a sensor for behavioral responses in Escherichia coli. *Antioxidants & redox signaling*, 3(5):867–879, 2001. 45

[125] I B Zhulin, V a Bespalov, M S Johnson, B L Taylor, Igor B Zhulin, Vyacheslav a Bespalov, and Mark S Johnson. Oxygen taxis and proton motive force in Azospirillum brasilense. *J. Bacteriol.*, 178(17):5199–5204, 1996. 45

[126] Barry L Taylor. Aer on the inside looking out: paradigm for a PAS-HAMP role in sensing oxygen, redox and energy. *Molecular microbiology*, 65(6):1415–1424, 2007. 46

[127] Karen S Conrad, Craig C Manahan, and Brian R Crane. Photochemistry of flavoprotein light sensors. *Nature Chemical Biology*, 10(10):801–809, sep 2014. 46, 70

[128] Sergei I Bibikov and Andrew C Miller. Methylation-independent aerotaxis mediated by the Escherichia coli Aer protein. *Journal of bacteriology*, 186(12):3730–3737, 2004. 46

[129] H Kondoh, C B Ball, and J Adler. Identification of a methyl-accepting chemotaxis protein for the ribose and galactose chemoreceptors of Escherichia coli. *Proceedings of the National Academy of Sciences of the United States of America*, 76(1):260–264, 1979. 47

[130] K Yamamoto, R M Macnab, and Y Imae. Repellent response functions of the Trg and Tap chemoreceptors of Escherichia coli. *Journal of bacteriology*, 172(1):383–8, 1990. 47

[131] Hai The Pham and John S Parkinson. Phenol sensing by Escherichia coli chemoreceptors: a nonclassical mechanism. *Journal of bacteriology*, 193(23):6597–604, dec 2011. 47

[132] Alexander N. Barnakov, Ludmila A. Barnakova, and Gerald L. Hazelbauer. Comparison in vitro of a high- and a low-abundance chemoreceptor of Escherichia coli: Similar kinase activation but different methyl-accepting activities. *Journal of Bacteriology*, 180(24):6713–6718, 1998. 47

[133] Junhua Yuan, Richard W Branch, Basarab G Hosu, and Howard C Berg. Adaptation at the output of the chemotaxis signalling pathway. *Nature*, 484(7393):233–6, apr 2012. 56

[134] John S. Parkinson. Crosslinking snapshots of bacterial chemoreceptor squads. 101(39):6314–6318, 2004. 58, 115

[135] Mingshan Li and Gerald L Hazelbauer. Core unit of chemotaxis signaling complexes. 2011, 2011. 58

[136] Khoosheh K. Gosink, Maria Del Carmen Burón-Barral, and John S. Parkinson. Signaling interactions between the aerotaxis transducer Aer and heterologous chemoreceptors in Escherichia coli. *Journal of Bacteriology*, 188(10):3487–3493, 2006. 58

[137] Mingshan Li and Gerald L Hazelbauer. Selective allosteric coupling in core chemotaxis signaling complexes. 111(45):1–6, 2014. 59

[138] Ariane Briegel, Davi R Ortega, Elitza I Tocheva, Kristin Wuichet, Zhuo Li, Songye Chen, Axel Mu, Cristina V Iancu, Gavin E Murphy, Megan J Dobro, Igor B Zhulin, and Grant J Jensen. Universal architecture of bacterial chemoreceptor arrays. 106(40):17181–17186, 2009. 59

[139] Victor Sourjik and Howard C Berg. Receptor sensitivity in bacterial chemotaxis. *Proceedings of the National Academy of Sciences of the United States of America*, 99(1):123–7, jan 2002. 59

[140] Allison C Lamanna, George W Ordal, and Laura L Kiessling. Large increases in attractant concentration disrupt the polar localization of bacterial chemoreceptors. 57:774–785, 2005. 59

[141] Ariane Briegel, Morgan Beeby, Martin Thanbichler, and Grant J Jensen. Activated chemoreceptor arrays remain intact and hexagonally packed. 82(3):748–757, 2011. 59

[142] White David. Membrane Bioenergetics: The Proton Potential, 2012. 64, 65, 67

[143] Jianhua Xing, Fan Bai, Richard Berry, and George Oster. Torque-speed relationship of the bacterial flagellar motor. *Proceedings of the National Academy of Sciences of the United States of America*, 103(5):1260–1265, 2006. 65

[144] Thierry Mora, Howard Yu, Yoshiyuki Sowa, and Ned S Wingreen. Steps in the bacterial flagellar motor. *PLoS computational biology*, 5(10):e1000540, oct 2009. 65

[145] D C Fung and H C Berg. Powering the flagellar motor of Escherichia coli with an external voltage source, 1995. 65

[146] Christopher V Gabel and Howard C Berg. The speed of the flagellar rotary motor of Escherichia coli varies linearly with protonmotive force. *Proceedings of the National Academy of Sciences of the United States of America*, 100:8748–8751, 2003. 65, 67

[147] A. Rebbapragada, M. S. Johnson, G. P. Harding, A. J. Zuccarelli, H. M. Fletcher, I. B. Zhulin, and B. L. Taylor. The Aer protein and the serine chemoreceptor Tsr independently sense intracellular energy levels and transduce oxygen, redox, and energy signals for Escherichia coli behavior. *Proceedings of the National Academy of Sciences*, 94(20):10541–10546, sep 1997. 66

[148] Suzanne E. Greer-Phillips, Gladys Alexandre, Barry L. Taylor, and Igor B. Zhulin. Aer and Tsr guide Escherichia coli in spatial gradients of oxidizable substrates. *Microbiology*, 149(2003):2661–2667, 2003. 66

[149] John Kasianowicz, Roland Benz, and Stuart McLaughlin. The kinetic mechanism by which CCCP (carbonyl cyanide m-Chlorophenylhydrazone) transports protons across membranes. *The Journal of Membrane Biology*, 82(2):179–190, 1984. 67

[150] Shunsuke Ozaki, Kenji Kano, and Osamu Shirai. Electrochemical elucidation on the mechanism of uncoupling caused by hydrophobic weak acids. *Physical Chemistry Chemical Physics*, 10(30):4449–4455, 2008. 67

[151] Frederic Reymond, Pierre-Alain Carrupt, Bernard Testa, and Hubert H Girault. Charge and delocalization effects on the lipophilicity of protonatable drugs. *Chemistry–A European Journal*, 5(1):39–47, 1999. 67

[152] Junichi Shiois, L Taylor, and Lorna Linda. Oxygen taxis and proton motive force in salmonella typhimurium. *The journal of biological chemistry*, 259(17):10983–10988, 1984. 67

[153] Wung-wai W Tso, J Adler, and American Society. Negative chemotaxis in Escherichia coli. *Journal of bacteriology*, 118(2):560–76, may 1974. 67

[154] Satoshi Nakamura, Takao Nakamura, and Yasuyuki Ogura. Absorption spectrum of flavin mononucleotide semiquinone. *Journal of biochemistry*, 53(2):143–146, 1963. 70

[155] Aba Losi and Wolfgang Gärtner. Old chromophores, new photoactivation paradigms, trendy applications: flavins in blue light-sensing photoreceptors. *Photochemistry and photobiology*, 87(3):491–510, 2011. 70

[156] G Unden and J Bongaerts. Alternative respiratory pathways of Escherichia coli: energetics and transcriptional regulation in response to electron acceptors. *Biochimica et biophysica acta*, 1320(3):217–34, jul 1997. 74

[157] P. S. Poole and J. P. Armitage. Motility response of Rhodobacter sphaeroides to chemotactic stimulation. *Journal of Bacteriology*, 170(12):5673–5679, 1988. 87

[158] Mila Kojadinovic, Judith P Armitage, Marcus J Tindall, and George H Wadhams. Response kinetics in the complex chemotaxis signalling pathway of Rhodobacter sphaeroides. *Journal of the Royal Society, Interface / the Royal Society*, 10(81):20121001, 2013. 87

[159] Steven L. Porter, Anna V. Warren, Angela C. Martin, and Judith P. Armitage. The third chemotaxis locus of Rhodobacter sphaeroides is essential for chemotaxis. *Molecular Microbiology*, 46(4):1081–1094, 2002. 87

[160] David Kentner and Victor Sourjik. Spatial organization of the bacterial chemotaxis system. *Current opinion in microbiology*, 9(6):619–24, dec 2006. 87

[161] Sisi Fan and Robert G. Endres. A minimal model for metabolism-dependent chemotaxis in Rhodobacter sphaeroides. *Interface Focus*, 4(6):20140002, 2014. 87

[162] D. E. Gauden and J. P. Armitage. Electron transport-dependent taxis in Rhodobacter sphaeroides. *Journal of Bacteriology*, 177(20):5853–5859, 1995. 87

[163] Hendrik N Happ, Stephan Braatsch, Vera Broschek, Lisa Osterloh, and Gabriele Klug. Light-dependent regulation of photosynthesis genes in Rhodobacter sphaeroides 2.4.1 is coordinately controlled by photosynthetic electron transport via the PrrBA two-component system and the photoreceptor AppA. *Molecular microbiology*, 58(3):903–14, nov 2005. 87

[164] Anja Steude, Matthias Jahnel, Michael Thomschke, Matthias Schober, and Malte C. Gather. Controlling the Behavior of Single Live Cells with High Density Arrays of Microscopic OLEDs. *Advanced Materials*, pages n/a–n/a, 2015. 92

[165] Honesty Kim, Lukas Cyrill Gerber, Daniel Chiu, Seung Ah Lee, Nate J Cira, Yuyang Xia, and Ingmar H Riedel-kruse. LudusScope : Accessible Interactive Smartphone Microscopy for Life-Science Education. pages 1–16, 2016. 92

[166] Kazunari Ozasa, June Won, Simon Song, and Mizuo Maeda. Autonomous oscillation/separation of cell density artificially induced by optical interlink feedback as designed interaction between two isolated microalgae chips. *Scientific Reports*, 6(August 2015):24602, 2016. 92

[167] Gaszton Vizsnyiczai, Giacomo Frangipane, Claudio Maggi, Filippo Saglimbeni, Silvio Bianchi, and Roberto Di Leonardo. Light controlled 3D micromotors powered by bacteria. *Nature Communications*, 8(15974):1–7, 2017. 92

[168] Introduction to Digital Micromirror Device (DMD) Technology. *Texas Instruments*, 2008. 92

[169] Colin Echeverría Aitken, R. Andrew Marshall, and Joseph D. Puglisi. An Oxygen Scavenging System for Improvement of Dye Stability in Single-Molecule Fluorescence Experiments. *Biophysical Journal*, 94(5):1826–1835, 2008. 97

[170] Oleg Paliy and Thusitha S Gunasekera. Growth of E. coli BL21 in minimal media with different gluconeogenic carbon sources and salt contents. *Applied microbiology and biotechnology*, 73(5):1169–72, jan 2007. 108

[171] Frederick M. Ausubel, Roger Brent, Robert E. Kingston, David D. Moore, J.G. Seidman, John A. Smith, and Kevin Struhl, editors. *Current Protocols in Molecular Biology*. John Wiley & Sons, Inc., Hoboken, NJ, USA, may 2001. 109

[172] J S Parkinson and S E Houts. Isolation and Behavior of Escherichia coli Deletion Mutants Lacking Chemotaxis Functions. 1982. 114

[173] U Alon, M G Surette, N Barkai, and S Leibler. Robustness in bacterial chemotaxis. *Nature*, 397(6715):168–71, jan 1999. 115